An investigation into the role of syntaxin 16 in GLUT4 trafficking

Nicola Samantha Hamilton
M.Res. B.Sc.(Hons)

Submitted in fulfilment of the requirements for the Degree of Master of Science

Institute of Molecular, Cell and Systems Biology
University of Glasgow

July 2011

Abstract

In muscle and fat cells, insulin stimulates the translocation of GLUT4 from unique intracellular storage site(s) to the cell surface. In type II diabetes this translocation is impaired. The translocation of GLUT4 in response to insulin is an example of regulated membrane trafficking.

Membrane trafficking involves the fusion of vesicles with specific target membranes and is mediated by SNARE proteins. The SNARE proteins involved in the intracellular trafficking of GLUT4 are poorly understood. Stx 16 is a t-SNARE located in the TGN which has been proposed to have a role in GLUT4 trafficking. Previous work has shown that expression of the cytosolic domain of stx 16 significantly slows the reversal of insulin-stimulated glucose transport and depletion of stx 16 using morpholino antisense oligonucleotides reduces glucose transport over a range of insulin concentrations. Stx 16 knockdown also reduces total cellular levels of GLUT4. It has been suggested that stx 16 has a role in sequestration of GLUT4 in its storage site(s). In this thesis the role of stx 16 in GLUT4 trafficking was further investigated.

First of all, stx 16 expression was stably depleted in 3T3-L1 adipocytes using a shRNA approach. Knockdown of stx 16 reduced the total GLUT4 cellular levels by 20% and the majority of GLUT4 appeared to be lost from fractions which included GSVs. Stx 16 depletion also resulted in a reduction in stx 6 levels and reduced recruitment of mVps45 to the membrane. Also, assays were developed to investigate GLUT4 trafficking kinetics using 3T3-L1 adipocytes expressing HA-GLUT4-GFP.

Stx 16 is phosphorylated under basal conditions and insulin stimulation decreases this phosphorylation. It is thought that this dephosphorylation regulates an important membrane trafficking event in GLUT4 sorting. Potential phosphorylation sites have been previously identified. Screening of phosphorylation site mutants in yeast suggested that stx 16 may be phosphorylated at Ser 95. Unfortunately it was not possible to confirm this in 3T3-L1 adipocytes.

In summary the data in this thesis suggests that stx 16 has a role in sorting GLUT4 to its storage site(s). The precise role of stx 16 will need to be further examined to determine the how stx 16 depletion affects GLUT4 trafficking

kinetics. The work presented in this thesis also suggests that stx 16 may be phosphorylated at Ser 95. This will need to be confirmed in 3T3-L1 adipocytes and the effect of stx 16 phosphorylation on GLUT4 trafficking examined.

Table of Contents

List of Figures

Chapter 1

Chapter 3

Chapter 4

Acknowledgements

There are many people I would like to thank for their help during this project. First of all I would like to thank my supervisor, Prof. Gwyn Gould for all his support and advice. I would also like to thank everyone in lab 241 past and present for their assistance in the lab. Thanks in particular to Dr. Scott Shanks for all his help with the yeast experiments.

Within the university I would like to thank Prof. William Cushley and Dr. Alastair Gracie for all their technical help with the flow cytometry experiments. I would also like to thank my PhD review panel, Prof. William Cushley, Prof. Joel Milner and Dr. Matthew Dalby for their advice. Outside the university, I would like to thank Douglas Lamont at the Fingerprint Proteomics Unit at the University of Dundee for his advice and technical expertise.

I would also like to thank other members of the Wellcome Trust PhD programme for interesting discussions during Forum and Awaydays. In particular I would like to thank Cecilia Lindestam Arlehamn, Rosie Williams and Sarah Jones for our coffee breaks and for lending an ear when things weren't going well. Finally I would like to thank my family for all their support even if they didn't really understand what I did everyday in the lab. Special thanks go to my husband Martin for all his love and support. I really couldn't have done this without him!

Dedication

To my wonderful husband Martin.

Declaration

I hereby declare that the thesis which follows is my own composition, that it is a record of the work done myself, except where otherwise acknowledged, and that it has not been presented in any previous application for a Higher Degree.

Nicola Samantha Hamilton

July 2011

Abbreviations

AP	Adaptor protein
APC	Allophycocyanin
APS	Adaptor protein containing a PH and SH2 domain
AS160	Akt substrate of 160 kDa
ATP	Adenosine-5'-triphosphate
BSA	Bovine serum albumin
CaMKII	Calcium/calmodulin-dependent protein kinase II
CAP	c-Cbl-associated protein
Cat. No.	Catalogue number
cDNA	Complementary DNA
cfu	Colony forming unit
CHAPS	3-[(3-Cholamidopropyl)dimethylammonio]-1 propanesulfonate
CKI	Casein kinase I
CKII	Casein kinase II
CPY	Carboxypeptidase Y
DAP kinase	Death-associated protein kinase
DMEM	Dulbecco's modified eagle medium
DMSO	Dimethyl sulphoxide
DNA	Deoxyribonucleic acid
dNTP	Deoxynucleotide triphosphate
DTT	Dithiothreitol

ECL	Enhanced chemiluminesence
E. coli	*Escherichia coli*
EDTA	Ethylenediaminetetraacetic acid
EPR	Electron paramagnetic resonance
ER	Endoplasmic reticulum
Ex/Em	Excitation/Emission wavelengths
FBS	Foetal bovine serum
g	Gravitational force
Gal	Galactose
GAP	GTPase-activating protein
GEF	Guanine-nucleotide exchange factor
GFP	Green fluorescent protein
GGA	Golgi-localised γ-ear-containing Arf-binding protein
GLUT4	Glucose transporter 4
Gly	Glycine
GSV	GLUT4 storage vesicle
GTP	Guanosine-5'-triphosphate
HA	Haemagglutinin
HDM	High density microsome
HEPES	4-(2-hydroxyethyl)-1-piperazineethanesulphonic acid
HRP	Horseradish peroxidase
Ig	Immunoglobulin
IMAC	Immobilised metal ion affinity chromatography

IP	Immunoprecipitation
IR	Insulin receptor
IRAP	Insulin-responsive aminopeptidase
IRC	Insulin-responsive compartment
IRS	Insulin receptor substrate
IRV	Insulin-responsive vesicle
kb	Kilobase
kDa	Kilodalton
LDM	Low density microsome
Leu	Leucine
Met	Methionine
MFI	Mean fluorescence intensity
M/N	Mitochondria and nuclei
MOI	Multiplicity of infection (cfu per cell)
NBD-PE	N-(7-nitro-2, 1, 3-benzoxadiazole-4-yl)-phosphatidylethanolamine
NCS	Newborn calf serum
NEAA	Non-essential amino acids
NSF	N-ethylmaleimide-sensitive factor
OD_{600}	Optical density at 600 nm
PBS	Phosphate-buffered saline
PCR	Polymerase chain reaction
PDK1	Phosphoinositide-dependent kinase 1

PFU	Plaque forming unit
Pfu	*Pyrococcus furiosus*
PH	Pleckstrin homology
PI3K	Phosphatidylinositol 3-kinase
PIKfyve	Phosphoinositide kinase, FYVE finger containing
PI(3)P	Phosphatidylinositol 3-phosphate
PI(3,5)P2	Phosphatidylinositol 3, 5-bisphosphate
PI(3,4,5)P3	Phosphatidylinositol 3, 4, 5-triphosphate
PKA	Protein kinase A
PKB	Protein kinase B
PKC	Protein kinase C
PM	Plasma membrane
Q-SNARE	Glutamine-containing SNARE
Raf	Raffinose
RNA	Ribonucleic acid
RNAi	RNA interference
RPE	R-Phycoerythrin
R-SNARE	Arginine-containing SNARE
Sap	Saponin
SCIMAC	SCX-IMAC
SCX	Strong cation exchange
SDS	Sodium dodecyl sulphate
SDS-PAGE	SDS-polyacrylamide gel electrophoresis

shRNA	Short hairpin RNA
siRNA	Short interfering RNA
SM	Sec1/Munc18
SNAP	Soluble NSF attachment protein
SNAP 23	Synaptosomal-associated protein, 23 kDa
SNARE	Soluble NSF attachment protein receptor
snc	Yeast cells lacking Snc1p and Snc2p
SOC	Super optimal broth with catabolite repression
Stx	Syntaxin
Supt.	Supernatant
TBC1D1	Tre-2/USP6,BUB2,cdc16 domain 1 family member 1
TfR	Transferrin receptor
TGN	*Trans*-Golgi network
TIRFM	Total internal reflection fluorescence microscopy
$\Delta tlg2$	Yeast cells lacking Tlg2p
T_m	Melting temperature
TORC2	Target of rapamycin complex 2
t-SNARE	Target-SNARE
TUG	Tether containing a UBX domain for GLUT4
Ura	Uracil
VAMP	Vesicle-associated membrane protein
v-SNARE	Vesicle-SNARE
v/v	Volume/volume ratio

w/v	Weight/volume ratio

Chapter 1 Introduction

1.1 Insulin resistance and diabetes

Diabetes mellitus is a global epidemic affecting approximately 150 million people worldwide, a figure which will double by the year 2025 (Zimmet *et al.*, 2001). The majority (90%) of these cases are of the type II form. Type II diabetes is a chronic disease characterised by defective insulin action, a condition known as insulin resistance, and/or abnormally high insulin secretion. Insulin resistance places a greater demand on the pancreas to produce insulin leading to hyperinsulinaemia. Insulin resistance also leads to dysfunctional glucose uptake into muscle and adipose tissue as well as increased release of glucose by the liver. Both of these processes result in hyperglycaemia. Type II diabetes is strongly associated with obesity and as the levels of obesity rise, the incidence of this condition, particularly in the younger population is increasing rapidly. Insulin resistance and type II diabetes are associated with many health complications. These include blindness, nerve damage, kidney failure and cardiovascular disease. Type II diabetes is one of the primary causes of cardiovascular disease. Overall type II diabetes can lead to increased risk of premature death. Although diabetes is a treatable condition, there is as yet no cure so it is important that the molecular mechanisms underlying this disease are more fully understood.

1.2 GLUT4

GLUT4 (glucose transporter 4) is a facilitative glucose transporter. It transports glucose down its concentration gradient into the cell in an energy-independent manner. It is a membrane protein with 12 transmembrane domains. There are 13 known members of the GLUT family of proteins (GLUT1-13) which can be divided into 3 classes. Class I includes GLUTs 1-4, class II includes GLUTs 5, 7, 9 and 11 and class III includes GLUTs 8, 10, 12 and the proton-myoinositol symporter H^+ -*myo*-inositol cotransporter (HMIT1) (Joost and Thorens, 2001). GLUT4 is expressed primarily in striated muscle and adipose tissue and is the major insulin-responsive GLUT isoform.

GLUT4 has been shown to be important for glucose homeostasis. Disruption of GLUT4 expression in all tissues of mice leads to insulin resistance (Stenbit *et al.*, 1997). Also, genetic ablation of the GLUT4 gene specifically in muscle tissue results in insulin resistance and glucose intolerance in mice as young as eight weeks old (Zisman *et al.*, 2000). Disruption of GLUT4 specifically in adipose tissue results in impaired glucose uptake and hyperinsulinaemia (Abel *et al.*, 2001). In addition, the adipose tissue shows insulin resistance and impaired glucose tolerance. Interestingly, liver and muscle tissue also develop insulin resistance, despite the fact that GLUT4 is only ablated in adipose tissue. Also insulin-stimulated glucose transport was markedly reduced in muscle tissue, even though the levels of GLUT4 expression in this tissue were normal (Abel *et al.*, 2001). These data suggest that perturbation of GLUT4 expression levels in specific tissues may be a contributing factor in insulin resistance and type II diabetes. In fact it has been shown that GLUT4 expression is reduced in adipocytes from obese subjects and those with impaired glucose tolerance and type II diabetes (Garvey *et al.*, 1991). It has also been shown that overexpression of GLUT4 ameliorates diabetes in the *db*/*db* mouse model (Brozinick, Jr. *et al.*, 2001).

1.3 Insulin

1.3.1 Role in glucose homeostasis

Insulin is an important hormone involved in metabolism. It has a role in cell growth, differentiation, and the storage of substrates in fat, muscle and the liver. One of its most important roles is in whole-body glucose homeostasis (Saltiel and Kahn, 2001). At high plasma glucose concentrations, for example after eating a meal, insulin stimulates the uptake of glucose by adipose and muscle tissue and inhibits glucose production by the liver. Insulin stimulates glucose uptake in adipocytes by stimulating the translocation of GLUT4 molecules from unique intracellular storage site(s) to the cell surface which results in an increase in glucose uptake into the cell. This returns glucose concentrations to their normal levels. In insulin resistance and type II diabetes this normal response to insulin is impaired.

1.3.2 Signalling regulating GLUT4 translocation

In the 1980s it was first demonstrated that insulin stimulates the translocation of glucose transport activity (Suzuki and Kono, 1980;Cushman and Wardzala, 1980). Insulin binds to a surface receptor on muscle and adipose cells and triggers a cascade of signalling events. Two independent signalling pathways have been shown to be involved in insulin-regulated GLUT4 translocation (Kanzaki, 2006;Leney and Tavare, 2009), a phosphatidylinositol 3-kinase (PI3K)-dependent pathway (Okada *et al.*, 1994) and a c-Cbl-dependent pathway (Baumann *et al.*, 2000) (Fig. 1.1). In both these pathways insulin binds to its heterotetrameric receptor composed of two α and two β subunits. This results in a conformational change in the receptor, which leads to activation of its tyrosine kinase domains in the intracellular portion of the β subunits. The receptor is then able to phosphorylate several potential substrates.

In the PI3K- dependent pathway (Okada *et al.*, 1994), the insulin receptor phosphorylates insulin receptor substrate (IRS)1 (White, 1998). IRS1 recruits PI3K to the plasma membrane where it catalyses the production of phosphatidylinositol 3, 4, 5-phosphate (PI(3,4,5)P3). PI(3,4,5)P3 recruits kinases including protein kinase B (PKB)/Akt via their pleckstrin homology (PH) domain (Stokoe *et al.*, 1997). This brings PKB/Akt in close proximity to the kinase phosphoinositide-dependent kinase-1 (PDK1) which phosphorylates PKB/Akt on Thr 308 and activates it (Alessi *et al.*, 1997). PKB is also activated by phosphorylation on Ser 473 by TORC2 (target of rapamycin complex 2) (Hresko and Mueckler, 2005;Sarbassov *et al.*, 2005). PDK1 also phosphorylates the atypical protein kinase C (PKC)s, PKCλ on Thr 402 and PKCζ on Thr 410 (Chou *et al.*, 1998;Le Good *et al.*, 1998).

PKB/Akt phosphorylates several substrates in the cell. One downstream target of PKB/Akt which is thought to be important in GLUT4 translocation is Akt substrate of 160 kDa (AS160) (Sakamoto and Holman, 2008). AS160 is a protein with Rab-GAP (GTPase-activating protein) activity (Kane *et al.*, 2002). It is thought that PKB/Akt phosphorylation of AS160 inhibits its Rab-GAP activity towards Rabs associated with GLUT4 storage vesicles (GSVs) which leads to translocation of GLUT4 (Sano *et al.*, 2003b;Zeigerer *et al.*, 2004). Further work has shown that AS160 is important for intracellular retention of GLUT4 under basal conditions

(Eguez *et al.*, 2005;Larance *et al.*, 2005). The membrane association of AS160 seems to be important in this process (Stockli *et al.*, 2008). PKB/Akt also phosphorylates TBC1D1 (tre-2/USP6,BUB2,cdc16 domain 1 family member 1) (Taylor *et al.*, 2008) and Ser 318 of PIKfyve (phosphoinositide kinase, FYVE finger containing) (Berwick *et al.*, 2004). TBC1D1 is a protein related to AS160 and is mostly expressed in fast twitch muscle fibres. TBC1D1 is likely to play an important role in the stimulation of muscle glucose uptake in response to insulin, contraction and AMPK activation (Taylor *et al.*, 2008). Phosphorylation of PIKfyve by PKB/Akt, activates the kinase which phosphorylates phosphatidylinositol 3-phosphate (PI(3)P) to yield phosphatidylinositol 3, 5-bisphosphate (PI(3,5)P2) on intracellular membranes. This may be important for intracellular trafficking of GLUT4 (Berwick *et al.*, 2004).

In the c-Cbl-dependent pathway (Baumann *et al.*, 2000), the insulin receptor phosphorylates APS (adapter protein containing a PH and SH2 domain) which binds to the receptor. Phosphorylated APS then recruits c-Cbl to the insulin receptor (Liu *et al.*, 2002;Ahn *et al.*, 2004). c-Cbl in a c-Cbl/CAP complex is phosphorylated by the insulin receptor (Ribon and Saltiel, 1997). This stimulates the movement of the c-Cbl-CAP complex into lipid rafts (Ribon *et al.*, 1998). The tyrosine-phosphorylated c-Cbl recruits a complex of an adaptor protein, CrkII and C3G, a guanine-nucleotide exchange factor (GEF). C3G then activates TC10 (Chiang *et al.*, 2001), which is a Rho family GTPase (Murphy *et al.*, 1999). TC10 is an actin regulator, (Kanzaki *et al.*, 2002) which may be important for GLUT4 translocation (Kanzaki and Pessin, 2001;Chang *et al.*, 2007). However, the precise mechanism by which TC10 stimulates GLUT4 translocation is yet to be described.

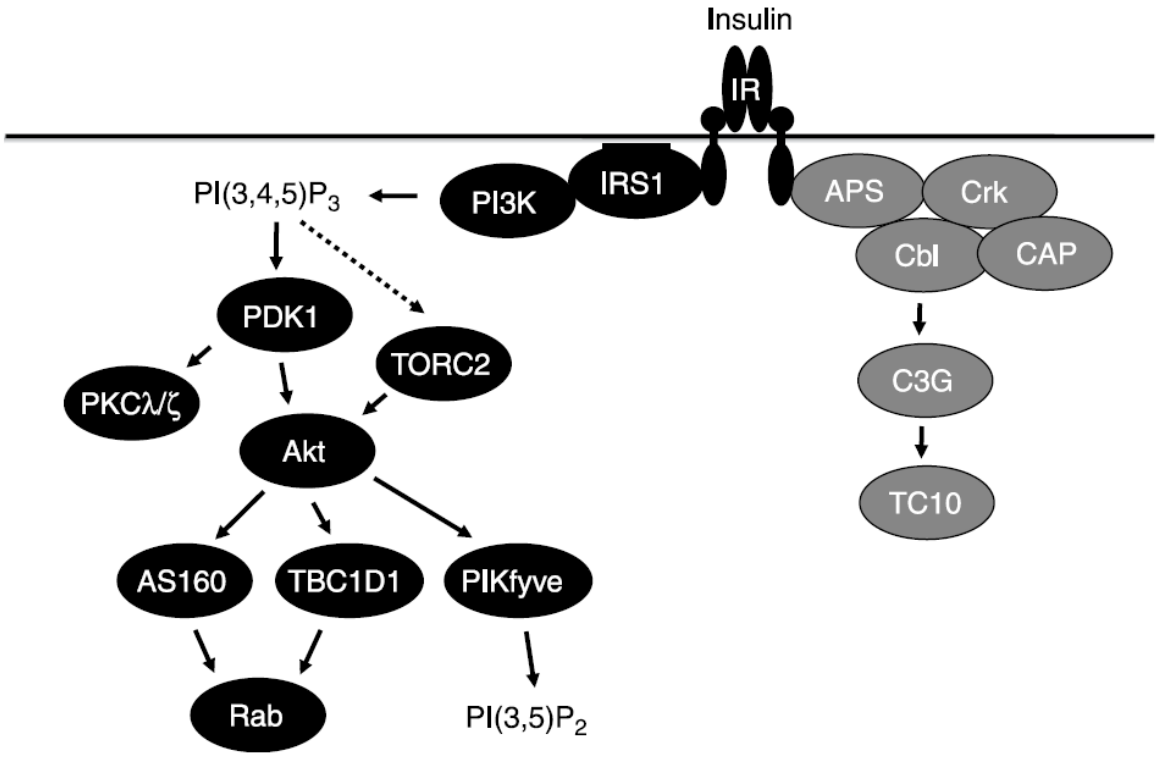

Figure 1.1. Insulin signalling pathways regulating GLUT4 translocation (Leney and Tavare, 2009).

Insulin binding to the insulin receptor (IR) activates both PI3K-dependent (shown in black) and c-Cbl-dependent (shown in grey) signalling pathways leading to translocation of GLUT4 vesicles to the plasma membrane.

In the PI3K-dependent pathway, the insulin receptor phosphorylates IRS1. Phosphorylated IRS1 recruits PI3K to the plasma membrane which catalyses the production of PI(3,4,5)P3. The increase in PI(3,4,5)P3 results in recruitment of PH domain-containing proteins, PDK1 and PKB/Akt. Once recruited to the plasma membrane, PKB/Akt is activated by phosphorylation by PDK1 and TORC2. PDK1 also phosphorylates the atypical PKCs, PKCλ and PKCζ. PKB/Akt phosphorylates several substrates including AS160, TBC1D1 and PIKfyve. PKB/Akt phosphorylation of AS160 inhibits its RabGAP activity against a number of Rab proteins thought to be associated with GLUT4 storage vesicles. In adipocytes AS160 acts on Rab 10 whereas in muscle cells it acts on Rabs 8A and 14. TBC1D1 is a protein related to AS160 and is mostly expressed in fast twitch muscle fibres. PKB/Akt also phosphorylates and activates PIKfyve which phosphorylates

PI(3)P to yield PI(3,5)P2 on intracellular membranes which may be important for intracellular trafficking of GLUT4.

In the c-Cbl-dependent pathway, the adaptor protein APS binds to and is phosphorylated by the IR. Phosphorylated APS recruits c-Cbl to the IR. C-Cbl in a c-Cbl/CAP complex is phosphorylated by the IR. Then the c-Cbl/CAP heterodimer dissociates from the IR and is recruited into lipid raft domains. Lipid raft-associated, phosphorylated c-Cbl recruits a signalling complex containing CrKII adaptor protein and C3G GEF. C3G activates TC10 which is a Rho-family GTPase. TC10 is an actin regulator which may be important for GLUT4 translocation.

See main text for further details.

The PI3K-dependent pathway and the c-Cbl-dependent pathway of insulin signalling have both been clearly defined and their role in GLUT4 translocation demonstrated. The two pathways have been shown to be independent. Disruption of CAP by expression of the N-terminal domain did not affect PI3K-dependent signalling (Baumann *et al.*, 2000). Also disruption of lipid raft domains in adipocytes inhibited TC10 activation without affecting PI3K signalling (Watson *et al.*, 2001). The roles of the individual proteins in each pathway have been determined using several methods including: using the PI3K inhibitor wortmannin (Okada *et al.*, 1994); truncation mutants (Baumann *et al.*, 2000;Ahn *et al.*, 2004); phosphosite mutants (Kane *et al.*, 2002;Sano *et al.*, 2003a;Berwick *et al.*, 2004); kinase assays (Alessi *et al.*, 1997;Chou *et al.*, 1998;Le Good *et al.*, 1998;Hresko and Mueckler, 2005); and RNA intereference (RNAi) (Eguez *et al.*, 2005;Larance *et al.*, 2005;Hresko and Mueckler, 2005;Sano *et al.*, 2007;Larance *et al.*, 2008).

However the exact nature and function of the downstream effectors which mediate GLUT4 translocation need to be further investigated. In particular the target Rabs of AS160 need to be clearly defined. *In vitro* the GAP domain of AS160 acts on Rabs 2A, 8A, 10 and 14 (Miinea *et al.*, 2005). Rabs 8A and 14 seem to be the targets of AS160 in muscle cells (Ishikura *et al.*, 2007). However, in adipocytes AS160 acts on Rab10 (Sano *et al.*, 2007;Sano *et al.*, 2008). This may indicate that there are cell-specific differences in the insulin signalling pathways regulating GLUT4 translocation.

Also the sites of insulin action on GLUT4 translocation need to be better understood. The main effect of insulin is on the exocytosis of GLUT4 (Satoh *et al.*, 1993). However exocytosis involves several steps each of which could be regulated by insulin (Holman and Sandoval, 2001;Zaid *et al.*, 2008). Insulin could regulate budding of vesicles from the GLUT4 storage compartment or the trafficking of these vesicles to the plasma membrane (Thurmond and Pessin, 2000;Xu and Kandror, 2002).

More recent data seems to suggest that insulin's main effect is on the docking (Lizunov *et al.*, 2005) and/or fusion of GLUT4 vesicles with the plasma membrane (Koumanov *et al.*, 2005;Bai *et al.*, 2007;Huang *et al.*, 2007;Jiang *et al.*, 2008). Lizunov *et al.* used time-lapse total internal reflection fluorescence

microscopy (TIRFM) to analyse the later stages of HA-GLUT4-GFP in primary rat adipose cells. Their data showed that under basal conditions, GLUT4 vesicles moved rapidly along a microtuble network under the plasma membrane, only stopping occasionally and only briefly and loosely. In contrast under insulin-stimulated conditions, GLUT4 vesicles were much less mobile and were tethered to the plasma membrane in clusters and then slowly fused with the plasma membrane (Lizunov *et al.*, 2005).

Several other studies have used TIRFM to analyse fusion of GLUT4 vesicles (Bai *et al.*, 2007;Huang *et al.*, 2007;Jiang *et al.*, 2008). Bai *et al.* used time-lapse TIRFM to observe the movement of vesicles containing GLUT4-EGFP in 3T3-L1 adipocytes and did a quantitive analysis of the docking, priming and fusion of the vesicles with the plasma membrane and the transition kinetics between these steps. The authors showed that preparation of GSVs for fusion competence after docking is a key step regulated by insulin. They also showed that docking of GSVs is PI3K- and AS160-dependent. This suggests that alternative Akt substrates or alternative signalling pathways downstream of docking are a key site of insulin regulation (Bai *et al.*, 2007). In another study, Huang *et al.* used TIRFM to track vesicles containg GLUT4-EGFP in 3T3-L1 adipocytes and developed a computer program to analyse docking/fusion kinetics. They showed that insulin increased the frequency of fusion of GLUT4 vesicles by approximately four –fold. Also insulin decreases the duration of docking prior to fusion. This suggests that insulin signalling accelerates the transition from docking to fusion with the plasma membrane (Huang *et al.*, 2007). Finally, Jiang *et al.* developed a novel dual-coloured probe to monitor the translocation of 3T3-L1 adipocytes. The probe was made up of the PH-sensitive fluorescence protein PHluorin attached to the luminal terminus of IRAP and the red fluorescence protein TDimer2 to the cytosolic end of IRAP. PHluorin will be located in the lumen of the GSVs, which is acidic prior to fusion and will be exposed to the extracellular medium, which is neutral upon fusion. This will cause a brightening of PHluorin fluorescence. This allowed easy identification of fusion of single GSVs and also allowed tracking of the GSVs prior to fusion. The authors used TIRFM to visualise single Tdimer2-IRAP-PHluorin vesicles.The study showed that insulin stimulation increased fusion of GSVs with the plasma membrane by approximately 40-fold (Jiang *et al.*, 2008).

In addition an *in vitro* fusion assay involving mixing GLUT4 vesicles containing DyLight647 streptavidin-tagged GLUT4 with plama membrane liposome containing EU(TMT) showed that the rate of GLUT4 vesicle fusion is stimulated 8-fold by insulin. Fusion was determined by analysing the FRET signal. Fusion was shown to be Akt-dependent and required the recruitment of Akt to the plasma membrane (Koumanov *et al.*, 2005).

Other data suggests that translocation of GLUT4 to the plasma membrane is not sufficient for glucose transport into the cell. The authors suggest that insulin stimulates the activation of the GLUT4 molecules once they are inserted into the plasma membrane (Funaki *et al.*, 2004).

1.4 Intracellular protein trafficking

Cells are highly organised and contain several different areas and compartments. An important aspect of this compartmentalisation is the localisation of proteins to specific compartments which ensures that the identity and function of the compartment is maintained. The sorting and transport of proteins to the correct compartment involves membrane trafficking (Rothman and Wieland, 1996). Membrane trafficking and the transport of proteins involves several steps. First of all, the cargo proteins to be transported are concentrated in a donor compartment or membrane. Transport vesicles, enriched in the cargo molecules are then formed from the donor membrane. These vesicles are then translocated to the target compartment or membrane. The vesicles then dock and fuse with the target membrane.

Two of the most studied examples of intracellular protein trafficking are the secretory pathway and the endocytic pathway.

1.4.1 Secretory pathway

In the secretory pathway (van Vliet *et al.*, 2003) newly synthesised membrane proteins and soluble proteins are first translocated into the endoplasmic reticulum (ER). The proteins are then packaged into vesicles and transported to the Golgi. Once at the Golgi, the proteins move through the Golgi cisternae to the *trans*-Golgi network (TGN). At the TGN, proteins are sorted according to

their final destinations. Proteins in the secretory pathway can be sorted to a number of different destinations. Soluble proteins can be secreted from the cell or membrane proteins inserted into the plasma membrane by a process known as exocytosis, in which an intracellular trafficking vesicle fuses with the plasma membrane (Jahn, 2004). Alternatively proteins can be sorted to lysosomes or retained in an organelle in the secretory pathway.

1.4.2 Endocytic pathway

The endocytic pathway is the process by which membrane proteins, receptor-associated ligands and solute molecules are delivered to various intracellular compartments (Maxfield and McGraw, 2004). First of all the proteins are packaged into an endocytic vesicle at the plasma membrane. The vesicle is then transported to an early endosome or sorting endosome compartment. From the sorting endosome proteins can be delivered to late endsomes and then the lysosome for degradation. Proteins can also be recycled back to the plasma membrane. Alternatively proteins can be transported from the sorting endosome to another part of the early endosome called the endocytic recycling compartment (ERC). Proteins in the ERC can either be recycled back to the plasma membrane or sorted to the TGN.

1.4.3 Sorting signals in the secretory and endocytic pathways

There are several signals which regulate the trafficking of proteins between compartments. A given protein can have multiple sorting signals, each specifying the fate of that protein at successive stages, i.e. whether the protein enters or avoids a transport vesicle. This determines the itinerary of the protein in the cell. A protein without sorting signals is transported by bulk flow of the membrane around the cell. Sorting motifs within the protein sequence can often bind to adaptor proteins which in turn bind to coat proteins, providing a link between cargo concentration and vesicle formation. Adaptor proteins such as APs (adaptor proteins) and GGAs (Golgi-localised γ-ear-containing Arf-binding proteins) have important roles in the sorting of membrane proteins (Robinson, 2004).

Examples of the sorting signals include; the KDEL or HDEL motif which is important for the retrieval of soluble ER-resident proteins from the Golgi. Soluble ER proteins contain the C-terminal KDEL or HDEL sequence. This sequence is recognised by the Golgi-localised receptor Erd2. Erd2 binds to the KDEL/HDEL sequence in the slightly acidic environment of the Golgi and releases it on arrival at the ER (Semenza *et al.*, 1990;Lewis and Pelham, 1992). Erd2 itself contains a dilysine retrieval sequence, K(X)KXX which interacts with the COPI coat protein (Cosson and Letourneur, 1994).

Also, tyrosine-based signals are require for the retrieval of Golgi-localised proteins from the plasma membrane. For example, TGN38 has a SDYQRL motif which interacts with the μ2 subunit of AP2 (Stephens *et al.*, 1997).In addition, CI-MPR trafficking is determined by an acidic-cluster dileucine motif which binds to GGA proteins and by an aromatic-residue motif (Chen *et al.*, 1993;Schweizer *et al.*, 1997).

There are other examples of sorting signals regulating the trafficking steps in the secretory and endocytic pathway, however many are not yet fully understood.

1.5 Intracellular trafficking of GLUT4

The translocation of GLUT4 in response to insulin is an example of regulated membrane trafficking (Bryant *et al.*, 2002). Under basal conditions, in the absence of insulin, GLUT4 is almost completely excluded from the cell surface. Insulin acts to greatly increase the exocytosis of GLUT4-containing vesicles to the plasma membrane, while only slightly decreasing their endocytosis (Suzuki and Kono, 1980;Cushman and Wardzala, 1980). This leads to a 10 to 20-fold increase in GLUT4 molecules at the cell surface. This effect of insulin is specific, as the plasma membrane level of the transferrin receptor (TfR) is only increased approximately two-fold.

1.5.1 Intracellular localisation of GLUT4

GLUT4 is found in many organelles including the plasma membrane, sorting endosome, recycling endosome, TGN (Shewan *et al.*, 2003), in tubulovesicular structures in the perinuclear region of the cell and at distinct loci throughout

the cytosol (Slot *et al.*, 1991). It is thought GLUT4 occupies a complex tubulovesicular network that is connected to the endosomal –TGN system. GLUT4 is also thought to reside in a specialised insulin-responsive compartment (IRC), insulin-responsive vesicles (IRVs) or GLUT4 storage vesicles (GSVs).

1.5.2 GSVs

The IRC or GSVs have been difficult to define and distinguish from the general endosomal system. GSVs are small insulin-responsive vesicles which are highly enriched in GLUT4 molecules. They also contain vesicle-associated membrane protein (VAMP)2 and insulin-responsive aminopeptidase (IRAP) (Martin *et al.*, 1996;Ramm *et al.*, 2000). IRAP traffics in concert with GLUT4 in response to insulin (Garza and Birnbaum, 2000) and enhances GLUT4 exocytosis in response to insulin (Yeh *et al.*, 2007). The GSVs are also lacking in several proteins including TfR, cellubrevin (VAMP3) (Hashiramoto and James, 2000), cellugyrin (synaptogyrin 2) (Kupriyanova *et al.*, 2002) and cation-dependent mannose-6-phosphate receptor (CD-MPR) (Martin *et al.*, 2000). GSVs are segregated from the general recycling endosomal system, as shown by chemical ablation of TfR-containing endosomal compartments (Martin *et al.*, 1996;Livingstone *et al.*, 1996).

The precise mechanism by which the GSVs are formed is not fully known. Sortillin, a major component of GSVs has been shown to be sufficient and essential for GSV formation (Shi and Kandror, 2005). Further work has shown that it is the lumenal Vsp10p domain of sortillin which interacts with GLUT4 and IRAP and plays an important role in GSV formation (Shi and Kandror, 2007). Also GGAs are required for the sorting of GLUT4 (Watson *et al.*, 2004;Li and Kandror, 2005) and IRAP (Hou *et al.*, 2006) into GSVs. It has been proposed that the formation of GSVs is driven by mass action, in which the expression of GLUT4, IRAP and sortillin, whose interaction and abundance fill the compartment, largely excludes other molecules (Pilch, 2008). Recently it has been shown that GSVs self-assemble during differention of 3T3-L1 adipocytes and that lumenal interactions of GLUT4 and IRAP have an important role in the assembly of GSVs (Shi *et al.*, 2008).

The specialised GSV compartment is thought to be an important mechanism of basal intracellular retention of GLUT4 and it is thought that GLUT4 in this compartment translocates to the cell surface in response to insulin.

1.5.3 Targeting sequences in GLUT4

GLUT4 contains several motifs which regulate its localisation and trafficking (Lalioti *et al.*, 2001). The majority of these motifs are found in the N- and C-terminal domains.

The FQQI motif in the N-terminus has been shown to be important for the internalisation of GLUT4 from the cell surface (Garippa *et al.*, 1994;Verhey *et al.*, 1995). Other studies have found it may be involved in other aspects of GLUT4 trafficking. Substitution of Phe (5) for Ser leads to transport of GLUT4 to the late endosome/lysosome, where it is degraded (Palacios *et al.*, 2001). FQQI is also involved in the entry of newly-synthesised GLUT4 into the IRC (Khan *et al.*, 2004) and the AS160-dependent exit of GLUT4 from the IRC (Capilla *et al.*, 2007). Recent work suggests that the FQQI motif may be involved in the basal retention of GLUT4 (Blot and McGraw, 2008).

The LL motif in the C-terminus of GLUT4 has also been shown to be important for the rapid endocytosis and retention of GLUT4 (Corvera *et al.*, 1994). It is thought that the LL motif regulates the transport of internalised GLUT4 out of a fast-recycling pathway into the retention pathway (Blot and McGraw, 2008).

The FQQI and LL motifs belong to the aromatic-based and dileucine-based family of trafficking motifs respectively. These motifs regulate intracellular trafficking of membrane proteins by interacting with adaptor proteins involved in vesicle formation and clathrin recruitment (Bonifacino and Traub, 2003). However the proteins which interact with the GLUT4 motifs have not been identified.

Several other residues and motifs in the C-terminus are thought to be important for GLUT4 trafficking. These residues and motifs tend to be acidic in nature. The last 30 amino acids of the C-terminus are sufficient for the correct localisation of GLUT4 into the IRC (Verhey *et al.*, 1995). A YXXPDEND motif has been shown to be important for the release of GLUT4 from the IRC (Martinez-Arca *et al.*, 2000) and a LXXLXPDEND motif is essential for insulin-stimulated GLUT4

translocation to the plasma membrane (Song *et al.*, 2008). Also a TELEYLGP motif regulates sorting of GLUT4 into a post-endosomal compartment (Shewan *et al.*, 2000;Cope *et al.*, 2000). The TELEY motif is conserved in IRAP (Shewan *et al.*, 2000). The post –endosomal compartment has been shown to be a subdomain of the TGN enriched with syntaxin(stx) 6 and 16 (Shewan *et al.*, 2003). Recently it has been shown that TELEY is required for the full basal retention of GLUT4 and that the trafficking step it is involved in is regulated by AS160 (Blot and McGraw, 2008). Other recent work suggests that the C-terminus of GLUT4 is required for targeting of GLUT4 to a perinuclear IRV donor compartment but is not required for entry into the IRVs (Li *et al.*, 2009).

In addition to the motifs in the N- and C-terminus, other motifs have been discovered which regulate GLUT4 trafficking. The large intracellular loop has been shown to be important for entry of GLUT4 into the IRC (Khan *et al.*, 2004) and also the AS160-dependent exit of GLUT4 from the IRC. This intracellular loop also binds to the protein TUG (Tether containing a UBX domain for GLUT4) which is required to retain GLUT4 intracellularly in 3T3-L1 adipocytes in the absence of insulin (Yu *et al.*, 2007). Also a phosphatidic acid binding motif, SQWL in the first intracellular loop of GLUT4 is involved in the insulin-stimulated fusion of GLUT4 vesicles with the plasma membrane (Heyward *et al.*, 2008).

1.5.4 Models of GLUT4 trafficking

There have been several models of GLUT4 trafficking proposed to explain the basal exclusion of GLUT4 from the plasma membrane and the high insulin responsiveness of GLUT4 translocation (Pessin *et al.*, 1999;Dugani and Klip, 2005). These models include retention mechanisms, dynamic sorting events and packaging GLUT4 into a more stationary population of secretory-type vesicles or a static specialised compartment (Fig. 1.2).

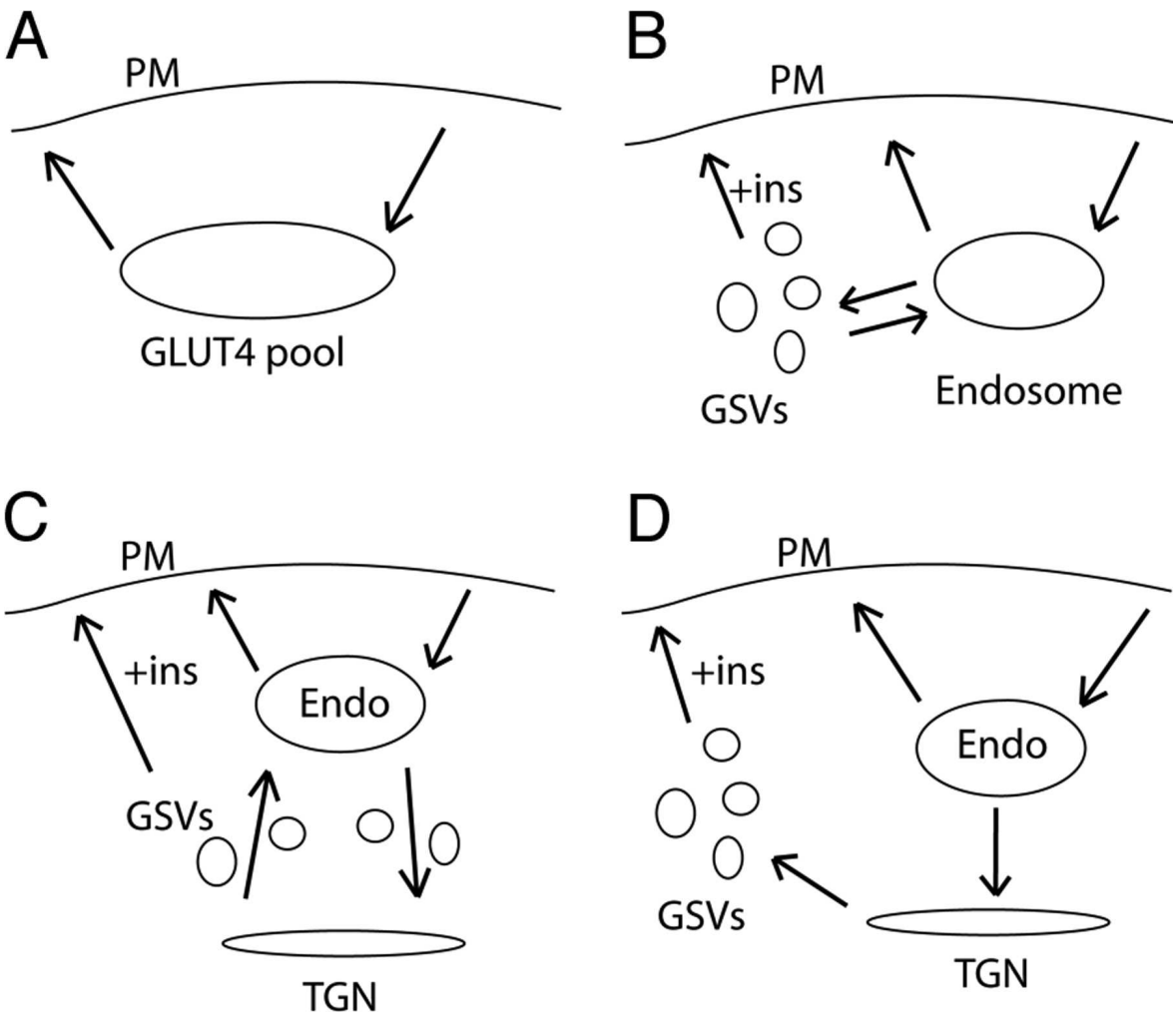

Figure 1.2 Dynamic *vs*. static models of intracellular GLUT4 retention (Larance *et al*., 2008).

A. In GLUT4 recycling experiments the intracellular GLUT4 is thought of as one pool. **B.** A dynamic recycling model in which GLUT4 recycles between endosomes and GSVs in the basal state. **C.** An alternative dynamic recycling model in which GSVs are an intermediate between the TGN and endosomes (Endo). **D.** Static retention model in which GSVs form a stable pool of GLUT4 which is only released to the plasma membrane/endosome cycle in response to insulin (ins).

The retention model predicts that sequences in GLUT4 specifically target GLUT4-containing vesicles away from the recycling endosome (Lalioti *et al.*, 2001). These sequences bind to retention receptors found in insulin-responsive cells, for example, TUG (Bogan *et al.*, 2003;Yu *et al.*, 2007). Insulin stimulation or competition by retention sequence peptides (Lee and Jung, 1997), disrupts the interaction between the GLUT4 sequences and the retention receptors, allowing the GLUT4-containing vesicles to enter the recycling endosomal system resulting in translocation to the plasma membrane.

In the dynamic recycling model, the entire complement of GLUT4 eventually recycles to the plasma membrane in the basal state (Martin *et al.*, 2006). GLUT4-containing vesicles undergo a futile cycle of fission and fusion with endosomes (Karylowski *et al.*, 2004). Insulin acts to switch the fusion of these vesicles to the plasma membrane. Insulin promotes two routes for GLUT4 mobilisation towards the plasma membrane, a direct route from the GLUT4-containing vesicles and an indirect one from the GLUT4-containing vesicles via the endosomal recycling system (Ramm *et al.*, 2000;Zeigerer *et al.*, 2002). A variation of this model is that only a fraction of GLUT4 recycles to the plasma membrane in the basal state. Insulin increases the quantity of GLUT4 available for translocation via the recycling endosomal system (Coster *et al.*, 2004). There also exists a latent pool of GLUT4 molecules which is never mobilised in response to insulin (Govers *et al.*, 2004).

In the secretory vesicle model GLUT4 is localised to both small synaptic-like vesicles as well as larger tubulovesicular compartments. Insulin stimulation results in association and fusion of the vesicles with the plasma membrane (Xu and Kandror, 2002). Evidence in support of this is the fact that ablation of endosomes does not prevent insulin-stimulated GLUT4 translocation (Martin *et al.*, 1998) and that GSVs share characteristics of small synaptic vesicles.

These models are not mutually exclusive. Recent work has shown that GLUT4 is regulated by both static and dynamic retention mechanisms (Muretta *et al.*, 2008). Also the authors suggest that cell culture conditions can affect GLUT4 trafficking, for example replating 3T3-L1 cells after differentiation inhibits static retention of GLUT4. Parts of each model can be incorporated into a model (Fig. 1.3). According to Bryant *et al*. GLUT4 transport is controlled by all three

mechanisms (Bryant *et al.*, 2002). It is proposed that intracellular GLUT4 occupies two interrelated and overlapping endosomal cycles. The first is a fast-trafficking cycle involving the plasma membrane and the early endosome. In the absence of insulin it is this cycle which internalises GLUT4. Once in the endosome, GLUT4 is further sorted into a slow-trafficking cycle involving the endosome, the TGN and GSVs. It is thought that it is the GLUT4 in these GSVs which translocates to the plasma membrane in response to insulin. Recent data also supports a model in which basal GLUT4 retention involves two intracellular trafficking cycles (Blot and McGraw, 2008).

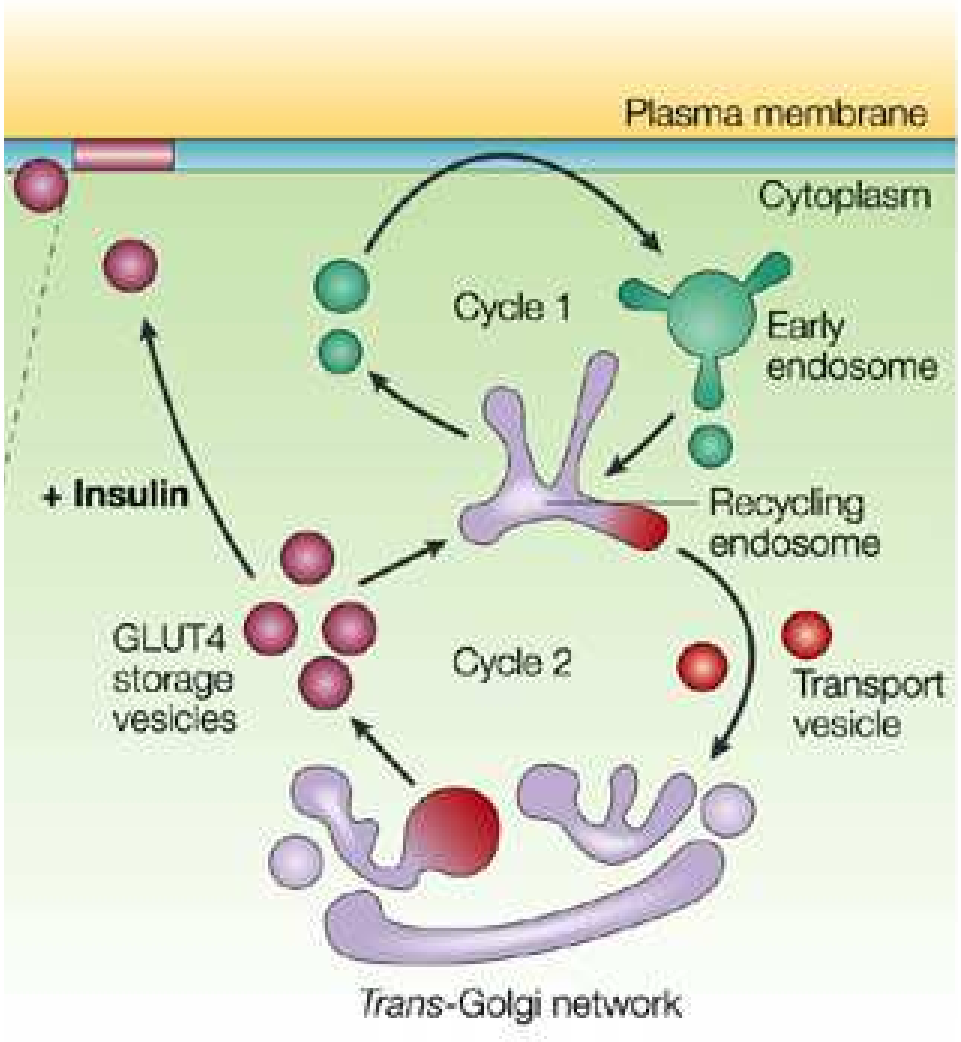

Figure 1.3. GLUT4 trafficking model. Modified from (Bryant *et al.*, 2002). GLUT4 occupies two intracellular overlapping trafficking cycles. Cycle 1 includes the plasma membrane and endosomes. Cycle 2 includes endosomes, TGN and GSVs. GLUT4 in the GSVs translocates to the cell surface in response to insulin.

1.6 SNAREs and membrane fusion

The trafficking of GLUT4 involves the fusion of vesicles with specific membranes which is mediated by target- (t-) and vesicle- (v-) SNAREs (soluble *N*-ethylmaleimide-sensitive factor attachment protein receptors) (Hong, 2005). During membrane trafficking or vesicle-mediated transport, vesicles are formed from a donor compartment or membrane. These transport vesicles are then translocated to the target compartment or membrane. Then the vesicles dock and fuse with the target membrane. SNAREs function in the final docking and fusion stages of this process and catalyse the final fusion step (Chen and Scheller, 2001).

1.6.1 Classification of SNAREs

SNAREs are small membrane proteins of around 100-300 amino acids in length, which function in membrane fusion. There are three main subfamilies of SNAREs; syntaxin (stx), synaptobrevin/ vesicle-associated membrane protein (VAMP) and synaptosomal-associated protein, 25 kDa (SNAP 25)/ light chain subfamily.

Functionally SNAREs can be classified into v-SNAREs that are associated with the vesicle and t-SNAREs that are associated with the target membrane (Hong, 2005). A v-SNARE consists of a single membrane-spanning protein containing one SNARE motif, whereas a t-SNARE consists of two or three proteins. There are two types of t-SNARE complex. A heterodimeric t-SNARE complex contains one member of the stx subfamily, contributing one SNARE motif and a member of the SNAP 25 subfamily which contributes two SNARE motifs. A heterotrimeric t-SNARE complex consists of one member of the stx subfamily, one SNARE related to the N-terminal half of SNAP 25 and one SNARE related to the C-terminal half of SNAP 25, each contributing one SNARE motif.

SNAREs are also classified structurally as R-SNAREs (arginine-containing SNARE) or Q-SNAREs (glutamine-containing SNARE) on the basis of a conserved residue in their SNARE motif (Fasshauer *et al.*, 1998). All members of the VAMP subfamily are R-SNAREs, the stx subfamily are Qa SNAREs, SNAREs related to the N-terminal half of SNAP-25 are Qb SNAREs and SNAREs related to the C-terminal half of SNAP-25 are Qc SNAREs.

1.6.2 Membrane fusion

The mechanism by which SNAREs mediate fusion involves several steps (Fig. 1.4) (Jahn and Scheller, 2006). First of all, during vesicle formation, the v-SNARE is packaged with cargo proteins into the budding vesicle. This ensures that the vesicle is competent to fuse with the target membrane. Meanwhile on the target membrane the heterodimeric or heterotrimeric t-SNARE complex forms. As the vesicle arrives at the target membrane, the vesicle is brought to the correct location in the membrane by tethering factors, such as Rab proteins. The tethering factors facilitate the pairing of the v-SNARE with its cognate t-SNARE complex. The v-SNARE binds to its cognate t-SNARE complex, docking the vesicle to the target membrane. The SNARE motifs of the proteins "zipper up," starting from the membrane-distal N-terminus to the membrane-proximal C-terminus, leading to the formation of the trans-SNARE complex. This involves the organisation of the SNARE motifs into a four helix bundle known as the core complex. This process brings the two opposing membranes closer together. The energy released during the formation of the stable trans-SNARE complex overcomes the energy barrier to membrane fusion which is created by the negative charges of the phospholipid headgroups in the lipid bilayers. The trans-SNARE complex is thought to directly catalyse fusion of the opposing membranes.

During membrane fusion, as the membranes are brought closer together, the outer leaflets of the two membranes start to merge, resulting in hemifusion. This follows with breakdown of the inner leaflets to form a fusion pore. The fusion pore expands leading to full fusion of the two membranes. The trans-SNARE complexes which were formed before membrane fusion are now on the same fused membrane and are known as cis-SNARE complexes. To allow subsequent rounds of vesicle transport, the cis-SNARE complex needs to be disassembled. This is catalysed by the ATPase N-ethylmaleimide-sensitive factor (NSF) and its cofactor α SNAP (soluble NSF attachment protein). The disassembled SNAREs are then sorted back to their correct compartment.

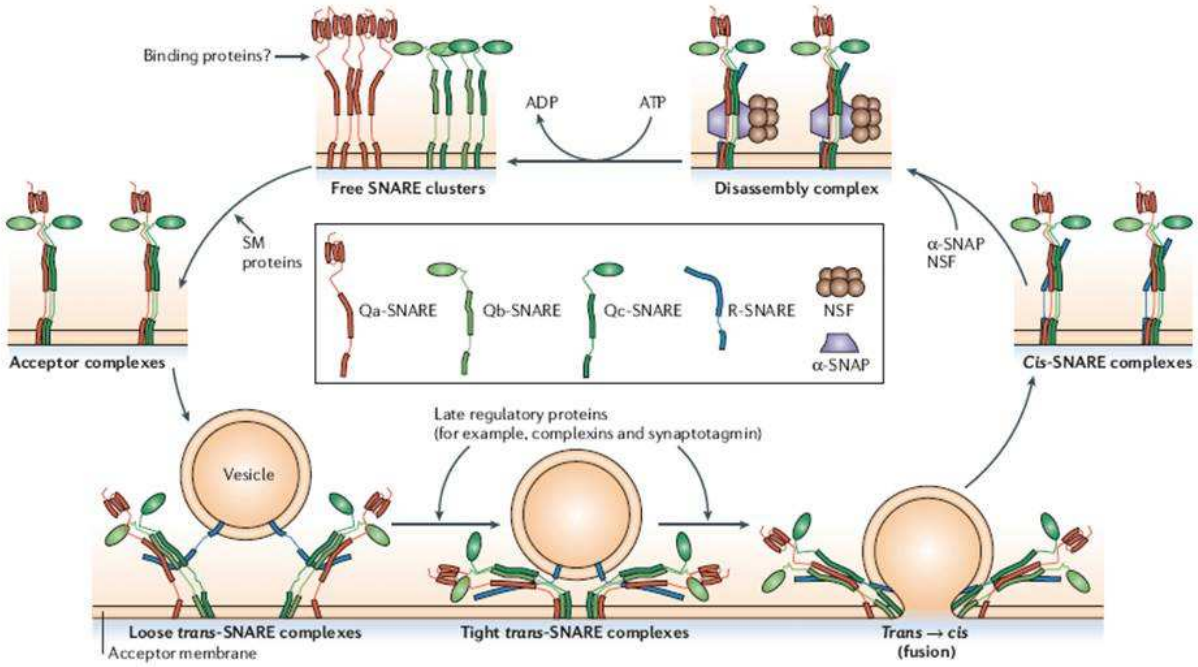

Figure 1.4. Membrane fusion (Jahn and Scheller, 2006).

Figure shows the main steps involved in membrane fusion. See main text for more details.

1.6.3 Structure of SNARE complexes

SNAREs have a highly conserved structure (Brunger, 2005). The majority of SNAREs contain three domains, an N-terminal domain, a SNARE domain and a transmembrane domain (Fig. 1.5). The main feature of these proteins is the SNARE domain of around 60 residues, which is found in all SNAREs. The SNARE domain consists of heptad repeats which form coiled-coil structures. Most SNAREs contain an extended N-terminal domain with coiled-coil regions. The structure of the N-terminal domain varies and this domain is involved in a variety of functions. The N-terminal domain of the stx subfamily has a three helical bundle consisting of Ha, Hb and Hc regions. These regions can bind to the C-terminal SNARE domain generating a closed conformation, which needs to be opened before assembly into a t-SNARE complex. The N-terminal domain of the stx subfamily can also be involved in interactions with regulators of SNARE assembly. For example the N-terminus of stx 16 binds to the Sec1/Munc18 (SM) protein mVps45 (Dulubova *et al.*, 2002). Finally the N-terminal domain can direct intracellular targeting of the SNARE, for example the N-terminal region of VAMP4 targets the SNARE to the TGN by a di-leucine motif and an acidic cluster (Zeng *et al.*, 2003).

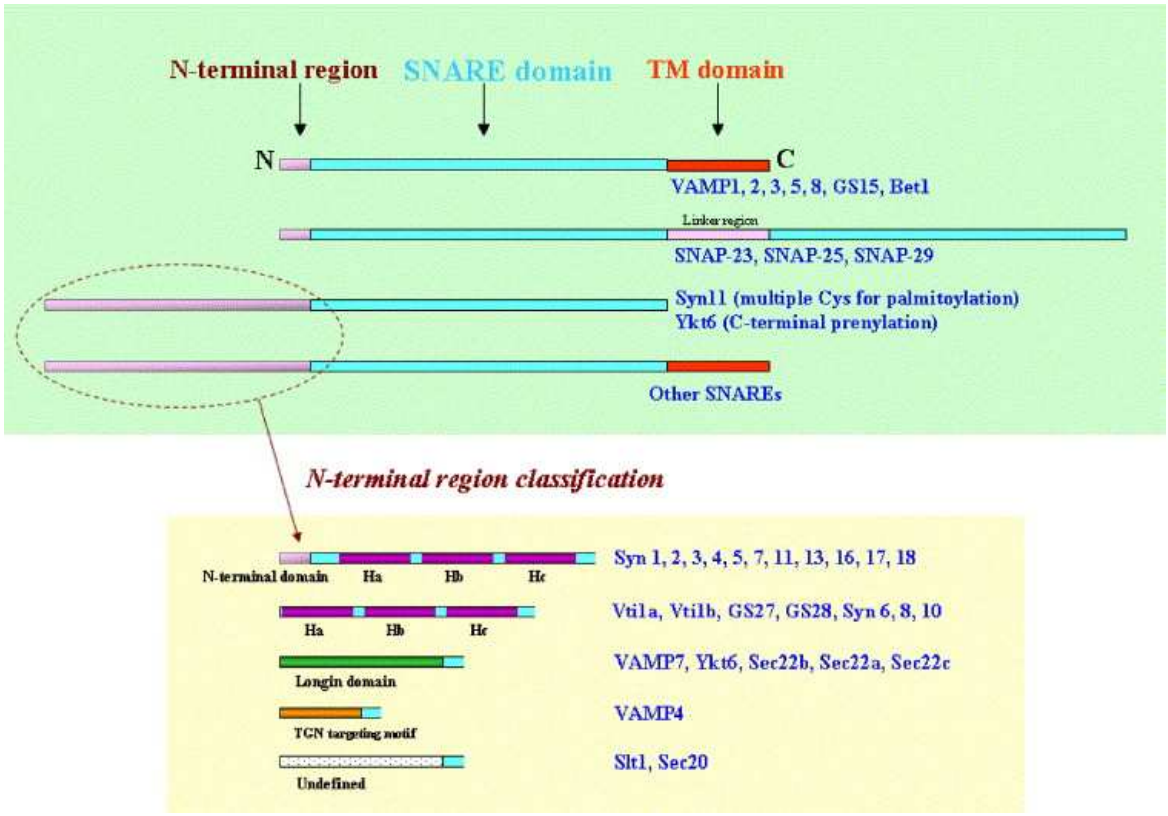

Figure 1.5. General structure of SNAREs (Hong, 2005).

General structure of different SNAREs. Upper panel shows the main domains in SNAREs. Lower panel shows the different N-terminal regions of SNAREs.

During membrane fusion a trans-SNARE complex is formed. The trans-SNARE complex is composed of a tightly packed parallel four-helix bundle, with each member of the SNARE subfamilies contributing one or two helices (Fasshauer, 2003) (Fig.1.6). In the interior of the SNARE bundle the four helices are connected by 16 layers (-7 to +8) of interacting amino acid side chains. These residues are mostly hydrophobic in nature and are highly conserved in SNAREs (Antonin *et al.*, 2002). In the middle of the bundle (0 layer) there is an unusual hydrophilic layer consisting of 3 Glutamine (Gln, Q) and 1 Arginine (Arg, R) residues (Fasshauer *et al.*, 1998). This is known as the 3Q:1R or QaQbQcR configuration. Mutations have shown that the 3Q:1R configuration is important for SNARE function in membrane fusion. However compensatory mutations in the 0 layer can restore membrane fusion (Fratti *et al.*, 2007).

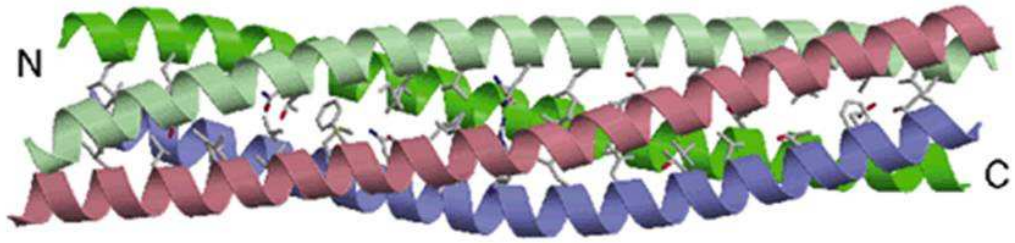

Figure 1.6. Structure of an endosomal SNARE complex. Modified from (Antonin *et al*., 2002).

Schematic view of an endosomal SNARE complex. Endobrevin is shown in blue, stx 7 in red, Vti1b in light green and stx 8 in dark green. N and C denote the N- and C-termini of the SNARE complex. Amino acid side chains are shown as sticks.

1.6.4 Role of SNARE function in membrane fusion

Several studies suggest that SNAREs have a role in membrane fusion. Clostridial neurotoxins inhibit neurotransmitter release in neurons. Schiavo *et al*. showed that clostridial neurotoxins such as tetanus toxin and botulinum toxin are zinc endopeptidases which act specifically on the SNARE synaptobrevin 2 (Schiavo *et al.*, 1992). They also showed that blocking of neurotransmitter release in Aplysia neurons by injection with tetanus or botulinum B toxin is delayed by the presence of synaptobrevin 2 peptides, containing the neurotoxin cleavage site. This suggests that tetanus and botulinum B neurotoxins block neurotransmitter release by cleaving synaptobrevin 2 and that synaptobrevin 2 plays an important role in neurotransmitter release. Another study examined catecholamine secretion from bovine adrenal chromaffin cells (Xu *et al.*, 1998). Using flash photolysis of caged intracellular calcium to induce exocytosis and capacitance measurements and amperometry the authors observed distinct kinetic components of vesicle fusion. These components were exocytic burst (which represents the fusion of release-competent vesicles) and a later slow component (which represents recruitment of vesicles to the ready-release pool). Botulinum A cleaves nine amino acids from the C-terminal of SNAP 25. This results in a reduction in the fast component of exocytic burst, which suggests that SNAP 25 is involved in final stage of exocytosis (i.e. the fusion of docked vesicles with the membrane) (Xu *et al.*, 1998). In a further study by Xu et al. it was shown that the inital fast component of exocytic burst was inhibited by a blocking antibody (specific to SNAP 25A) which prevented the assembly of the ternary SNARE complex containing syntaxin 1A, synaptobrevin 2 and SNAP 25A (Xu *et al.*, 1999).

Genetic studies have also shown the importance of SNAREs in membrane fusion. A temperature-sensitive paralytic mutation in syntaxin of *D. Melanogaster* rapidly blocks synaptic transmission at non-permissive temperatures. The mutation (a substitution of Ile for Thr at position 254 in the SNARE domain of syntaxin), specifically and selectively decreases binding of syntaxin to synaptobrevin and abolishes assembly of the SNARE complex between syntaxin, snaptobrevin and SNAP 25. This failure to assemble the SNARE complex results in an increase in docked vesicles and leads to a block in synaptic transmission. This suggests that syntaxin-synaptobrevin interaction and SNARE complex assembly

are required for exocytosis (Littleton *et al.*, 1998). In a VAMP2 knockout mouse, the rate of spontaneous synaptic vesicle fusion was decreased by approximately 10-fold and the rate of calcium-triggered synaptic vesicle fusion was decreased by over 100-fold (Schoch *et al.*, 2001).

An *In vitro* study using a synthetic liposome fusion system has shown that SNAREs are both necessary and sufficient for fusion to occur (Weber *et al.*, 1998). The SNAREs VAMP 2, syntaxin 1A and SNAP 25 were reconstituted into vesicles. Fusion was monitored by measuring lipid mixing. The vesicles containing the v-SNARE VAMP2 also contained a quenched mixture of fluorescent phospholipids NBD-PE (N-(7-nitro-2, 1, 3-benzoxadiazole-4-yl)-phosphatidylethanolamine) and rhodamine-PE. When the fluorescent "donor" vesicles fused with non-fluorescent "acceptor" vesicles (containing the t-SNAREs syntaxin 1A and SNAP 25) the fluorescent lipid was diluted and the quenching decreased, resulting in an increase in NBD fluorescence at 538 nm. Fusion was disrupted by pre-incubation of free SNAREs with botulinum toxin D or with soluble cytoplasmic domains of SNAREs. However this disruption did not occur once SNARE complexes have been formed. This suggests that SNARE complex assembly is necessary and sufficient for fusion. However the rate of fusion *in vitro* was much slower than *in vivo* with a half time of around 10 minutes, which suggests that although SNAREs are sufficient for membrane fusion, other factors are required *in vivo* to aid fusion.

Despite this large amount of evidence in support of SNAREs as mediators of membrane fusion, some studies have suggested that perhaps SNAREs are not involved in the fusion process. A yeast study of vacuolar fusion showed that disruption of SNARE complexes by a blocking antibody did not affect content mixing of vacuoles (Ungermann *et al.*, 1998). Also in fusion of sea urchin egg cortical vesicles, calcium ions were found to dissociate SNARE complexes without disrupting fusion (Tahara *et al.*, 1998). It has also been suggested that proteins other than SNAREs can mediate fusion *in vitro* which may mediate fusion *in vivo*. (Jahn and Grubmuller, 2002).

More recent papers have focussed on how SNARE assembly leads to membrane fusion and whether the energy released during assembly is sufficient to induce membrane fusion.

Sorensen *et al.* investigated whether SNARE complex assembly of the SNAREs, SNAP 25, syntaxin and synaptobrevin occurs in the N- to C-terminal direction (Sorensen *et al.*, 2006).Using alanine mutations in the N- and C-terminal regions of the SNARE complex, they showed that C-terminal mutations in SNAP 25 reduced fusion triggering in embryonic chromaffin cells and lead to unfolding of the SNARE complex *in vitro*. This suggests that the C-terminal region of SNAREs can assemble /disassemble independently. In contrast N-terminal mutations in SNAP 25 were without effect on fusion. These results suggest that SNARE complex assembly occurs from the N-terminal end to the C-terminal end.

The linker region between the SNARE domain and the transmembrane domain is thought to have important role in transducing the energy from SNARE assembly to the membrane, leading to fusion. Two studies have illustrated the importance of the linker region in fusion. Introduction of two "helix-breaking" proline residues in the juxtamembrane region of syntaxin reduced fusion by 50% in a liposome fusion assay. Also insertion of a flexible linker to increase the distance between the cytoplasmic and transmembrane domain of syntaxin lead to a 50% decrease in fusion (McNew *et al.*, 1999). In a further study, replacement of the transmembrane domain anchors of VAMP2 and syntaxin 1A with a covalently-attached phospholipid (phosphatidylethanolamine) completely inhibited fusion in a liposome fusion assay (McNew *et al.*, 2000b).

Studies have also investigated the energy produced during SNARE assembly and whether this energy is sufficient to fuse membranes. Li *et al.* used surface forces apparatus to determine the energetics and dynamics of SNARE complex formation (Li *et al.*, 2007). The authors found that the energy stabilising a single SNARE complex (35 K_BT) corresponds closely with the energy required to fuse the outer leaflet of a lipid bilayer (hemifusion). Sorenson *et al.* used free energy perturbation simulations to determine the effect of mutations in the C-terminal region of SNAP 25 on the thermodynamic stability of the SNARE complex between SNAP 25, syntaxin and synaptobrevin. The $\Delta\Delta G$ for the SNAP 25 L78A, L81A, M201A mutant was 45KJ/mol. This suggests that assembly of the C-terminal end of the SNARE complex may provide substantial energy for membrane fusion.

A number of studies have also investigated how many SNAREs are necessary for fusion of a vesicle with a membrane. Using a permeablised PC12 cell system, the effect of an increasing concentration of the soluble domain of VAMP2 on membrane fusion was determined. The increased inhibition of fusion with increasing concentration of VAMP2 best fit to a model in which three SNARE complexes mediate fusion of a single vesicle (Hua and Scheller, 2001). Han *et al*. showed that mutations in the transmembrane domain of syntaxin altered neurotransmitter flux through fusion pores and altered pore conductance in PC12 cells (Han *et al.*, 2004). The mutations were on the same face of the transmembrane alpha helix and lined the fusion pore. This suggested a model in which the syntaxin transmembrane domains form a circular arrangement of 5-8 molecules in the plasma membrane forming a fusion pore. Kinetic analysis of the docking and fusion of synaptobrevin-containing vesicles with a t-SNARE complex-containing planar membrane in a single vesicle fusion assay using TIRFM, suggested a kinetic model in which fusion sites consisted of 8 SNARE complexes that each activate a single rate-limiting step (Domanska *et al.*, 2009). Electron paramagnetic resonance (EPR) and fluorescence analyses also show that at least three copies of t-SNAREs self assemble through interaction between the transmembrane domains (Lu *et al.*, 2008). This multimeric structure serves as a scaffold for trans-SNARE complex formation leading to hemifusion.

1.6.5 Specificity of membrane fusion and the SNARE hypothesis

In addition to their function in promoting fusion, SNAREs also have a role in ensuring specificity of membrane fusion. In 1993 Sollner *et al*. proposed the SNARE hypothesis (Sollner *et al.*, 1993). It proposes that each transport vesicle has its own v-SNARE that pairs up with its unique cognate t-SNARE complex in the appropriate target membrane, and that this specific interaction docks vesicles at the correct membrane.

Several studies support the SNARE hypothesis. Firstly for most trafficking steps there is only one set of SNAREs involved. Also it has been shown that for exocytosis in PC12 cells only specific SNAREs inhibit or rescue this process (Scales *et al.*, 2000). In addition several liposome-based fusion studies have shown specificity in SNARE pairing (McNew *et al.*, 2000a;Parlati *et al.*, 2002;Paumet *et al.*, 2004).

However some SNAREs can function in more than one trafficking step and in some cases substitute for other SNAREs (Gotte and von Mollard, 1998). Several studies have shown promiscuity of SNARE interactions (von Mollard *et al.*, 1997;Yang *et al.*, 1999;Fasshauer *et al.*, 1999;Tsui and Banfield, 2000). The SNARE hypothesis suggests that SNAREs dock vesicles at the correct membrane. However disruption of SNAREs does not seem to affect vesicle docking (Hunt *et al.*, 1994;Broadie *et al.*, 1995). SNAREs have a high level of structural conservation which may explain their promiscuity. Also SNAREs localise to specific membranes and compartments and this may be the mechanism by which they mediate specificity of membrane fusion events. It has been suggested that *in vivo* other proteins are required for the docking of vesicles with specific membranes (Zerial and McBride, 2001). Recent data suggests that in biological membranes SNARE specificity is mediated by both a preference for cognate SNAREs in the trans configuration (which may involve proof reading proteins such as SM proteins) and lateral segregation of SNAREs at the site of fusion (Bethani *et al.*, 2007).

1.6.6 Regulation of SNARE function

The action of SNAREs can be regulated by several factors including SNARE binding proteins, for example SM proteins and post-translational modifications such as phosphorylation (Gerst, 2003;Malsam *et al.*, 2008). This regulation ensures that functional SNARE complexes and therefore membrane fusion only occurs at the right time and place. Regulation is needed to prevent inappropriate trans-SNARE pairing between cognate SNAREs before they are required, to ensure that only SNARE molecules at the site of fusion are activated for fusion and to aid catalysis of SNARE assembly. SNARE regulators act by maintaining SNARE proteins in conformations which are either well or poorly disposed to assembly.

SM proteins are a family of proteins which have been shown to be essential for vesicle trafficking. For example, a temperature-sensitive mutant of the yeast SM protein Vps45p causes an accumulation of post-Golgi vesicles (Piper *et al.*, 1994). SM proteins bind to stxs and regulate SNARE complex assembly (Toonen and Verhage, 2003;Sudhof and Rothman, 2009). They function to positively regulate SNARE complex assembly by regulating t-SNARE receptivity. SM proteins bind to stxs in three different modes (Carpp *et al.*, 2006;D'Andrea-Merrins *et al.*,

2007;Aran *et al.*, 2009;Furgason *et al.*, 2009). In the first mode the SM protein binds to the stx in a closed conformation, preventing the formation of SNARE complexes (mode A Fig. 1.7). In the second mode (mode B) the N-terminal lobe of the SM protein binds to the N-terminal peptide of the stx. This mode of binding allows the t-SNARE complex to assemble and then accept the v-SNARE, forming a trans-SNARE complex. SM proteins also bind the trans-SNARE complex. Interaction of the SM protein with the trans-SNARE complex (mode C) stimulates membrane fusion and adds specificity to membrane trafficking.

There is a lot of data to support the binding of SM proteins to the closed conformation of stxs. For example, stx 4 lacking the N-terminal 36 amino acids (Stx 4 –NΔ) is still able to bind to Munc 18c (Aran *et al.*, 2009). Also Tlg2p-NΔ is able to bind to the mutant Vps45p-L117R (Furgason *et al.*, 2009). Vps45p-L117R is a "pocket-fill" mutant which is unable to bind the N-terminal peptide of Tlg2p. Also Tlg2p(37-192), containing the Habc domain and Tlg2p(221-318), containing the linker and SNARE motif, are unable to bind Vps45p or compete with Tlg2p-NΔ for binding to Vps45p (Furgason *et al.*, 2009). In addition, mutation of I285, a residue present in the SNARE motif which should contact Vps45p when in the closed conformation, inhibits C-terminal binding of Tlg2p to Vps45p (Furgason *et al.*, 2009).

There is also evidence to support binding of the N-terminal peptide of stx to SM proteins. The Vps45p-L117R "pocket fill" mutation completely abolishes binding of Vps45p with Tlg2p (Carpp *et al.*, 2006). In another study, a D3R mutation in the N-terminal peptide of stx 4-CFP resulted in a 40% reduction in FRET with cYFP-Munc 18c. In addition D3R mutation in a constitutively open mutant of stx 4 (stx 4 L173A, E174A) completely eliminated binding to Munc 18c (D'Andrea-Merrins *et al.*, 2007). Another mutation in the N-terminal peptide of stx 4 (L8K), significantly reduced binding of Munc 18c to both wildtype and constitutively open stx 4 (Aran *et al.*, 2009). The crystal structure of the N-terminal peptide bound to Munc 18c identified Leu 8 of stx 4 as making a crucial contact with the hydrophobic pocket in domain 1 of Munc 18c (Hu *et al.*, 2007).

Finally, there is some evidence to support the binding of SM proteins to the trans-SNARE complex. His_6-Vps45p interacts directly with the cytosolic domains of the Tlg2p and the V-SNARE Snc2p. Also this interaction is specific to Vps45p as Snc2p does not bind to the SM protein Munc 18c (Carpp *et al.*, 2006). The

interaction between Snc2p is mediated by its SNARE motif as a version of Snc2p lacking its N-terminal region ($Snc2p_{\Delta 2\text{-}19}$) binds efficiently to Vsp45p. This supports a bridging hypothesis, whereby the SM protein forms a bridge between t-SNAREs and their cognate v-SNAREs (Peng and Gallwitz, 2004).

In addition to a role in SNARE complex assembly, SM proteins have been implicated in stx stabilisation and transport (Bryant and James, 2001;Carpp *et al.*, 2007).

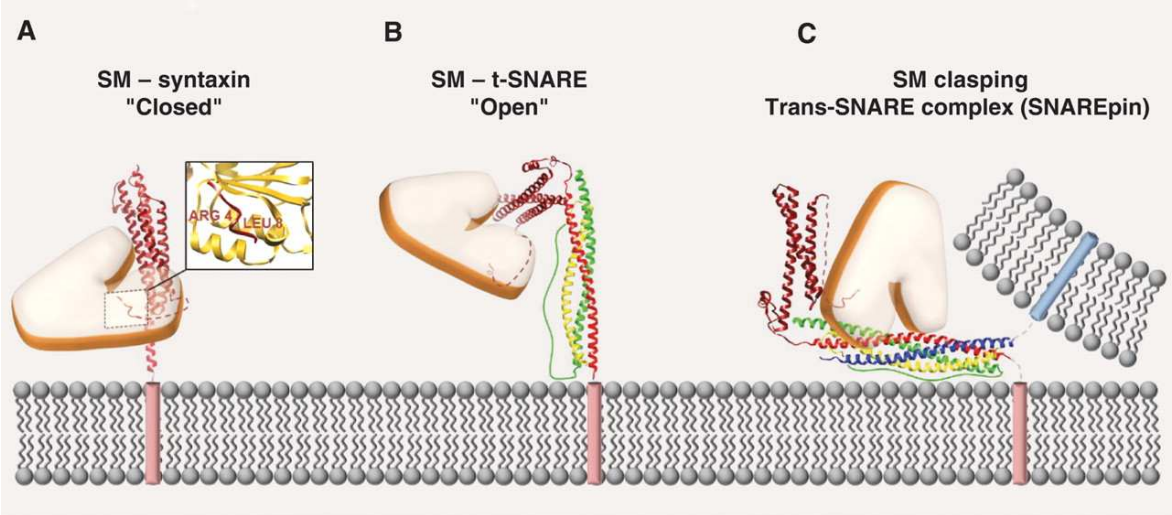

Figure 1.7. Binding modes of SM proteins (Sudhof and Rothman, 2009).
A. SM protein binds to the closed conformation of the stx. Inset shows the residues of the stx N-terminus which interact with the SM protein in this mode. **B.** SM protein binds to the N-terminal peptide of the stx. **C.** SM protein binds to the trans-SNARE complex. Positions of the SM protein in **B** and **C** are arbitrary.

SNAREs can also be regulated by phosphorylation. It has been shown that dephosphorylation of t-SNAREs modulates exocytosis and endocytosis in yeast, by regulating the assembly of SNARE complexes (Marash and Gerst, 2001;Gurunathan *et al.*, 2002). Yeast cells lacking Snc1p and Snc2p (*snc)* are defective in exocytosis. This defect can be ameliorated by treatment with ceramide which results in dephosphorylation of Ssop t-SNAREs and the formation of complexes between Ssop and Sec9p t-SNAREs. Sso1p has a protein kinase A (PKA) phosphorylation site at Ser 79. Mutation of this site to alanine rescues *snc* cells in the absence of ceramide. Also phosphorylation of Sso1p *in vitro* by Tpk1p prevents assembly of Sso1p into complexes with Sec9p (Marash and Gerst, 2001). These results suggest that t-SNARE phosphorylation by PKA inhibits SNARE assembly and subsequent fusion in yeast. The results also suggest a ceramide-regulated pathway can restore exocytosis in *snc* cells by dephosphorylating t-SNAREs.

Yeast cells lacking the v-SNAREs Snc1p and Snc2p and Tlg1p or Tlg2p t-SNAREs are defective in endocytosis. Treatment of these yeast cells with ceramide restores endocytosis. Ceramide treatment also promotes assembly of Tlg1p and Tlg2p into complexes in *snc* cells. Also mutation of single PKA sites in Tlg1p (Ser 31) or Tlg2p (Ser 90) to alanine is sufficient to restore endocytosis in *snc* cells in the absence of ceramide. *In vitro* phosphorylation of Tlg1p and Tlg2p by Tpk1p inhibits complex assembly (Gurunathan *et al.*, 2002). These results suggest that like exocytosis, endocytosis is regulated by t-SNARE phosphorylation *in vivo*. It is thought that phosphorylation regulates the availability of t-SNAREs to participate in trafficking events.

In addition to the yeast SNAREs Sso1p, Tlg1p and Tlg2p, there are other SNAREs which have been found to be phosphorylated. Stx 1 is phosphorylated by several kinases including, casein kinase I (CKI) (Dubois *et al.*, 2002), CKII (Bennett *et al.*, 1993;Hirling and Scheller, 1996;Foster *et al.*, 1998;Risinger and Bennett, 1999;Dubois *et al.*, 2002), calcium/calmodulin-dependent protein kinase II (CaMKII) (Hirling and Scheller, 1996;Ohyama *et al.*, 2002) and death-associated protein (DAP) kinase (Tian *et al.*, 2003). Stx 4 is phosphorylated by CKII (Foster *et al.*, 1998;Risinger and Bennett, 1999) and PKA (Foster *et al.*, 1998). SNAP 25 is phosphorylated by PKC (Shimazaki *et al.*, 1996;Genoud *et al.*, 1999) and PKA (Risinger and Bennett, 1999). SNAP 23 is also phosphorylated by PKC (Polgar *et*

al., 2003). Finally VAMP2 is phosphorylated by CKII and CaMKII (Nielander *et al.*, 1995).

Stx 1 is phosphorylated at Ser 14 by CKII (Bennett *et al.*, 1993). This phosphorylation of stx 1 by CKII enhances its interaction with synaptotagmin I (Risinger and Bennett, 1999). Phosphorylated stx 1 also associates with SNAP 25 and localises to discrete domains of axonal plasma membranes which may define fusion sites (Foletti *et al.*, 2000). In addition, phosphorylation of stx 1 at Ser 14 decreases the N-terminal interaction of stx 1 with Munc 18-1 at the plasma membrane and reduces vesicle mobility and exocytosis (Rickman and Duncan, 2010). Stx 1 is also phosphorylated by CaMKII at Thr 161 in the linker domain. Phosphorylation at Thr 161 by CaMKII does not affect the binding of CaMKII to stx 1 (Ohyama *et al.*, 2002). Stx 1 is phosphorylated by DAP kinase at Ser 188 in the linker domain of stx 1 both *in vitro* and *in vivo* in a Ca^{2+}-dependent manner. Stx 1 phosphorylation by DAP kinase decreases stx 1 binding to Munc 18-1 (Tian *et al.*, 2003).

The phosphorylation sites of stx 4 for CKII and PKA were not determined (Foster *et al.*, 1998;Risinger and Bennett, 1999). However it was shown that phosphorylation of stx 4 by PKA disrupted its binding to SNAP 23 (Foster *et al.*, 1998). The authors suggest that PKA may modulate stx 4-dependent SNARE complex formation to regulate exocytosis in non-neuronal cells.

SNAP 25 is phosphorylated at Ser 28, Ser 187 and Thr 29 by PKC (Shimazaki *et al.*, 1996;Genoud *et al.*, 1999). Phosphorylation of SNAP 25 at Ser 187 decreases binding of SNAP 25 to syntaxin (Shimazaki *et al.*, 1996). Phosphorylation of SNAP 25 at Ser 187 *in vivo* increases vesicle recruitment in chromaffin cells (Nagy *et al.*, 2002). The authors suggest that the decreased binding of SNAP 25 to syntaxin prevents inappropriate SNARE interactions. SNAP 25 is also phosphorylated at Thr 138 by PKA, although this phosphorylation does not affect binding to syntaxin (Risinger and Bennett, 1999). However PKA phosphorylation at Thr 138 increases the size of the ready-releasable pool of vesicles in chromaffin cells (Nagy *et al.*, 2004).

SNAP 23 is phosphorylated at Ser 13/Thr 14 and Ser161 by PKC (Polgar *et al.*, 2003). The authors could not determine which of Ser 13 or Thr 14 were phosphorylated but did show that phosphorylation at these sites inhibits the

interaction between SNAP 23 and syntaxin. SNAP 23 is also phosphorylated at Ser 95 and Ser 120 in rodent mast cells (Hepp *et al.*, 2005). This phosphorylation occurs after degranulation and after stimulation occurs, essentially all of the SNAP23 that is bound to stx 4 and VAMP 2 is phosphorylated.

VAMP 2 is phosphorylated *in vitro* at Thr 35 and Ser 61 by CaMKII and at Ser 75 by CKII (Nielander *et al.*, 1995). As the study was done *in vitro* the significance of these phosphorylations was not determined.

1.7 SNAREs involved in GLUT4 trafficking

The SNAREs involved in fusion of GLUT4-containing vesicles with the plasma membrane have been well characterised (Thurmond and Pessin, 2001). The v-SNARE VAMP2 has been found to reside in GSVs (Martin *et al.*, 1996) and has been shown to be important for translocation of GSVs to the plasma membrane in response to insulin (Martin *et al.*, 1998). VAMP2 forms a complex with the t-SNAREs stx 4 and SNAP 23 which are highly enriched in the plasma membrane of fat and muscle cells. This results in fusion of the GLUT4-containing vesicle with the plasma membrane. The assembly of the trans-SNARE complex between VAMP2, stx 4 and SNAP 23 is regulated by the SM protein Munc18c (Brandie *et al.*, 2008).

In contrast the identity of the SNAREs involved in GLUT4 intracellular trafficking remains largely unknown. It has been shown that the t-SNARE stx 6 has a role in GLUT4 trafficking. Stx 6 colocalises with perinuclear GLUT4 in a subdomain of the TGN and is highly enriched in immunoisolated GLUT4 vesicles. Also insulin stimulates movement of stx 6 from intracellular membranes to the plasma membrane of adipocytes (Shewan *et al.*, 2003). Overexpression of the cytosolic domain of stx 6 in adipocytes increases basal levels of glucose transport and cell surface levels of GLUT4, but does not affect insulin-stimulated glucose transport or GLUT4 translocation (Perera *et al.*, 2003). However reversal of insulin-stimulated glucose transport and the rate of internalisation of GLUT4 from the plasma membrane after insulin withdrawal are significantly slowed in cells overexpressing the cytosolic domain of stx 6. Also overexpression of the cytosolic domain of stx 6 significantly reduces the amount of GLUT4 reaching the GSV compartment after insulin withdrawal (Perera *et al.*, 2003). This data suggests that stx 6 may be involved in trafficking of GLUT4 into its storage site.

1.8 Syntaxin 16

Stx 16 is a member of the stx subfamily of SNAREs (Teng *et al.*, 2001). Its yeast homologue is Tlg2p (Struthers *et al.*, 2009). Stx 16 is located in the TGN (Simonsen *et al.*, 1998;Tang *et al.*, 1998) and is known to be involved in early endosome to TGN transport (Mallard *et al.*, 2002). It is required for the efficient retrograde transport of Shiga toxin, cholera toxin, ricin and the mannose 6-phosphate receptor (Amessou *et al.*, 2007). Stx 16 forms a t-SNARE complex with stx 6 and Vti1a (Mallard *et al.*, 2002) and also with stx 10 and Vti1a, however the latter complex is not formed in murine cells and is specifically required for the retrograde transport of mannose 6-phosphate receptor (Ganley *et al.*, 2008). Stx 16 also binds to the SM protein mVps45 (Dulubova *et al.*, 2002) which regulates its assembly into SNARE complexes.

1.9 Role of syntaxin 16 in GLUT4 trafficking

In addition to its role in retrograde transport, stx 16 is proposed to have a role in GLUT4 trafficking. There are data to support a role for stx 16 in GLUT4 trafficking. The expression of stx 16 is significantly upregulated during adipocyte differentiation. It colocalises with GLUT4 in a subdomain of the TGN and is highly enriched in GLUT4 vesicles. Also insulin stimulation results in the translocation of stx 16 to the cell surface in a similar manner to GLUT4 (Shewan *et al.*, 2003). Recently it has been shown that overexpression of the cytosolic domain of stx 16 significantly slows the reversal of insulin-stimulated glucose transport. Depletion of stx 16 using a morpholino antisense oligonucleotide reduces insulin-stimulated glucose transport over a range of insulin concentrations and slows the reversal of glucose transport after insulin withdrawal (Proctor *et al.*, 2006).Stx 16 knockdown also reduces the translocation of GLUT4 to the cell surface in response to insulin. It was also noted in stx 16-depleted cells that total GLUT4 cellular levels were reduced by 30% which suggests that GLUT4 is missorted to a degradative pathway in these cells. The effect of stx 16 is specific to GLUT4 trafficking as there was no effect on the delivery of TfR to the cell surface (Proctor *et al.*, 2006). This data suggests that stx 16 regulates intracellular trafficking of GLUT4. In particular it

suggests stx16 has a crucial role in sorting GLUT4 from the fast-trafficking pathway to the slow-trafficking pathway. It has been proposed that stx 16 may control sequestration of GLUT4 in its storage site(s).

Stx 16 is also phosphorylated in the absence of insulin and this phosphorylation decreases upon insulin treatment (Perera *et al.*, 2003). It is thought that this dephosphorylation may control an important membrane trafficking event in GLUT4 sorting.

1.10 Aims of this thesis

The aim of this thesis was to further investigate the role of stx 16 in GLUT4 trafficking. The results obtained in this thesis were divided into three chapters as follows.

In chapter three, a shRNA approach was used to knockdown stx 16 expression in 3T3-L1 adipocytes. The effect of stx 16 knockdown on GLUT4 trafficking was investigated. In chapter four, assays were developed to examine the translocation and recycling of GLUT4. In chapter five, the phosphorylation site of stx 16 was investigated.

Chapter 2 Materials and Methods

2.1 Materials

2.1.1 General reagents

All reagents were ordered from Fisher Scientific UK Ltd, Loughborough, Leicestershire, UK or Sigma-Aldrich Company Ltd, Gillingham, Dorset, UK unless stated below.

BD Biosciences, Oxford, UK

Round-bottomed flow cytometry tubes

Syringes

26 gauge needles

Beckman Coulter (UK) Ltd, High Wycombe, Buckinghamshire, UK

Thinwall polyallomer 2.2 ml tubes, 11 x 35 mm

Thinwall Ultra-Clear™ 5 ml tubes, 13 x 51 mm

Bio-Rad Laboratories Ltd, Hemel Hempstead, Hertfordshire, UK

Bio-Rad protein assay reagent

Dako UK Ltd, Cambridgeshire, UK

R-Phycoerythrin (RPE)-conjugated goat anti-mouse antibody

ForMedium™, Hunstanton, Norfolk, UK

Agarose

Amino acid supplements –uracil (Ura) –leucine (Leu)

Amino acid supplements –Ura –methionine (Met)

Peptone

Tryptone

Yeast extract

Yeast nitrogen base without amino acids

GE Healthcare Life Sciences, Little Chalfont, Buckhamshire, UK

All horseradish peroxidase (HRP)-conjugated secondary antibodies

Cy3 antibody labelling kit

Invitrogen Ltd, Paisley, UK

Super optimal broth with catabolite repression (SOC) medium

Deoxynucleotide triphosphates (dNTPs)

Kodak Ltd, Hemel Hempstead, Hertfordshire, UK

X-ray film

Jackson ImmunoResearch Laboratories Inc, West Grove, Pennsylvania, US

Cy3-conjugated goat anti-mouse antibody

Merck Chemicals Ltd, Nottingham, UK

Calbiochem® Proteoextract® phosphopeptide enrichment TiO_2 kit

Calbiochem® Proteoextract® phosphopeptide enrichment SCIMAC (strong cation exchange- immobilised metal ion affinity chromatography) kit

New England Biolabs (UK) Ltd, Hitchin, Hertfordshire, UK

Pre-stained broad range protein marker 6-175 kilodaltons (kDa)

T4 deoxyribonucleic acid (DNA) ligase

1 kilobase (kb) DNA ladder

Premier Brands UK, Knighton, Adbaston, Staffordshire, UK

Marvel low-fat milk powder

Promega, Southampton, UK

All restriction endonucleases

Pfu DNA polymerase

Wizard® Plus SV miniprep kit

Qiagen, Crawley, West Sussex, UK

PhosphoProtein purification kit

QIAfilter Maxi plasmid purification kit

Roche Diagnostics Ltd, Burgess Hill, UK

Complete and complete ethylenediaminetetraacetic acid (EDTA)-free protease inhibitor tablets

Trypsin (sequencing grade)

Severn Biotech Ltd, Kidderminster, Worcestershire, UK

30% weight/volume ratio (w/v) acrylamide/bisacrylamide

Sterilin Limited, Caerphily, UK

90 mm petri dishes

Whatman plc, Maidstone, Kent, UK

Protran® nitrocellulose

2.1.2 Cell culture materials

ATCC, LGC Standards, Teddington, Middlesex, UK

NIH 3T3 cell line

ATCC, P.O. Box 1549, Manassas, Virginia, US

3T3-L1 cell line

BD Biosciences, Oxford, UK

BD Falcon™ 10 cm plates, 6-well plates, 12-well plates and 96-well plates

Clontech-Takara Bio Europe, Saint-Germain-en-Laye, France

EcoPack 2-293 cell line

Corning B.V. Life Sciences, Schiphol-Rijk, The Netherlands

75 cm^2 flasks and 150 cm^2 flasks

GE Osmonics, Minnetonka, Minnesota, US

0.45 μm cellulose acetate filters

Invitrogen Ltd, Paisley, UK

Dulbecco's modified eagle medium (DMEM)

Foetal bovine serum (FBS, US origin)

Lipofectamine™ 2000

Newborn calf serum (NCS, New Zealand origin)

Non-essential amino acids (NEAA)

Opti-MEM® reduced serum medium

Penicillin and streptomycin

Sodium pyruvate

0.25 % (w/v) trypsin-EDTA

Roche Diagnostics Ltd, Burgess Hill, UK

Collagenase

293T cell line was a kind gift of Prof. R. Everett (University of Glasgow).

2.1.3 Primary antibodies

Abcam plc, Cambridge, UK

Green fluorescent protein (GFP) rabbit polyclonal antibody. Catalogue number (Cat. No.) ab290

mVps45 goat polyclonal antibody. Cat. No. ab52013

BD Biosciences, Oxford, UK

Stx 6 mouse monoclonal antibody. Cat. No. 610636

Vti1a mouse monoclonal antibody. Cat. No. 611220

Vti1b mouse monoclonal antibody. Cat. No. 611405

Cambridge BioScience Ltd, Cambridge, UK

Covance® haemagglutinin (HA).11 mouse monoclonal antibody. Cat. No. MMS-101R

Invitrogen Ltd, Paisley, UK

ZYMED® TfR mouse monoclonal antibody. Cat. No. 13-6800

Millipore Ltd, Watford, UK

CHEMICON® GLUT4 C-terminus rabbit polyclonal antiserum. Cat. No. CBL243

Roche Diagnostics Ltd, West Sussex, UK

HA rat monoclonal antibody (clone 3F10). Cat. No. 11867423001

Sigma-Aldrich Company Ltd, Gillingham, Dorset,UK

Rabbit anti-sheep immunoglobulin (Ig)G antiserum. Cat. No. S 1140

IgG1 isotype control from murine myeloma clone MOPC-21. Cat. No. M 5284

IgG2b isotype control from murine myeloma clone MOPC-141. Cat. No. M 5534

Synaptic Systems GmbH, Goettingen, Germany

SNAP 23 rabbit polyclonal antiserum. Cat. No. 111 202

Stx 16 mouse monoclonal antibody. Cat. No. 110 161

Stx 16 rabbit polyclonal antiserum. Cat. No. 110 162

IRAP rabbit antibody was a kind gift of Prof. D. E. James (Garvan Institute of Medical Research, Sydney) (Keller *et al.*, 1995).

Tlg2p rabbit antiserum was purified in house as described in (Bryant and James, 2001).

2.1.4 Plasmids

Clontech-Takara Bio Europe, Saint-Germain-en-Laye, France

Ribonucleic acid interference (RNAi)-Ready pSIREN-RetroQ vector. Cat. No. 631526. Retroviral expression vector designed to express short hairpin RNA (shRNA). ShRNA was cloned into the vector using *Bam*H I and *Eco*R I sites.

HA-GLUT4-GFP in the pRRL-PGK plasmid and the ViraPower™ packaging mix were a kind gift of Prof. C.C. Mastick (University of Nevada) (Muretta *et al.*, 2008). HA-GLUT4-GFP was constructed by cloning cDNA encoding HA-GLUT4 (from Dr Samuel Cushman, National Institutes of Health, Bethesda) at the *Age* I site in frame upstream of the GFP reporter of the pRRL-PGK-GFP lentiviral expression vector. The HA tag is in the first exofacial loop of GLUT4 and the GFP tag is at the C-terminus of GLUT4. The GLUT4 used in the plasmid is human and contains the residues 1-509.

Myc-stx 16A in the pShuttle-CMV plasmid was made by Dr K. Proctor (University of Glasgow) (Proctor *et al.*, 2006). A N-terminally myc-tagged (EQKLISEEDL) version of human stx 16A (residues 1-304) was cloned into the pShuttle-CMV adenoviral expression vector at the *Pme* I site.

pVT102U (Vernet *et al.*, 1987). Yeast expression vector (2μ *URA3*) containing the *ADH1* promoter.

pHA-TLG2 (Seron *et al.*, 1998). pHA-TLG2 was constructed to express a N-terminally HA-tagged (YPYDVPDYA) version of Tlg2p (residues 1-396) under the control of the constitutive *ADH1* promoter in pVT102U. HA-TLG2 was cloned into the pVT102U vector at the *Xba* I site.

pSGS025 and pSGS036 were made by Dr. S. Shanks (University of Glasgow). pSGS025 was constructed to express a N-terminally HA-tagged (YPYDVP) version

of human stx 16A (residues 1-304) under the control of the constitutive *ADH1* promoter in pVT102U. HA-stx 16A was cloned into the pVT102U vector at the *Xba* I and *Xho* I sites. pSGS036 was constructed to express a N-terminally HA-tagged (YPYDVP) version of human stx 4 (residues 1-297) under the control of the constitutive *ADH1* promoter in pVT102U. HA-stx 4 was cloned into the pVT102U vector at the *Xba* I and *Xho* I sites.

pSL2099 (Davis *et al.*, 1993). pSL2099 was constructed to express a C-terminally myc-tagged (*c-myc* 9E10 epitope) version of Ste3p (residues 1-470) under control of the *GAL1* promoter in pRS315.

2.1.5 Oligonucleotides

All oligonucleotides were made by Yorkshire Bioscience Ltd, York, UK.

Name	Sequence (5' to 3')
Stx16 shRNA1 5'	GATCC**GTATGATGTTGGCCGCATT**TTCAAGAGAAATGCGGCCAACAT CATACTTTTTTACGCGTG
Stx16 shRNA1 3'	AATTCACGCGTAAAAAAGTATGATGTTGGCCGCATTTCTCTTGAAAAT GCGGCCAACATCATACG
Stx16 shRNA2 5'	GATCC**AGGAGAGATCGCAGCATTT**TTCAAGAGAAAATGCTGCGATCT CTCCTTTTTTTACGCGTG
Stx16 shRNA2 3'	AATTCACGCGTAAAAAAAGGAGAGATCGCAGCATTTTCTCTTGAAAAA TGCTGCGATCTCTCCTG
Stx16 shRNA3 5'	GATCCG**CATTTAGACGGGCCAGTTA**TTCAAGAGATAACTGGCCCGTC TAAATGTTTTTTACGCGTG
Stx16 shRNA3 3'	AATTCACGCGTAAAAAACATTTAGACGGGCCAGTTATCTCTTGAATAAC TGGCCCGTCTAAATGCG
Stx16 shRNA4 5'	GATCC**GTGCTACTGTGTGGATTAT**TTCAAGAGAATAATCCACACAGTA GCACTTTTTTACGCGTG
Stx16 shRNA4 3'	AATTCACGCGTAAAAAAGTGCTACTGTGTGGATTATTCTCTTGAAATAA TCCACACAGTAGCACG
Stx16 T90AS94AS95A	CATTTAAACAGACCC**GCC**CTGGATGAC**GCCGCC**GAAGAGGAACATGCC

5’	
Stx16 T90AS94AS95A 3’	GCCATGTTCCTCTTCGGCGGCGTCATCCAGGGCGGGTCTGTTTAAATG
Stx16 T90DS94DS95D 5’	CATTTAAACAGACCC**GAC**CTGGATGAC**GACGAC**GAAGAGGAACATGCC
Stx16 T90DS94DS95D 3’	GGCATGTTCCTCTTCGTCGTCGTCATCCAGGTCGGGTCTGTTTAAATG
Stx16 S94A 5’	CCCACCCTGGATGAC**GCC**AGCGAAGAGGAACATGC
Stx16 S94A 3’	GCATGTTCCTCTTCGCTGGCGTCATCCAGGGTGGG
Stx16 S95A 5’	CCCACCCTGGATGACAGC**GCC**GAAGAGGAACATGC
Stx16 S95A 3’	GCATGTTCCTCTTCGGCGCTGTCATCCAGGGTGGG
Stx16 T90D 5’	AAACAGACCC**GAC**CTGGATGACA
Stx16 T90D 3’	TGTCATCCAGGTCGGGTCTGTTT
Stx16 S94D 5’	CCTGGATGAC**GAC**AGCGAAGAGGAA
Stx16 S94D 3’	TTCCTCTTCGCTGTCGTCATCCAGG
Stx16 S95D 5’	CCTGGATGACAGC**GAC**GAAGAGGAA
Stx16 S95D 3’	TTCCTCTTCGTCGCTGTCATCCAGG

Target sequences in the shRNA oligonucleotides are highlighted in bold and underlined. Mutations in the primers for site-directed mutagenesis are also highlighted in bold and underlined.

2.1.6 Escherichia coli (E.coli) strains

Clontech-Takara Bio Europe, Saint-Germain-en-Laye, France

Fusion-Blue™ competent cells
*end*A1, *hsd*R17 (r_{K12-}, m_{K12+}), *sup*E44, *thi*-1, *rec*A1, *gyr*A96, *rel*A1, *lac* F'[*proA*$_+$*B*$_+$, *lacI*^{q}ZΔ*M15*::Tn*10*(tet^R)]

Invitrogen Ltd, Paisley, UK

Stbl3 competent cells
F- *mcr*B *mrr hsd*S20(r_B-, m_B-) *rec*A13 *sup*E44 *ara*-14 *gal*K2 *lac*Y1 *pro*A2 *rps*L20(Str^R) *xyl*-5 λ- *leu mtl*-1

Top 10 competent cells
F- *mcr*A Δ(*mrr-hsd*RMS-*mcr*BC) φ80*lac*ZΔM15 Δ*lac*X74 *rec*A1 *ara*D139 Δ(*araleu*) 7697 *gal*U *gal*K *rps*L (StrR) *end*A1 *nup*G

2.1.7 Yeast strains

RPY10
*MAT*α *ura*3-52 *leu*2-3 112 *his*4-519 *ade*6 *gal*2
(Piper *et al.*, 1994)

NOzY4
*MAT*α *ura*3-52 *leu*2-3 112 *his*4-519 *ade*6 *gal*2 *tlg*2Δ*::Kan*^{r}
(Bryant and James, 2001)

SF838-9D
*MAT*α *ura*3-52 *leu*2-3 112 *his*4-519 *ade*6 *gal*2 *pep*4-3
(Rothman and Stevens, 1986)

NOzY3
*MAT*α *ura*3-52 *leu*2-3 *his*4-519 *ade*6 *gal*2 *pep*4-3 *tlg*2Δ*::Kan*^{r}
(Bryant and James, 2001)

2.1.8 General buffers

BSA/Gly buffer

2% (w/v) bovine serum albumin (BSA) in 20 mM glycine (Gly) in phosphate-buffered saline (PBS)

BSA/Gly/Sap buffer

0.1% (w/v) saponin (Sap) in BSA/Gly buffer

DNA loading buffer (6 x)

0.25% (w/v) bromophenol blue, 15% (w/v) Ficoll

HES buffer

20 mM HEPES(4-(2-hydroxyethyl)-1-piperazineethanesulphonic acid), 225 mM sucrose, 1 mM EDTA, EDTA-free protease inhibitors, pH 7.4

High sucrose HES buffer

20 mM HEPES, 1.12 M sucrose, 1 mM EDTA, EDTA-free protease inhibitors, pH 7.4

Immunoprecipitation (IP) buffer

50 mM HEPES, 5 mM EDTA, 10 mM sodium pyrophosphate, 10 mM NaF, 150 mM NaCl, 2 mM sodium orthovanadate, 50 mM β-glycerolphosphate, 1 mM dithiothreitol (DTT), 1% volume/volume ratio (v/v) Triton X-100, EDTA-free protease inhibitors, pH 7.4

IP wash buffer

20 mM Tris base, 150 mM NaCl, pH 7.4

LiTE-Sorb

0.1 M LiOAc, 10 mM Tris.HCl pH 7.6, 1 mM EDTA, 1.2 M sorbitol

Phosphate-buffered Saline (PBS)

136 mM NaCl, 10 mM Na_2HPO_4, 2.5 mM KCl, 1.8 mM KH_2PO_4, pH 7.4

PBS-T

PBS, 0.01% (v/v) Tween-20

Recycling assay wash buffer

150 mM NaCl, 20 mM HEPES, 1mM $CaCl_2$, 5 mM KCl, 1 mM $MgCl_2$, pH 7.2

Running buffer

25 mM Tris base, 190 mM glycine, 0.1% (w/v) sodium dodecyl sulphate (SDS)

S-D –Ura –Leu plates

0.67% (w/v) yeast nitrogen base without amino acids, 0.075% (w/v) amino acid supplements –Ura –Leu, 2% (w/v) (D)- glucose, 2% (w/v) agarose

S-Raf/Gal –Ura –Leu

0.67% (w/v) yeast nitrogen base without amino acids, 0.075% (w/v) amino acid supplements –Ura –Leu, 2% (w/v) galactose (Gal), 2% (w/v) raffinose (Raf)

S-D –Ura -Met

0.67% (w/v) yeast nitrogen base without amino acids, 0.075% (w/v) amino acid supplements –Ura –Met, 2% (w/v) (D)- glucose

S-D –Ura -Met plates

0.67% (w/v) yeast nitrogen base without amino acids, 0.075% (w/v) amino acid supplements –Ura –Met, 2% (w/v) (D)- glucose, 2% (w/v) agarose

SDS-PAGE sample buffer (2 x)

100 mM Tris.HCl pH 6.8, 20 mM DTT (added immediately before use), 20% (w/v) glycerol, 4% (w/v) SDS, 0.2% (w/v) bromophenol blue

TAE buffer

40 mM Tris-acetate, 1 mM EDTA pH 7.8

Transfer buffer

25 mM Tris base, 192 mM glycine, 20% (v/v) methanol

TWIRL buffer

8 M Urea, 50 mM Tris.HCl pH 6.8, 10% (w/v) glycerol, 5% (w/v) SDS, 0.2% (w/v) bromophenol blue, 10% (v/v) β-mercaptoethanol (added immediately before use)

2YT

1% (w/v) yeast extract, 1.6% (w/v) tryptone, 85 mM NaCl

YEPD

1% (w/v) yeast extract, 2% (w/v) peptone, 2% (w/v) (D)-glucose

2.2 Molecular biology methods

2.2.1 2YT agar plates

2YT was prepared as described in 2.1.8. 2% (w/v) agarose was added to the 2YT and then autoclaved. After autoclaving the mixture was cooled to approximately 50 ^{o}C prior to addition of antibiotic. Ampicillin was used at a final concentration of 100 μg/ml and Kanamycin was used at a final concentration of 50 μg/ml. The medium was mixed gently and approximately 25 ml poured into each 90 mm petri dish. The plates were left to set at room temperature and then stored at 4 ^{o}C. Unused plates were disposed of one month after preparation.

2.2.2 Transformation of E. coli

An aliquot of Top10 (Stbl3 for HA-GLUT4-GFP plasmid) competent cells was thawed on ice. 1-10 μl of DNA was added to the cells and incubated on ice for 30 minutes. The cells were then incubated at 42 ^{o}C for 45 seconds to heat shock. After heat shock the cells were incubated on ice for 2 minutes. 300 μl of SOC

medium was added to the cells which were then incubated for 90 minutes at 37 °C. After incubation, 50 μl and 250 μl was plated on 2YT agar plates (section 2.2.1) containing the appropriate antibiotic. The plates were inverted and incubated overnight at 37 °C.

2.2.3 E. coli cultures

To prepare a small overnight culture (10 ml) a colony of the transformed bacteria was picked from the 2YT agar plate (section 2.2.2) using a pipette tip. This was put into 10 ml 2YT (section 2.1.8) containing the appropriate antibiotic. The culture was incubated overnight at 37 °C with shaking.

To prepare a larger culture the small overnight culture was diluted 1:1000 into a large volume of 2YT containing the appropriate antibiotic. The culture was incubated overnight at 37 °C with shaking.

2.2.4 Small-scale preparation of plasmid DNA (Mini-preps)

Plasmid DNA was purified from bacterial cultures using the Wizard® Plus SV miniprep kit and the buffers therein. A small overnight culture was prepared as described in section 2.2.3. 10 ml of bacterial culture was centrifuged at 10,000 x g for 5 minutes at 4 °C and the supernatant removed. The pellet was resuspended in 250 μl of cell resuspension solution and transferred to a 1.5 ml microcentrifuge tube. 250 μl of cell lysis solution was added to the tube followed by 10 μl of alkaline protease solution. The mixture was then incubated for 5 minutes at room temperature. Then 350 μl of neutralization solution was added. The bacterial lysate was centrifuged at 14,000 x g for 10 minutes. The cleared lysate was decanted into a spin column. The spin column was centrifuged at 14,000 x g for 1 minute to allow DNA binding. The spin column was washed twice with column wash solution and centrifuged at 14,000 x g for 1 minute. DNA was eluted by adding 100 μl of nuclease-free water to the spin column (which had been placed into a 1.5 ml microcentrifuge tube) and then centrifugation at 14,000 x g for 1 minute.

2.2.5 Large-scale preparation of plasmid DNA (Maxi-preps)

Plasmid DNA was purified using the QIAfilter Maxi plasmid purification kit and the buffers therein. A 100 ml culture was prepared as described in 2.2.3. Bacterial cells were harvested by centrifugation at 6000 x g for 15 minutes at 4 ^{o}C. The pellet was resuspended in 10 ml of chilled P1 buffer. 10 ml of P2 buffer was added and the mixture incubated at room temperature for 5 minutes. To neutralise the reaction 10 ml of chilled P3 buffer was added to the mixture. The lysate was then poured into a capped QIAfilter Maxi cartridge and incubated at room temperature for 10 minutes. Meanwhile a QIAGEN-tip 500 was equilibrated by applying 10 ml of QBT buffer and allowing the column to empty by gravity flow. After incubation the cap was removed from the QIAfilter Maxi cartridge and a plunger inserted to filter the lysate into the equilibrated QIAGEN-tip 500. The cleared lysate was then allowed to enter the resin by gravity flow. The QIAGEN-tip 500 was washed twice with 30 ml of QC buffer. DNA was eluted with 15 ml of QF buffer. To precipitate the DNA, 10.5 ml of isopropanol was added to the eluted DNA. This mixture was then centrifuged at 5000 x g for 60 minutes at 4 ^{o}C. The pellet was washed with 5ml 70% (v/v) ethanol and centrifuged again at 5000 x g for 30 minutes at 4 ^{o}C. The pellet was air-dried for 10 minutes and then resuspended in 250 μl of nuclease-free water.

2.2.6 DNA quantification

The concentration of a DNA sample was determined by measuring the absorbance of a 1:1000 dilution of the sample at 260 nm using a Jenway Genova life science analyser (Bibby Scientific Ltd, Dunmow, Essex, UK). An A_{260} of 1 corresponds to 50 μg/ml of double stranded DNA.

2.2.7 Sequencing

Sequencing reactions were performed at The Sequencing Service, University of Dundee.

2.2.8 Preparation of glycerol stocks of transformed E.coli

A 10 ml overnight culture was prepared as described in section 2.2.3. 0.75 ml of the bacterial culture was placed into a 1.8 ml cryovial. 0.75 ml of 50% (v/v) glycerol was then added and mixed. The cryovial was stored at -80 ^{o}C.

2.2.9 Digestion of DNA with restriction endonucleases

Restriction digests of DNA were performed to check that a ligation reaction had been successful. To check a ligation reaction 5 μl of DNA miniprep (section 2.2.4) was digested using the appropriate enzymes and buffers in a final volume of 10 μl. Control reaction mixtures did not contain any restriction endonuclease. Restriction digest reaction mixtures were incubated from 2 hours to overnight at 37 ^{o}C.

2.2.10 Agarose gel electrophoresis

Digested DNA samples were examined using gel electrophoresis. A 1% (w/v) agarose gel was prepared by mixing agarose with 1 x TAE buffer (section 2.1.8). The agarose was heated until it had melted. 2.5 μg/ml ethidium bromide was added and the gel poured into a horizontal gel tank. Once the gel had set 1 x TAE was added to the tank. DNA samples were mixed with 6 x DNA loading dye (section 2.1.8) and then loaded onto the gel. The gel was then run for approximately 30 minutes at 100 V. The DNA fragments were visualised under ultraviolet light and their sizes determined by comparison with a 1 kb ladder.

2.2.11 Site-directed mutagenesis

Site directed mutagenesis was performed using the QuikChange® Site-Directed Mutagenesis Kit. Polymerase chain reaction (PCR) reaction mixtures containing 5 μl of 10 x *Pfu* buffer, 50 ng of dsDNA template 125 ng of forward and reverse primer, 1 μl of dNTP mix and 1 μl *Pfu* DNA polymerase were prepared in a total volume of 50 μl. Control reaction mixtures did not contain any *Pfu* DNA polymerase. Reactions were cycled in a Proteus thermocycler (Helena Bioscience, Gateshead, Tyne and Wear, UK) as described below:

Cycle 1: 95 °C for 2 minutes

Cycle 2-19: 95 °C for 30 seconds

50 °C for 1 minute

68 °C for 1 minute per kb of plasmid length

Cycle 20: 68 °C for 1 minute per kb of plasmid length

After themocycling, the PCR products were treated with 1 μl of Dpn1 and incubated for 1 hour at 37 °C. 5 μl of the digested PCR product was then transformed as described in section 2.2.2.

2.3 Mammalian cell culture methods

2.3.1 Cell maintenance

2.3.1.1 3T3-L1

3T3-L1 fibroblasts were cultured in 75 cm^2 flasks in DMEM containing 10% (v/v) NCS and 1% (v/v) penicillin and streptomycin. The cells were incubated at 37 °C in a humidified atmosphere of 10% CO_2. The medium was replaced every 48 hours.

2.3.1.2 NIH 3T3

NIH 3T3 cells were cultured in 75 cm^2 flasks in DMEM containing 10% (v/v) NCS and 1% (v/v) penicillin and streptomycin. The cells were incubated at 37 °C in a humidified atmosphere of 10% CO_2. The medium was replaced every 48 hours.

2.3.1.3 EcoPack 2-293

EcoPack 2-293 cells were cultured in 150 cm^2 flasks in DMEM containing 10% (v/v) FBS, 1 mM sodium pyruvate and 1% (v/v) penicillin and streptomycin. The cells were incubated at 37 °C in a humidified atmosphere of 5% CO_2. The medium was replaced every 48 hours.

2.3.1.4 293T

293T cells were cultured in 10 cm plates in DMEM containing 10% (v/v) FBS, 1 mM sodium pyruvate, 1% (v/v) NEAA and 1% (v/v) penicillin and streptomycin. The cells were incubated at 37 ^{o}C in a humidified atmosphere of 5% CO_2. The medium was replaced every 48 hours.

2.3.2 Cell sub-culture

When the cells were sub-confluent they were sub-cultured into 75 cm^2 flasks, 10 cm, 6-well, 12-well or 96-well plates. The medium was removed by aspiration. 1 ml of 0.25% (w/v) trypsin-EDTA solution was added to the cells to wash them. The trypsin solution was removed and a further 2 ml added. The cells were then incubated with the trypsin for 5 minutes at 37 ^{o}C. Once the cells had detached complete medium was added to the appropriate volume and the cells dispensed into new flasks and plates.

2.3.3 Freezing down and thawing of cells

To freeze down cells, a freeze medium was prepared by adding 10% (v/v) dimethyl sulfoxide (DMSO) to complete medium. Cells were detached from a 75 cm^2 flask as described in 2.3.2. A small volume of complete medium was added to the cells and the cells sedimented by centrifugation at 183 x g for 5 minutes at 4 ^{o}C. The cells were then resuspended in 2 ml of freeze medium. A 1 ml aliquot was placed into a 1.8 ml cryovial. The cryovials were kept at -80 ^{o}C overnight before storing in liquid nitrogen.

To thaw cells, a cryovial was taken from storage in liquid nitrogen and incubated at 37 ^{o}C until the cells had just thawed. The cells were then transferred into 5 ml of pre-warmed complete medium and gently mixed. A further 5 ml of medium was added and then mixed. This was to wash the DMSO from the cells. The cells were then sedimented by centrifugation at 183 x g for 5 minutes at 4 ^{o}C. The cells were resuspended in complete medium and placed into a culture plate.

2.3.4 Differentiation of 3T3-L1s.

3T3-L1 fibroblasts in 10 cm plates were allowed to grow to confluency. The DMEM containing 10% (v/v) NCS, 1% (v/v) penicillin and streptomycin was replaced at confluency. After 48 hours the cells were incubated in DMEM containing 10% (v/v) FBS, 1% (v/v) penicillin and streptomycin, 1 μg/ml insulin, 110 μg/ml isobutylmethylxanthine and 0.25 μM dexamethasone. After a further 48 hours the medium was replaced with DMEM containing 10% (v/v) FBS, 1% (v/v) penicillin and streptomycin and 1 μg/ml insulin. Thereafter the medium was replaced every 48 hours with DMEM containing 10% (v/v) FBS, 1% (v/v) penicillin and streptomycin. The cells were ready to use between 8 and 12 days post-differentiation.

2.4 Biochemical methods

2.4.1 Cell membrane preparation

3T3-L1 adipocytes were incubated in serum-free medium for 2 hours. Then the cells were washed twice with 5 ml of ice-cold HES buffer (section 2.1.8). The cells were then scraped into 0.5 ml HES buffer per 10 cm plate. The lysate was passed through a 26 gauge needle twenty times. The lysate was then centrifuged at 250 x g for 10 minutes at 4 ^{o}C to pellet debris. The resulting supernatant was then centrifuged at 104300 x g for 60 minutes at 4 ^{o}C. The pellet which contains the cell membranes was then resuspended in HES buffer. The sample was then mixed with 2 x SDS-PAGE (SDS-polyacrylamide gel electrophoresis) sample buffer (section 2.1.8) and incubated at 65 ^{o}C for 15 minutes.

2.4.2 Subcellular fractionation

3T3-L1 adipocytes were incubated in serum-free medium for 2 hours. Then the cells were washed three times with 5 ml of ice-cold HES buffer (section 2.1.8). The cells from two 10 cm plates were then scraped into 2 ml of HES buffer. The lysate was passed through a 26 gauge needle twenty times and then centrifuged at 500 x g for 10 minutes at 4 ^{o}C in a bench-top refrigerated microcentrifuge to pellet debris. The supernatant was placed in a Thinwall Ultra-Clear™ tube and

centrifuged at 6000 x g for 12 minutes at 4 °C using a TLA 110 rotor in an Optima™ ultracentrifuge (Beckman Coulter (UK) Ltd, High Wycombe, Buckinghamshire, UK). The pellet contains the plasma membrane (PM) and mitochondria and nuclei (M/N) fractions. The supernatant contains the cytosol, low density microsome (LDM) and high density microsome (HDM) fractions.

The pellet which contained the PM and M/N fractions was resuspended in 10 ml HES buffer and centrifuged at 6000 x g for 12 minutes at 4 °C. The resulting pellet was resuspended in 1 ml HES, layered over high sucrose HES (section 2.1.8) in a Thinwall polyallomer tube and then centrifuged at 42000 x g for 60 minutes at 4 °C in a TLS-55 rotor. The resulting pellet contains the M/N fraction and was resuspended in 100 μl HES. The PM fraction was collected from a layer above the high sucrose HES and placed into a Thinwall Ultra-Clear™ tube. Three volumes of HES were added to the PM fraction and the mixture was centrifuged at 9400 x g for 15 minutes at 4 °C in a TLA 110 rotor. The resulting pellet contains the PM fraction and was resuspended in 100 μl HES.

The supernatant which contained the cytosol, LDM and HDM fractions was further centrifuged at 9400 x g for 17 minutes at 4 °C in a TLA 110 rotor. The resulting pellet contains the HDM fraction and was resuspended in 100 μl HES. The supernatant was then centrifuged at 104300 x g for 75 minutes at 4 °C in a TLA 110 rotor. The resulting pellet contains the LDM fraction and was resuspended in 100 μl HES. The supernatant contains the cytosol. To recover the soluble proteins from the cytosol, 0.1 ml 100% (w/v) trichloroacetic acid was added to 1 ml of the cytosol fraction. The mixture was vortexed and then kept on ice for 10 minutes. The mixture was then centrifuged at 22000 x g in a bench-top refrigerated microcentrifuge. The pellet which contains the soluble proteins was resuspended in 100 μl HES. The fractions were mixed with 2 x SDS-PAGE sample buffer (section 2.1.8) and then incubated at 65 °C for 15 minutes.

2.4.3 Protein concentration determination

Protein concentration was determined using the Bio-Rad protein assay reagent. The standard curve and test samples were placed in a 96-well plate. For the standard curve, between 0 and 20 μg of BSA was put into duplicate wells. Water was added to the wells to make a total volume of 160 μl. For the test samples

159 μl of water was put into duplicate wells and 1 μl of sample added. Then 40 μl of Bio-Rad protein assay reagent was added to all the wells and the plate incubated at room temperature for 5 minutes. After incubation the colour change was determined by measuring the A_{595} using a FLUOstar OPTIMA microplate reader (BMG LABTECH Ltd, Aylesbury, UK).

2.4.4 SDS-PAGE

Samples were loaded onto a SDS-PAGE gel consisting of a 5% (v/v) stacker gel and a 10% (v/v) resolving gel. The molecular weight of the samples was determined using a pre-stained protein marker. The gel was placed in running buffer (section 2.1.8) and run at 120V using a BioRad mini protean 3 system until the dye front reached the bottom of the gel.

2.4.5 Transfer to nitrocellulose

The gel was removed from the plate and placed onto a nitrocellulose membrane soaked in transfer buffer (section 2.1.8). The gel and nitrocellulose membrane were placed between filter paper and sponges soaked in transfer buffer and placed into a tank. Proteins were transferred to the nitrocellulose membrane at 200 mAmp for 2 hours.

2.4.6 Western blotting

The nitrocellulose membrane was incubated with PBS-T (section 2.1.8) containing 5% (w/v) low-fat milk power for 30 minutes on a roller to block non-specific binding sites. The membrane was then incubated overnight at 4 ^{o}C with primary antibody usually at a dilution of 1:1000 in PBS-T containing 1% (w/v) low-fat milk powder. The next day the membrane was washed five times with PBS-T for 5 minutes each wash. After washing, the membrane was incubated for 1 hour at room temperature with a HRP-conjugated secondary antibody usually at a dilution of 1:2500 in PBS-T containing 5% (w/v) low-fat milk powder. The membrane was washed five times with PBS-T for 5 minutes each wash. The membrane was then incubated in enhanced chemiluminesence (ECL) solution and exposed to blue Kodak film and developed using an X-OMAT machine. Blots

were analysed by densitometry using ImageJ software (National Institutes of Health, NIH, Maryland, US).

2.4.7 Immunoprecipitation

3T3-L1 adipocytes were incubated in serum-free medium for 2 hours. The cells were then washed three times with 5 ml of IP buffer (section 2.1.8). After washing, the cells from three 10 cm plates were scraped into 1 ml of IP buffer. The lysate was passed through a 26 gauge needle ten times and then incubated on ice for 30 minutes. After incubation the lysate was centrifuged at 22000 x g for 20 minutes at 4 ^{o}C. 1 ml of the clarified lysate was incubated with each antibody. For stx 16 immunoprecipitations, 5 μg of stx 16 rabbit polyclonal antiserum was added to the lysate. As a control 5 μg of rabbit anti-sheep IgG antiserum was used. Alternatively 5 μg of stx 16 mouse monoclonal antibody was added to the lysate and 5 μg of IgG2b isotype control from murine myeloma clone MOPC-141 was used as a control. The lysate was then inverted ten times to mix. The lysate was incubated with the antibody for 60 minutes on ice. Meanwhile, Protein A-agarose slurry was washed three times with 1 ml of IP wash buffer (section 2.1.8). For each lysate mixture, 50 μl of slurry was used. After washing, the lysate mixtures were added to each tube of Protein A-agarose and mixed gently. The tubes were rotated overnight at 4 ^{o}C. The next day the agarose was sedimented by centrifugation at 22000 x g for 1 minute at 4 ^{o}C. The supernatant was carefully removed and kept as the unbound control. The Protein A-agarose was then washed twice with wash buffer containing 1% (v/v) thesit and again with wash buffer containing 0.1% (v/v) thesit. 50 μl of 2 x SDS-PAGE sample buffer (section 2.1.8) was added to each IP sample and boiled for 5 minutes. After boiling the samples were placed on ice for 5 minutes. The samples were then centrifuged at 22000 x g for 1 minute at 4 ^{o}C. The supernatant containing the immunoprecipitated proteins was then carefully transferred to a new microcentrifuge tube. 2 x SDS-PAGE sample buffer was also added to the unbound controls and the samples boiled as described above.

2.4.8 Colloidal Coomassie staining

Samples were separated by SDS-PAGE as described in section 2.4.4. After electrophoresis the gel was stained with Brilliant Blue G-Colloidal concentrate

according to the manufacturer's instructions. First the gel was fixed for one hour in 7% (v/v) glacial acetic acid in 40% (v/v) methanol. Meanwhile Brilliant Blue G-Colloidal working solution was diluted 4:1 with methanol. This solution was then used to stain the gel for 2 hours. The gel was de-stained with 10% (v/v) acetic acid in 25% (v/v) methanol for 30 seconds with shaking. The gel was then rinsed with 25% (v/v) methanol and de-stained with 25% (v/v) methanol overnight.

2.4.9 Phosphoprotein purification

Phosphoproteins were purified from basal and insulin-stimulated 3T3-L1 adipocytes using a PhosphoProtein purification kit. 10^7 cells were lysed in 5 ml of PhosphoProtein lysis buffer containing 0.25% (w/v) CHAPS (3-[(3-Cholamidopropyl)dimethylammonio]-1-propanesulphonate), a protease inhibitor tablet and 250 U of Benzonase® nuclease. The lysate was incubated at 4 °C for 30 minutes and vortexed briefly every 10 minutes. After incubation the lysate was centrifuged at 10000 x g for 30 minutes at 4 °C. Meanwhile a PhosphoProtein purification column was equilibrated using 4 ml of PhosphoProtein lysis buffer containing 0.25% (w/v) CHAPS. The supernatant from the centrifugation was harvested and the protein concentration was determined as described in 2.4.3. A volume of lysate containing 2.5 mg of protein was diluted to 0.1 mg/ml using PhosphoProtein lysis buffer containing 0.25% (w/v) CHAPS. The diluted lysate was poured into the PhosphoProtein purification column. The flow-through fraction was collected for analysis of unphosphorylated proteins. The column was then washed with 6 ml of PhosphoProtein lysis buffer containing 0.25% (w/v) CHAPS. The phosphorylated proteins were eluted using 5 x 500 µl of PhosphoProtein elution buffer containing 0.25% (w/v) CHAPS. The protein concentration was determined as described in section 2.4.3 of all eluates to determine the most concentrated fraction.

The most concentrated fractions were then further concentrated using a Nanosep ultrafiltration column. Each 500 µl protein fraction was placed into the sample reservoir of the column. The column was centrifuged at 10000 x g for 10 minutes. After centrifugation the concentrated protein sample was removed from the retentate chamber, mixed with 2 x SDS-PAGE sample buffer (section 2.1.8) and heated at 65 °C for 15 minutes. The flow-through and eluate samples

were analysed by SDS-PAGE and western blotting as described in sections 2.4.4, 2.4.5 and 2.4.6 to determine in which fractions stx 16 was present.

2.4.10 Phosphopeptide purification

Stx 16 was immunoprecipitated from basal and insulin-stimulated 3T3-L1 adipocytes as described in section 2.4.7 except the samples were not boiled in 2 x SDS-PAGE sample buffer. The immunoprecipitated proteins remained bound to the Protein A-agarose. The proteins were denatured and digested according to a protocol by T.E.Thingholm (Thingholm *et al.*, 2006). The proteins were first incubated with 50 mM ammonium bicarbonate, pH 7.8, 10 mM DTT at 37 ^{o}C for 1 hour to reduce the proteins. After reduction, 20 mM iodoacetate was added and the samples incubated at room temperature for 1 hour. The reaction was quenched with 10 mM DTT and then digested with sequencing-grade trypsin (2% v/v) at 37 ^{o}C overnight.

2.4.10.1 TiO_2 method

Phosphorylated peptides were purified using the Calbiochem® Proteoextract® phosphopeptide enrichment TiO_2 kit. The trypsin-digested samples were diluted 1:4 with TiO_2 Phosphobind buffer containing dihydrobenzoic acid to give a final volume of 200 μl. The diluted samples were then mixed with 50 μl of TiO_2 Phophobind resin and incubated for 10 minutes at room temperature with gentle agitation. After incubation the samples were centrifuged at 2500 x g for 3 minutes at 4 ^{o}C and the supernatant removed. The samples were washed twice with 100 μl of Wash buffer 1 and the samples centrifuged at 2500 x g for 3 minutes at 4 ^{o}C. The samples were then washed twice with 100 μl of Wash buffer 2 as described above. 30 μl of Elution buffer was then added to the samples and incubated with gentle agitation for 10 minutes at room temperature. The samples were then centrifuged at 10000 x g for 5 minutes at 4 ^{o}C and the supernatant carefully transferred to a new microcentrifuge tube. The supernatant was centrifuged again at 10000 x g for 3 minutes at 4 ^{o}C. The supernatant containing the phosphopeptides was sent for phophosite analysis at the Fingerprint Proteomics unit at the University of Dundee.

2.4.10.2 SCIMAC method

Phosphorylated peptides were purified using the Calbiochem® Proteoextract® phosphopeptide enrichment SCIMAC kit. The trypsin-digested samples were diluted 1:10 with 1 x Phosphobind buffer to give a total volume of 200 μl. 100 μl SCX resin was pelleted by centrifugation at 2500 x g for 2 minutes at 4 °C. The resin was then washed three times with 500 μl of 1 x Phosphobind buffer and centrifuged at 2500 x g for 3 minutes at 4 °C. The diluted samples were then mixed with the washed resin and incubated at room temperature for 15 minutes with gentle agitation. The mixture was then centrifuged at 2500 x g for 3 minutes at 4 °C and the supernatant removed. 100 μl of SCX Elute buffer was added to the resin and incubated at room temperature for 10 minutes with gentle agitation. After incubation, the mixture was centrifuged at 2500 x g for 3 minutes at 4 °C. The supernatant was transferred to a new microcentrifuge tube and centrifuged again at 10000 x g for 3 minutes at 4 °C. The final SCX eluate was transferred to a new microcentrifuge tube and 50 μl of 1 x Phosphobind buffer was added.

The diluted SCX eluate was mixed with 50 μl of MagPrep® Phosphobind particles. The mixture was incubated at room temperature for 10 minutes with gentle agitation. The mixture was centrifuged at 2000 x g for 1 minute at 4 °C and the supernatant removed. The particles were washed twice with 100 μl of Wash buffer 1 and centrifuged at 2000 x g for 1 minute at 4 °C. Then the particles were washed twice with 100 μl of Wash buffer 2 and centrifuged at 2000 x g for 1 minute at 4 °C. 25 μl of Elution buffer was added to the particles and incubated at room temperature for 10 minutes with gentle agitation. After incubation the mixture was centrifuged at 10000 x g for 5 minutes at 4 °C. The supernatant containing the phosphopeptides was sent for phophosite analysis at the Fingerprint Proteomics unit at the University of Dundee.

2.4.11 Cy3 antibody labelling

HA.11 antibody was labelled with a Cy3 antibody labelling kit. 1 mg of the HA.11 antibody was dissolved at 1 mg/ml in PBS (section 2.1.8). The antibody solution was added to the vial of coupling buffer and mixed thoroughly by inverting ten times. The antibody and coupling buffer mixture was transferred to the vial of

reactive Cy3 dye and mixed thoroughly. The reaction mixture was incubated at room temperature for 30 minutes and mixed every 10 minutes. Meanwhile the gel filtration column was equilibrated with 13 ml of elution buffer. The reaction mixture was then added to the column. 2 ml of elution buffer was added to the column to separate the faster-moving pink band of labelled antibody from the unconjugated dye. An additional 2.5 ml of elution buffer was added to the column to elute the labelled antibody from the column. The molar dye/protein ratio was determined by measuring the absorbance at 552 nm and 280 nm using the Jenway Genova life science analyser (Bibby Scientific Ltd, Dunmow, Essex, UK). The kit produced a dye/protein ratio of approximately 12.

2.5 Virus preparation methods

2.5.1 Stx16 shRNA retrovirus

Stx 16 shRNA retrovirus was prepared using the Clontech RNAi-Ready pSIREN-RetroQ Vector system. Stx 16 shRNA target sequences and oligonucleotides were designed using Clontech's online designer tool. Four different shRNA targets were designed (see table in 2.1.5). To anneal the oligonucleotides, 100 μM 5' and 3' strands were mixed at a 1:1 ratio. The mixture was heated in a Proteus thermocycler (Helena Bioscience, Gateshead, Tyne and Wear, UK) as described below:

95 ^{o}C for 30 seconds

72 ^{o}C for 2 minutes

37 ^{o}C for 2 minutes

25 ^{o}C for 2 minutes

Then the annealed shRNA oligonucleotides were ligated into the RNAi-Ready pSIREN-RetroQ vector using a T4 DNA ligase. 1 μl of 0.5 μM annealed shRNA oligonucleotide was mixed with 50 ng of linearised pSIREN vector. 1.5 μl of 10 x ligase buffer and 0.5 μl of T4 DNA ligase were added to give a final volume of 15

μl. As a control 1 μl of negative control annealed shRNA oligonucleotide was used. The reaction mixtures were incubated at room temperature for 3 hours. 2 μl of the ligation reaction mixtures were then transformed into Fusion-Blue™ competent cells as described in section 2.2.2. Colonies were picked the next day and small cultures prepared as described in section 2.2.3. The plasmid DNA was purified as described in section 2.2.4.

In order to identify clones which contained the shRNA target sequence, the DNA was digested with *Mlu* I restriction endonuclease. The *Mlu* I site had been designed into the shRNA oligonucleotide sequence. The restriction digest was performed as described in section 2.2.9. Once positive clones were identified a large culture was prepared as described in section 2.2.3 and the plasmid DNA was purified as described in 2.2.5.

Next the shRNA plasmids were transfected into EcoPack 2-293 cells using Lipofectamine™ 2000. EcoPack2-293 cells were grown to approximately 90% confluency in a 150 cm^2 flask. The medium was then replaced with growth medium without antibiotics. 60 μg of shRNA plasmid was diluted in 3.75 ml of Opti-MEM® reduced serum medium. Then 150 μl of Lipofectamine™ 2000 was diluted in 3.75 ml of Opti-MEM® reduced serum medium and incubated at room temperature for 5 minutes. After incubation the diluted DNA was mixed gently with the diluted Lipofectamine™ 2000 and incubated at room temperature for 20 minutes. After incubation the DNA and Lipofectamine™ 2000 mixture was added to the EcoPack 2-293 cells and medium. The medium was changed after 4 hours to complete medium containing antibiotics.

The supernatant from the transfected EcoPack 2-293 cells containing the shRNA retroviral particles was harvested after 24 hours and 48 hours. To remove any unwanted debris from the cells the supernatants were centrifuged at 183 x g for 5 minutes at 4 °C. The 24 hour and 48 hour supernatants were then combined, aliquoted and then stored at -80 °C.

The titre of the virus was determined using NIH 3T3 cells. 1 x 10^5 cells were seeded into each well of a 6-well plate in 2 ml of complete medium. The next day 60 μl of 4 mg/ml polybrene was added to 20 ml of complete medium. The virus-containing medium was thawed and filtered through a 0.45 μm cellulose

acetate filter. The virus-containing medium was then diluted 10-fold by adding 150 μl to 1.35 ml of complete medium. This diluted virus-containing medium was then diluted as above a further five times. To infect the NIH 3T3 cells, 1 ml of diluted virus-containing medium was added to each well. The next day the medium on the NIH 3T3 cells was replaced with complete medium containing 2.5 μg/ml puromycin. The NIH 3T3 cells were grown in puromycin for a week, after which the number of colonies present at the highest dilution of the virus-containing medium was determined. This number was multiplied by the dilution factor to give the number of colony forming units (cfu)/ml.

To infect 3T3-L1 cells, 2 x 10^5 cells were seeded into a 10 cm plate. The next day the virus-containing medium was thawed and filtered through a 0.45 μm cellulose acetate filter. The virus-containing medium was added to the cells at a multiplicity of infection (MOI) of 50 and polybrene was added to a final concentration of 5 μg/ml. The cells were then incubated for 24 hours. After 24 hours the infected 3T3-L1 cells were sub-cultured at a 1 in 10 dilution into new 10 cm and 12-well plates as described in section 2.3.2. After a further 24 hours the medium on the infected 3T3-L1 cells was replaced with complete medium containing 1 μg/ml puromycin. The infected cells were grown in puromycin-containing medium for a least a week to select for cells stably expressing the shRNA construct. When the infected 3T3-L1 cells reached confluency they were differentiated as described in section 2.3.4.

2.5.2 HA-GLUT4-GFP lentivirus

HA-GLUT4-GFP lentivirus was prepared using Invitrogen™ ViraPower™ Lentiviral systems.

293T cells were co-transfected with the HA-GLUT4-GFP plasmid and the ViraPower™ packaging mix using Lipofectamine™ 2000. As a negative control some 293T cells were transfected without DNA. A reverse transfection procedure was employed. 9 μg ViraPower™ packaging mix and 3 μg HA-GLUT4-GFP plasmid was diluted in 1.5 ml Opti-MEM® reduced serum medium. In a separate tube 36 μl of Lipofectamine™ 2000 was diluted in 1.5 ml of Opti-MEM® reduced serum medium and incubated at room temperature for 5 minutes. After the incubation, the diluted DNA and diluted Lipofectamine™ 2000 were mixed gently and

incubated at room temperature for 20 minutes. During this incubation 293T cells were detached from the plates as described in section 2.3.2 and then counted. The 293T cells were resuspended at 1.2 x 10^6 cells/ml in growth medium without antibiotics. The DNA and Lipofectamine™ 2000 mixture was added to a 10 cm plate containing 5 ml of growth medium without antibiotics. Then 5 ml of the 293T cell suspension (6 x 10^6 total cells) was added to the plate and the cells incubated overnight at 37 ^oC. The next day the medium was replaced with growth medium without antibiotics. Lentivirus –containing supernatants were harvested 72 hours after transfection.

The day before lentivirus harvesting the 3T3-L1 fibroblasts to be infected were plated. 3T3-L1 fibroblasts were seeded at 1 x 10^5 cells per well of a 6-well plate. The next day the lentivirus-containing supernatants were harvested from the transfected 293T cells. The supernatants were centrifuged at 183 x g for 15 minutes at 4 ^oC to remove unwanted debris. The viral supernatants were then filtered through a 0.45 μm cellulose-acetate filter and aliquoted into crovials. Any virus not used was then stored at -80 ^oC. To infect 3T3-L1 fibroblasts a 2-fold serial dilution was used. Viral supernatant and 6 μg/ml polybrene was added to the cells and incubated for 24 hours at 37 ^oC. After incubation the medium on the infected 3T3-L1 fibroblasts was replaced with complete medium and the cells were incubated at 37 ^oC for a further 48 hours. After incubation the infected 3T3-L1 fibroblasts were sub-cultured as described in section 2.3.2 and diluted into 10 ml of complete medium. 2.5 ml was plated into a well of a 6-well plate and 7.5 ml was plated into a 10 cm plate. When the cells were just sub-confluent, the cells in the 6-well plate were analysed using flow cytometry as described in section 2.6.1 and the cells in the 10 cm plate were further sub-cultured and frozen down as described in sections 2.3.2 and 2.3.3. The infected cells will express HA-GLUT4-GFP for several passages.

2.5.3 Myc-stx 16 adenovirus

Myc-stx 16 adenovirus was produced by ViraQuest Inc. North Liberty, Iowa, US, using the myc-stx 16A in pShuttle-CMV plasmid in section 2.1.4.

To infect 3T3-L1 cells, 3T3-L1 fibroblasts were seeded in a 12-well plate and differentiated as described in section 2.3.4. At day 6 post-differentiation, 500 μl

of serum-free DMEM was placed in each well. Between 0 and 1000 plaque forming units (PFU)/cell was added to each well. The cells were then incubated at 37 ^{o}C for 6 hours. After incubation, 500 μl of DMEM containing 20% (v/v) FBS was added to each well and the cells were incubated overnight at 37 ^{o}C. The next day the medium was replaced with DMEM containing 10% (v/v) FBS. The following day (day 8 post-differentiation) the cells were lysed in 100 μl HES buffer (section 2.1.8) per well.

2.6 Flow cytometry methods

2.6.1 HA-GLUT4-GFP infection efficiency

The level of HA-GLUT4-GFP expression in the lentivirus-infected 3T3-L1 cells was determined by flow cytometry. The method was suggested by Prof. C. C. Mastick (University of Nevada) (Muretta *et al.*, 2008).

Cells were detached from the 6-well plate as described in section 2.3.2. A small volume of complete medium was added to the cells and the cells sedimented by centrifugation at 183 x g for 5 minutes at 4 ^{o}C. The cells were then washed twice and resuspended in ice-cold PBS (section 2.1.8). The level of GFP fluorescence (which corresponds to the level of HA-GLUT4-GFP expression) was determined using a Becton Dickinson FACScan machine and CellQuest software (BD Biosciences, Oxford, UK). The total number of cells (counts) analysed in each sample was set at 10,000. The cells were counted by the flow cytometer as each cell passed the laser.

The mean fluorescence intensity (MFI) of the GFP fluorescence was determined by calculating the geometric mean. The percentage of cells positively expressing HA-GLUT4-GFP was defined as the percentage of cells with a higher GFP fluorescence than the negative control cells. The percentage of cells positively expressing HA-GLUT4-GFP was determined by calculating the area under the HA-GLUT4-GFP-infected sample curve to the right of the negative control curve.

2.6.2 Cell sorting

Cell sorting was used to determine the population of 3T3-L1 adipocytes. The method of cell sorting is based on a paper by Prof. C. C. Mastick (University of Nevada) (Muretta *et al.*, 2008).

Wildtype 3T3-L1 adipocytes were detached from 10 cm plates by incubation with 1 mg/ml collagenase in PBS for 5 minutes at 37 ^{o}C. A small volume of complete medium was added to the cells and the cells sedimented by centrifugation at 183 x g for 5 minutes at 4 ^{o}C. The cells were then washed twice and resuspended in ice-cold PBS (section 2.1.8).

Cells were sorted using a Becton Dickinson FACSaria machine (BD Biosciences, Oxford, UK). The number of cells (events) sorted was set at 50,000. Cells were sorted on the basis of scattered light in terms of forward scatter (FSC-A) and side scatter (SSC-A) into P1 and P2 populations. FSC measures the size of the cell or cell volume. SSC measures the internal complexity of the cell or granularity. The P1 population was then sorted into P3 and P4 populations on the basis of autofluorescence which was measured as fluorescence in the allophycocyanin (APC) channel. During cell sorting, droplets containing individual cells were charged depending on which population they belonged to. Then each droplet was deflected into the correct container using an electrostatic deflection system.

Sorted cells were viewed using a Zeiss Axiovert microscope (Carl Zeiss Ltd, Hetrfordshire, UK), with a x 32 lens, numerical aperture 0.4.

2.6.3 HA-GLUT4-GFP surface labelling assay

To determine the level of HA-GLUT4-GFP translocation in 3T3-L1 adipocytes a flow cytometry assay was used. This assay is based on a paper by Prof. C. C. Mastick (University of Nevada) (Muretta *et al.*, 2008).

3T3-L1 adipocytes expressing HA-GLUT4-GFP were incubated with serum-free medium for 2 hours. The cells were then stimulated with or without 100 nM insulin for 30 minutes. After stimulation the cells were detached from the plates by incubation with 1 mg/ml collagenase in PBS for 5 minutes at 37 ^{o}C, and the

cells sedimented by centrifugation at 183 x g for 5 minutes at 4 ^{o}C. The cells were then washed twice and resuspended in ice-cold PBS (section 2.1.8). The cell suspension was incubated with HA.11 mouse monoclonal primary antibody or IgG isotype control from murine myeloma clone MOPC21 at 50 μg/ml for 60 minutes at 4 ^{o}C. The cells were washed three times with ice-cold PBS and then incubated with RPE-conjugated goat anti-mouse secondary antibody or Cy3-conjugated goat anti-mouse secondary antibody for 60 minutes at 4 ^{o}C. The cells were then washed three times and resuspended in ice-cold PBS. The cells were analysed using a MACSQuant™ Analyzer (Miltenyi Biotec Ltd, Surrey, UK) and FlowJo software (Tree Star, Inc. Oregon, US). The total number of cells (events) analysed in each sample was set at 10,000.

2.7 Confocal microscopy methods

All images were taken with using a Zeiss LSM Exciter confocal microscope (Carl Zeiss Ltd, Hetrfordshire, UK), under oil immersion with a x 64 lens, numerical aperture 1.4.

2.7.1 HA-GLUT4-GFP surface staining

3T3-L1 cells infected with a 1 in 2 or 1 in 4 dilution of HA-GLUT4-GFP lentivirus (section 2.5.2) were seeded onto glass coverslips in a 6-well plate. As a control cells infected without HA-GLUT4-GFP DNA were used. The cells were allowed to grow to confluency and differentiated as described in section 2.3.4. At 8 days post-differentiation the cells were incubated in serum-free medium for 2 hours and then treated with or without 100 nM insulin for 30 minutes.

To fix the cells, the coverslips were washed twice with PBS (section 2.1.8). Then 800 μl 3% (w/v) paraformaldehyde was added to each coverslip and incubated for 20-30 minutes. The paraformaldehyde was removed and the coverslips washed again with PBS. To quench the paraformaldehyde the coverslips were washed with 20 mM glycine in PBS.

After fixing, the cells were blocked by adding 800 μl BSA/Gly buffer (section 2.1.8) to the each coverslip and incubating for 20 minutes. The cells were then stained with HA.11 mouse monoclonal primary antibody at 1:500 dilution in

BSA/Gly buffer and incubated for 45 minutes. After staining the coverslips were washed 4 times with BSA/Gly. The cells were then stained with Cy3-conjugated goat anti-mouse secondary antibody or RPE-conjugated goat anti-mouse secondary antibody at 1:200 dilution in BSA/Gly buffer and incubated for 30 minutes. The cells were then washed 4 times with BSA/Gly. Finally the coverslips were dipped into PBS, dried and mounted onto a slide.

If internal staining of HA was required the cells were permeablised after the 20 mM glycine wash step with BSA/Gly/Sap buffer (section 2.1.8) and incubated for 20 minutes. The staining of the coverslips was perfomed as described above except with BSA/Gly/Sap buffer replacing BSA/Gly buffer in all steps.

2.8 96-well plate assays

2.8.1 HA-GLUT4-GFP surface labelling assay

3T3-L1 cells infected with a 1 in 4 dilution of HA-GLUT4-GFP lentivirus (section 2.5.2) were seeded in a 96-well plate (see plate diagram below). As a control cells infected without HA-GLUT4-GFP DNA were used. The cells were allowed to grow to confluency and differentiated as described in section 2.3.4. At 8 days post-differentiation the cells were incubated in serum-free medium for 2 hours and then treated with or without 100 nM insulin for 30 minutes.

Plate diagram:

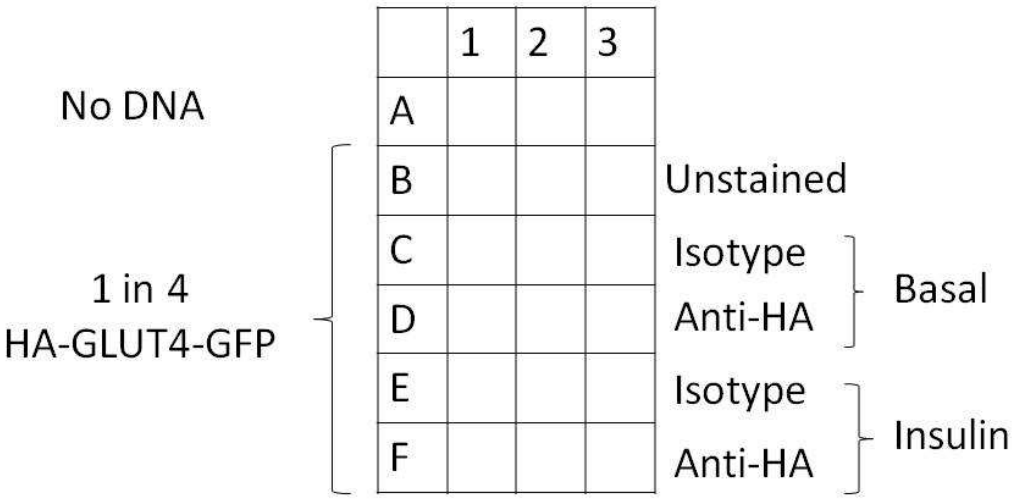

To fix the cells, they were washed three times with PBS (section 2.1.8). Then 200 µl 3% (w/v) paraformaldehyde was added to each well and incubated for 20-30 minutes. The paraformaldehyde was removed and the cells washed again with PBS. To quench the paraformaldehyde the cells were washed with 20 mM glycine in PBS. The cells were washed again with PBS. Then the cells were stained with HA.11 mouse monoclonal primary antibody or IgG isotype control from murine myeloma clone MOPC21 at 50 µg/ml for 60 minutes. After staining the cells were washed with PBS and stained with Cy3-conjugated goat anti-mouse secondary antibody for 60 minutes. Then the cells were washed with PBS and 200 µl PBS added to each well. The GFP and Cy3 fluorescence of the cells was determined using a FLUOstar OPTIMA microplate reader (BMG LABTECH Ltd, Aylesbury, UK).

The GFP and Cy3 fluorescence of the cells were used to calculate the mean fluorescence ratio (MFR) of basal or insulin-stimulated cells. The MFR of surface to total HA-GLUT4-GFP was used as a measure of HA-GLUT4-GFP translocation.

$$\text{MFR} = \frac{\text{MFI of HA-GLUT4-GFP at the cell surface}}{\text{MFI of total HA-GLUT4-GFP expression}}$$

$$\text{MFI of HA-GLUT4-GFP at the cell surface} = \text{mean Cy3 fluorescence of HA-stained cells} - \text{mean Cy3 fluorescence of isotype-stained cells}$$

$$\text{MFI of total HA-GLUT4-GFP expression} = \text{mean GFP fluorescence of HA-stained cells} - \text{mean GFP fluorescence of No DNA control cells}$$

2.8.2 HA-GLUT4-GFP recycling assay

3T3-L1 cells infected with a 1 in 4 dilution of HA-GLUT4-GFP lentivirus (section 2.5.2) were seeded in a 96-well plate (see plate diagram below). As a control cells infected without HA-GLUT4-GFP DNA were used. The cells were allowed to grow to confluency and differentiated as described in section 2.3.4. At 8 days post-differentiation the cells were incubated in serum-free medium for 2 hours and then treated with or without 170 nM insulin for 30 minutes. After treatment, the medium was replaced at specific time points with pre-warmed serum-free DMEM containing 50 µg/ml Cy3-HA.11 antibody (section 2.4.11) and with or

without 170 nM insulin. For basal cells the time points were 0, 2, 5 and 10 hours. For insulin-stimulated cells the time points were 0, 30, 60 and 120 minutes.

Plate diagram:

One plate was basal. A second plate was stimulated with 170 nM insulin. The plate below shows the time points for basal cells.

Time points (hours)		No DNA				1 in 4 HA-GLUT4-GFP		
		1	2	3		6	7	8
0	A				A			
2	B				B			
5	C				C			
10	D				D			

When the cells had finished incubating with the Cy3-HA.11 antibody, the 96-well plates were placed on ice and then washed four times with recycling assay wash buffer (section 2.1.8). The cells were fixed by adding 200 µl 3% (w/v) paraformaldehyde to each well and incubating for 20-30 minutes. The paraformaldehyde was removed and the cells were washed with PBS (section 2.1.8) and finally 200 µl PBS added to each well. The GFP and Cy3 fluorescence of the cells was determined using a FLUOstar OPTIMA microplate reader (BMG LABTECH Ltd, Aylesbury, UK).

The GFP and Cy3 fluorescence of the cells were used to calculate the mean Cy3: GFP ratio at each time point of basal or insulin-stimulated cells. The mean Cy3: GFP ratio was used as a measure of HA-GLUT4-GFP recycling.

$$\text{Mean Cy3: GFP ratio} = \frac{\text{MFI of Cy3-labelled HA-GLUT4-GFP}}{\text{MFI of total HA-GLUT4-GFP expression}}$$

$$\text{MFI of Cy3-labelled HA-GLUT4-GFP} =$$

mean Cy3 fluorescence of Cy3-HA-labelled HA-GLUT4-GFP cells
− mean Cy3 fluorescence of Cy3-HA-labelled No DNA control cells

MFI of total HA-GLUT4-GFP expression =
mean GFP fluorescence of HA-GLUT4-GFP cells
− mean GFP fluorescence of No DNA control cells

2.9 Yeast methods

2.9.1 Yeast cultures

Yeast cells were picked from a colony or a frozen glycerol stock using a pipette tip. The cells were put into YEPD, S-D –Ura –Met or S-Raf/Gal –Ura –Leu medium (section 2.1.8) and incubated at 30 °C until the culture had reached the required OD_{600} (optical density at 600 nm) or overnight.

2.9.2 Preparation of competent cells

A 50 ml culture was prepared as described in section 2.9.1 in YEPD (section 2.1.8). The culture was grown to an OD_{600} of 0.5-1.0. Yeast cells were harvested by centrifugation at 3000 x g for 2 minutes. The cells were resuspended in 10 ml LiTE-Sorb (section 2.1.8) and then sedimented as above. The resulting pellet was resuspended in 1 ml LiTE-Sorb and incubated at 30 °C for 1 hour. After incubation the cells were placed on ice for 20 minutes. The cells were now ready for transformation. Any remaining cells not used for transformation were stored at -80 °C after the addition of an equivalent volume of 40% (w/v) glycerol, 0.5% (w/v) NaCl.

2.9.3 Yeast transformation

10 μg DNA was added to 100 μl competent cells (section 2.9.2). An equivalent volume of 70% (w/v) PEG-3350 was added and mixed by inversion. The mixture was incubated for 30-45 minutes at 30 °C and then incubated at 42 °C for 20 minutes to heat shock. After heat shock the cells were sedimented by centrifugation at 4000 x g for 2 minutes and resuspended in sterile water or YEPD (section 2.1.8), 1.2 M sorbitol. The transformed yeast cells were plated on

S-D –Ura –Met or S-D –Ura –Leu plates (section 2.1.8) and incubated at 30 °C for 2-4 days. The transformed yeast cells could be stored on the plate at 4 °C for up to one month.

2.9.4 Preparation of samples for SDS-PAGE analysis

To prepare samples of yeast cells, a 10 ml overnight culture was prepared as described in section 2.9.1. The next day the OD_{600} of the culture was determined. A volume corresponding to 10 OD_{600} was centrifuged at 4000 x g for 2 minutes and resuspended in 100 µl TWIRL buffer (section 2.1.8). The samples were then incubated at 65 °C for 10 minutes before analysis by SDS-PAGE as described in sections 2.4.4, 2.4.5 and 2.4.6.

2.9.5 Ste3p-myc endocytosis assay

A 10 ml overnight culture was prepared as described in section 2.9.1 in S-Raf/Gal –Ura –Leu medium (section 2.1.8) for each strain. The OD_{600} of the cultures was checked the next day. Each culture was diluted into 50 ml S-Raf/Gal –Ura –Leu medium to an OD_{600} of 0.2 and then incubated at 30 °C until the OD_{600} reached 0.4. Once the OD_{600} had reached this value, (D)-glucose was added to a final concentration of 3 % (w/v) to repress the *GAL1* promoter and inhibit expression of Ste3p-myc. 4 ml of culture was harvested at 0, 20, 40, 60 and 80 minutes after the addition of (D)-glucose. At each time point the OD_{600} of the remaining culture was also measured. To harvest the cells, 4 ml of culture was added to 40 µl of 1 M sodium azide and the cells placed on ice for 5 minutes. The cells were then sedimented by centrifugation at 6000 x g for 5 minutes at 4 °C. The supernatant was decanted and the pellet was resuspended and transferred to a 1.5 ml microcentrifuge tube. The cells were sedimented by centrifugation at 2500 x g for 2 minutes. The supernatant was removed by aspiration. The pellet was resuspended in TWIRL buffer (section 2.1.8) in a volume corresponding to the OD_{600} of the culture when the cells were harvested. The samples were then incubated at 65 °C for 10 minutes.

2.9.6 KCl osmotic stress assay

A 10 ml overnight culture was prepared as described in section 2.9.1 in S-D –Ura –Met medium (section 2.1.8) for each strain. The OD_{600} of each strain was determined the next day and the cultures were diluted to 1 OD_{600}/ml. Ten-fold serial dilutions were made of each culture. 5 μl aliquots of the 1 OD_{600}/ml culture and the serial dilutions were spotted onto S-D –Ura –Met plates with or without 1.5 M KCl. The plates were incubated at 30 °C for 2-4 days.

Chapter 3 Effect of syntaxin 16 on GLUT4 trafficking

3.1 Introduction

In adipocytes insulin stimulates the translocation of GLUT4 from unique intracellular storage sites to the cell surface (Bryant *et al.*, 2002). In type II diabetes this translocation is impaired. The translocation of GLUT4 is an example of regulated membrane trafficking and involves the fusion of vesicles with specific target membranes. This is mediated by SNARE proteins (Hong, 2005).

Stx 16 is a t-SNARE found in the TGN and is known to mediate transport between the early endosome and the TGN (Mallard *et al.*, 2002). There is a lot of data to suggest that stx 16 has a role in GLUT4 trafficking. Firstly stx 16 colocalises with GLUT4 in a subdomain of the TGN and is highly enriched in GLUT4 vesicles. Also insulin stimulates the translocation of stx 16 to the cell surface (Shewan *et al.*, 2003). Recent data from our lab has shown that overexpression of the cytosolic domain of stx 16 significantly slows the reversal of insulin-stimulated glucose transport. Also depletion of stx 16 by RNAi reduces insulin-stimulated glucose transport over a range of insulin concentrations. It was also noted in these cells that the total GLUT4 cellular levels were reduced by 30% (Proctor *et al.*, 2006). This suggests that GLUT4 may be missorted to a degradation pathway in stx 16-depleted cells. The above data suggests that stx 16 may control sequestration of GLUT4 in its storage site(s).

3.2 Aims of this chapter

In this chapter the effect of stx 16 on GLUT4 trafficking was investigated. In order to blockade stx 16 function a shRNA approach was used to produce 3T3-L1 adipocytes stably depleted of stx 16. The level of GLUT4 and a number of other proteins was examined in these cells. Also the distribution of GLUT4 and other insulin-responsive proteins was investigated. Finally a myc-tagged human stx 16 (which is resistant to the shRNA constructs) was expressed in the stx 16-depleted cells to rescue the stx 16 knockdown.

3.3 Results

3.3.1 Knockdown of stx 16 expression in 3T3-L1 adipocytes

As mentioned in section 3.1 stx 16 seems to play a role in GLUT4 trafficking. In order to further investigate the role of stx 16 in GLUT4 trafficking, the expression of stx 16 was knocked-down using a shRNA approach. This method was used to generate 3T3-L1 cells which were stably depleted of stx 16. Four different stx 16-targeting shRNAs were used and scrambled shRNA was used as a negative control. After infection with the shRNA retroviruses membrane extracts from the 3T3-L1 adipocytes were blotted for the presence of stx 16.

As shown in figure 3.1, compared with the negative control the level of stx 16 is reduced in cells infected with shRNAs 1-4 to varying degrees, whereas the level of the unrelated SNARE SNAP 23 is not affected. In particular shRNA4 gave the greatest reduction of 96.74 ± 2.22% (mean ± S.D.) ($P < 0.001$).

3.3.2 Effect of stx 16 knockdown on the expression of other SNARE proteins

Stx 16 is a t-SNARE found in the TGN and it forms a t-SNARE complex with stx 6 and Vti1a (Mallard *et al.*, 2002). Stx 16 is also known to interact with the SM protein mVps45 (Dulubova *et al.*, 2002). Therefore the effect of stx 16 knockdown on these important proteins was investigated.

Figure 3.2 shows that in shRNA4-infected cells the levels of stx 6 and mVps45 were significantly reduced compared with the negative control. Stx 6 was reduced by 83.01 ± 5.74% ($P < 0.05$) and mVps45 was reduced by 57.09 ± 32.68% ($P < 0.05$). However the level of Vti1a remained unaffected. Also the level of Vti1b (a closely related isotype of Vti1a) was not significantly affected.

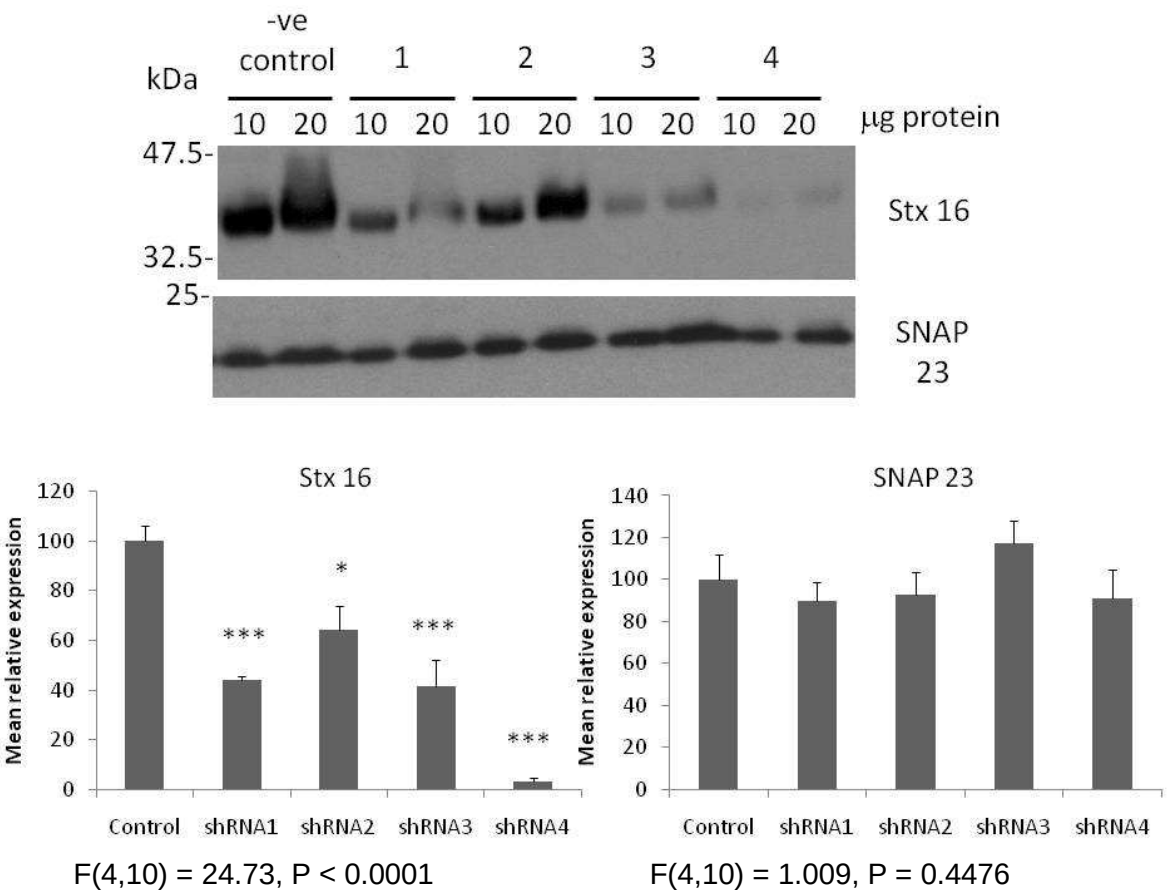

Figure 3.1. Knockdown of syntaxin 16 expression in 3T3-L1 adipocytes.

3T3-L1 fibroblasts were infected with retrovirus expressing negative control shRNA or shRNA targeting syntaxin (stx) 16 (1-4) as described in section 2.5.1.

Upper panel: Membrane samples were prepared as described in section 2.4.1 and blotted for stx 16 and SNAP 23 (section 2.4.4-2.4.6). Rabbit stx16 antiserum and rabbit SNAP23 antiserum were used at 1:1000 dilution. SNAP 23 was used as a loading control. The amount of protein loaded in each lane is indicated at the top of the blots. The numbers at the side of the blots indicate molecular weight in kDa.

Lower panel: Mean relative expression, compared to the negative control which was set at 100%. The mean is calculated from 3 independent experiments. Blots were quantified by densitometry using ImageJ software. Error bars are S.E.M (n = 3). Statistical analysis was performed using the software program GraphPad Prism 5. The significance between groups was determined by one-way ANOVA. F ratio and probability values are quoted. Dunnett's multiple comparison post-test was performed to determine which shRNA significantly differed from the negative control. * denotes Dunnett's $P < 0.05$. *** denotes $P < 0.001$.

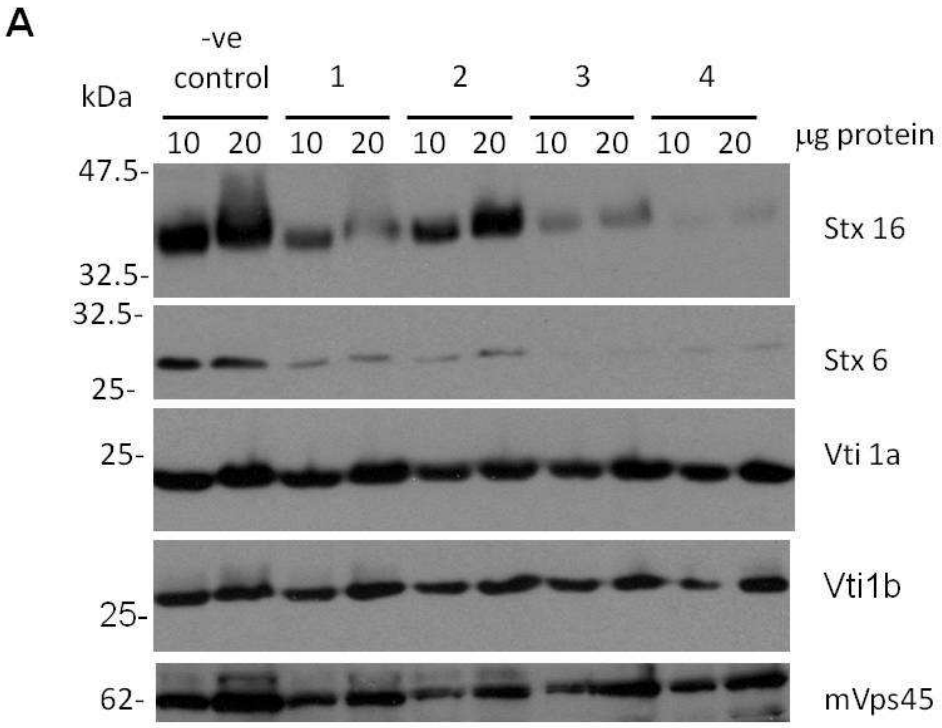

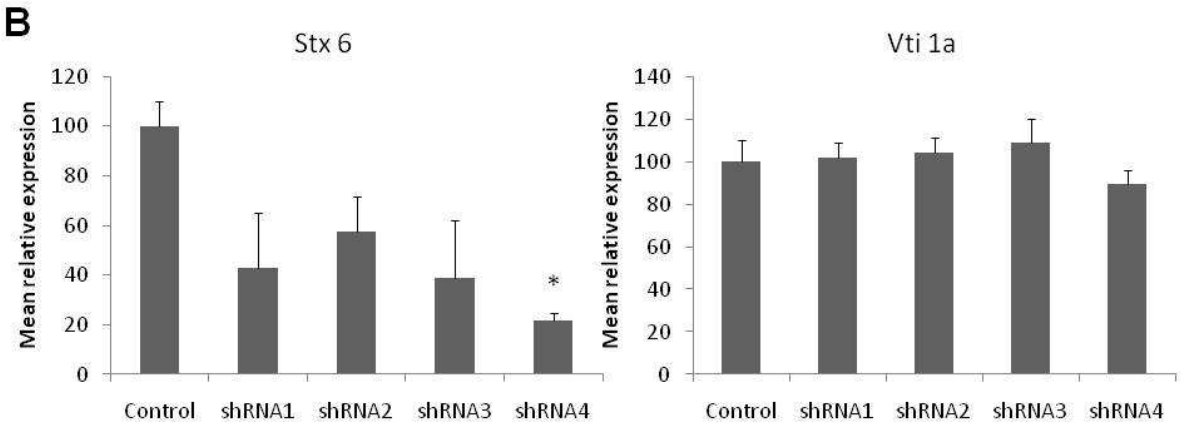

F(4,10) = 3.567, P = 0.0468

F(4,10) = 0.7231, P = 0.5957

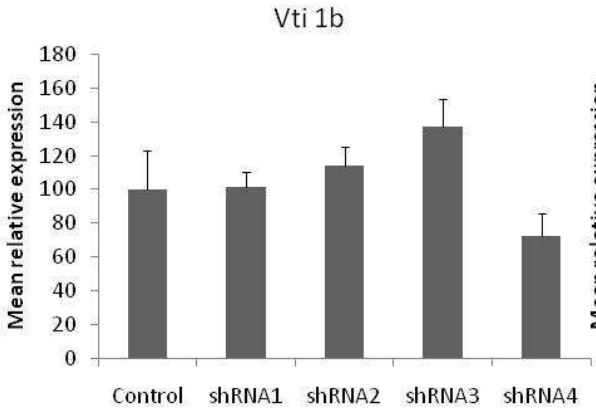

F(4,10) = 2.322, P = 0.1276

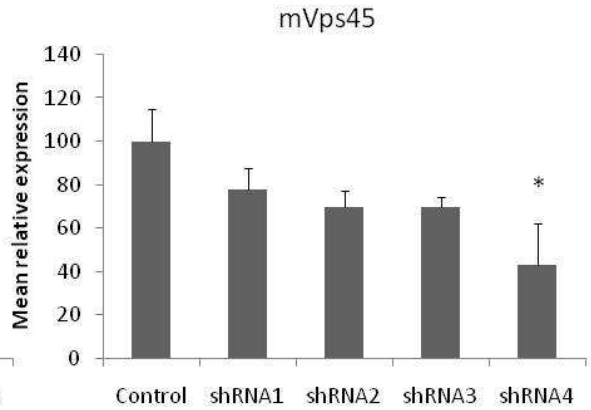

F(4,10) = 3.451, P = 0.0485

Figure 3.2.Effect of syntaxin 16 knockdown on expression of other SNARE proteins.

3T3-L1 fibroblasts were infected with retrovirus expressing negative control shRNA or shRNA targeting syntaxin (stx) 16 (1-4) as described in section 2.5.1.

A. Membrane samples were prepared as described in section 2.4.1 and blotted for stx 16, stx 6, vti1a, vti1b and mVps45 (section 2.4.4-2.4.6). All antibodies were used at a 1:1000 dilution. The stx 16 blot from figure 3.1 is included as a reference. The amount of protein loaded in each lane is indicated at the top of the blots. The numbers at the side of the blots indicate molecular weight in kDa.

B. Mean relative expression, compared to the negative control which was set at 100%. The mean is calculated from 3 independent experiments. Blots were quantified by densitometry using ImageJ software. Error bars are S.E.M (n = 3). Statistical analysis was performed using the software program GraphPad Prism 5. The significance between groups was determined by one-way ANOVA. F ratio and probability values are quoted. Dunnett's multiple comparison post-test was performed to determine which shRNA significantly differed from the negative control. * denotes Dunnett's $P < 0.05$.

3.3.3 Stx 16 knockdown affects total GLUT4 cellular levels

It was important to show whether the role of stx 16 on GLUT4 trafficking was specific or whether stx 16 knockdown had a general effect on proteins in the endosomal system. Therefore the levels of GLUT4, IRAP, which traffics in concert with GLUT4 (Garza and Birnbaum, 2000) and TfR were determined in the stx 16-depleted cells.

As shown in figure 3.3, compared with the negative control, the level of GLUT4 was significantly reduced in cells infected with shRNA2 and 4. The level of GLUT4 was reduced by 34.34 ± 3.82% ($P < 0.01$) in shRNA2-infected cells. The level of GLUT4 was reduced by 21.42 ± 5.16% ($P < 0.05$) in shRNA4-infected cells. In contrast the level of IRAP was not significantly affected. Also the level of TfR was unaffected.

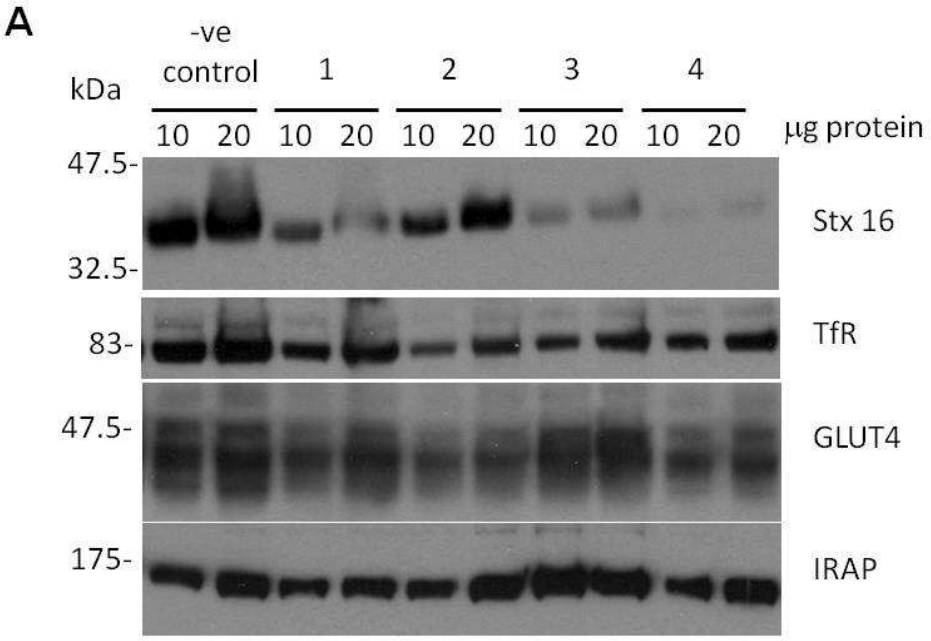

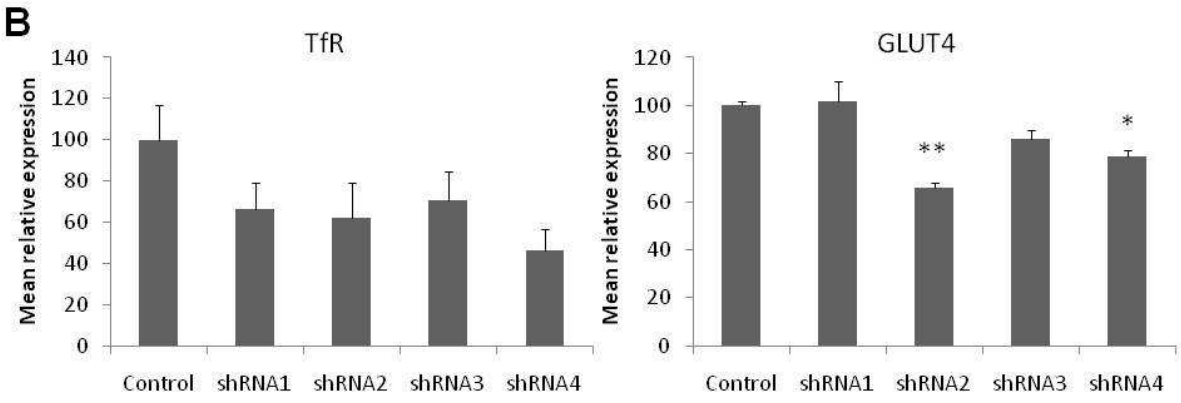

F(4,10) = 1.833, P = 0.1992

F(4,10) = 11.23, P = 0.0010

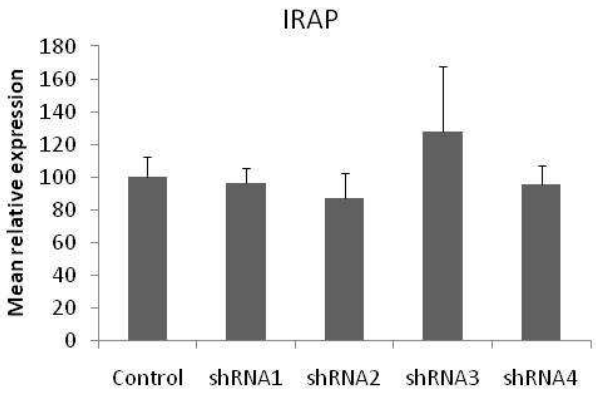

F(4,10) = 0.5615, P = 0.6961

Figure 3.3.Effect of syntaxin 16 knockdown on expression of GLUT4.

3T3-L1 fibroblasts were infected with retrovirus expressing negative control shRNA or shRNA targeting syntaxin (stx) 16 (1-4) as described in section 2.5.1.

A. Membrane samples were prepared as described in section 2.4.1 and blotted for stx 16, transferrin receptor (TfR), glucose transporter 4 (GLUT4), and insulin-responsive aminopeptidase (IRAP) (section 2.4.4-2.4.6). All antibodies were used at 1:1000 dilution. The stx 16 blot from figure 3.1 is included as a reference. The amount of protein loaded in each lane is indicated at the top of the blots. The numbers at the side of the blots indicate molecular weight in kDa.

B. Mean relative expression, compared to the negative control which was set at 100%. The mean is calculated from 3 independent experiments. Blots were quantified by densitometry using ImageJ software. Error bars are S.E.M (n = 3). Statistical analysis was performed using the software program GraphPad Prism 5. The significance between groups was determined by one-way ANOVA. F ratio and probability values are quoted. Dunnett's multiple comparison post-test was performed to determine which shRNA significantly differed from the negative control. * denotes Dunnett's $P < 0.05$. ** denotes $P < 0.01$.

3.3.4 Effect of stx 16 knockdown on GLUT4 cellular distribution

After discovering a reduction in total GLUT4 cellular levels in stx 16-depleted cells, the distribution of GLUT4 within the cell was investigated. 3T3-L1 adipocytes infected with negative control shRNA or shRNA4 (the highest stx 16 knockdown) were fractionated into mitochondria/nuclei (M/N), high density microsome (HDM), low density microsome (LDM), plasma membrane (P/M) and soluble protein (Sol.) fractions.

Figure 3.4 shows that in the shRNA4-infected cells, stx 16 was found only in the LDM fraction, whereas in the negative control stx 16 was found in both the HDM and LDM fractions. The LDM fraction represents endosomal membranes and GSVs. The HDM fraction represents the ER and Golgi. This suggests that in shRNA4-infected cells the remaining stx 16 is localised to the endosomal membranes and perhaps the GSVs. GLUT4 was present in both the HDM and LDM fractions of negative control and shRNA4-infected cells. This suggests that the overall localisation of GLUT4 may not be altered in stx 16-depleted cells. TfR was mostly found in the LDM fraction in both negative control and shRNA4-infected cells which is expected for a protein which is localised to endosomal membranes. Finally SNAP23 was only present in the P/M fraction in negative control and shRNA4-infected cells which is where SNAP23 is normally localised.

Perhaps stx 16 knockdown might not affect the localisation of GLUT4 but the level of GLUT4 in each fraction. In figure 3.5 a comparison was made of the HDM fractions and the LDM fractions of negative control and shRNA1-4-infected cells. In the HDM fractions, stx 16 is greatly reduced in shRNA3 and 4-infected cells compared with the negative control. A lower level of stx 16 is also seen in the LDM fractions of these cells. This suggests that majority of stx 16 is depleted from the ER and Golgi and that the remaining stx 16 is localised to the endosomal membranes and perhaps the GSVs which agrees with figure 3.4.

GLUT4 is much lower in the HDM and LDM fractions of shRNA2 and 3-infected cells compared with the negative control. This suggests that there is much less GLUT4 in the ER, Golgi, endosomal membranes and GSVs in shRNA2 and 3-infected cells. A smaller reduction is seen in the HDM and LDM fractions of

shRNA1 and 4-infected cells. The levels of IRAP are quite similar in the HDM fraction of the negative control and shRNA1, 2 and 4-infected cells. This suggests that there is very little change in the levels of IRAP in the ER and Golgi of those cells. But the levels of IRAP are very low in the shRNA3-infected cells. In the LDM fractions there seems to be little difference between the levels of IRAP in the negative control and shRNA4-infected cells, which suggests that the level of IRAP in the endosomal membranes and GSV in these cells is similar to that in the negative control. However, the levels of IRAP are a little lower in the shRNA1-3-infected cells.

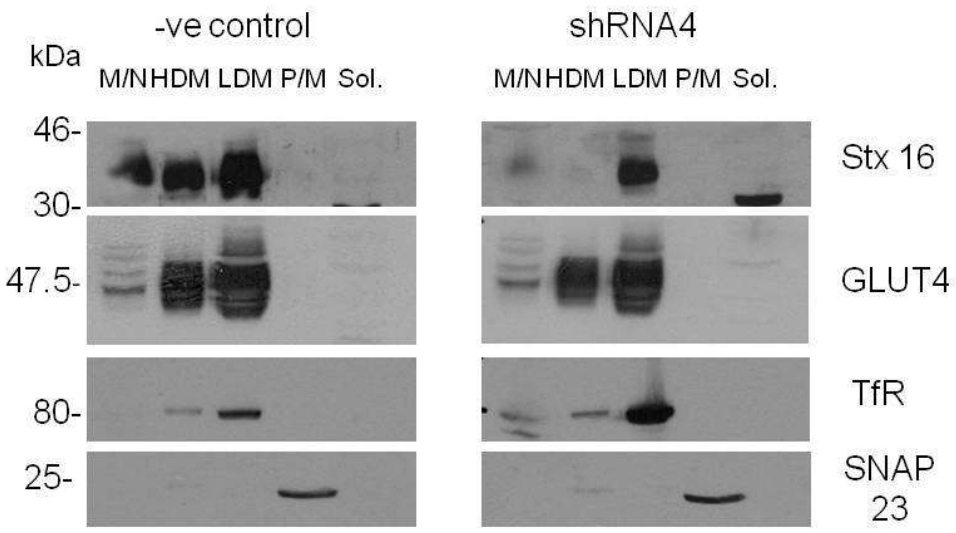

Figure 3.4.Distribution of GLUT4 in stx 16-depleted 3T3-L1 adipocytes.

3T3-L1 fibroblasts were infected with retrovirus expressing negative control (-ve control) shRNA or shRNA targeting stx 16 (shRNA4) as described in section 2.5.1. Lysate from two 10 cm plates of 3T3-L1 adipocytes was fractionated as described in section 2.4.2 into mitochondria and nuclei (M/N), heavy density microsome (HDM), low density microsome (LDM), plasma membrane (P/M) and soluble (Sol.) fractions. 1/20 of the fractions (10 μl) were blotted for stx 16, GLUT4, TfR and SNAP 23 (sections 2.4.4-2.4.6). All antibodies were used at a 1:1000 dilution. The numbers at the side of the blots indicate molecular weight in kDa. The figure shows a representative set of blots (n = 2).

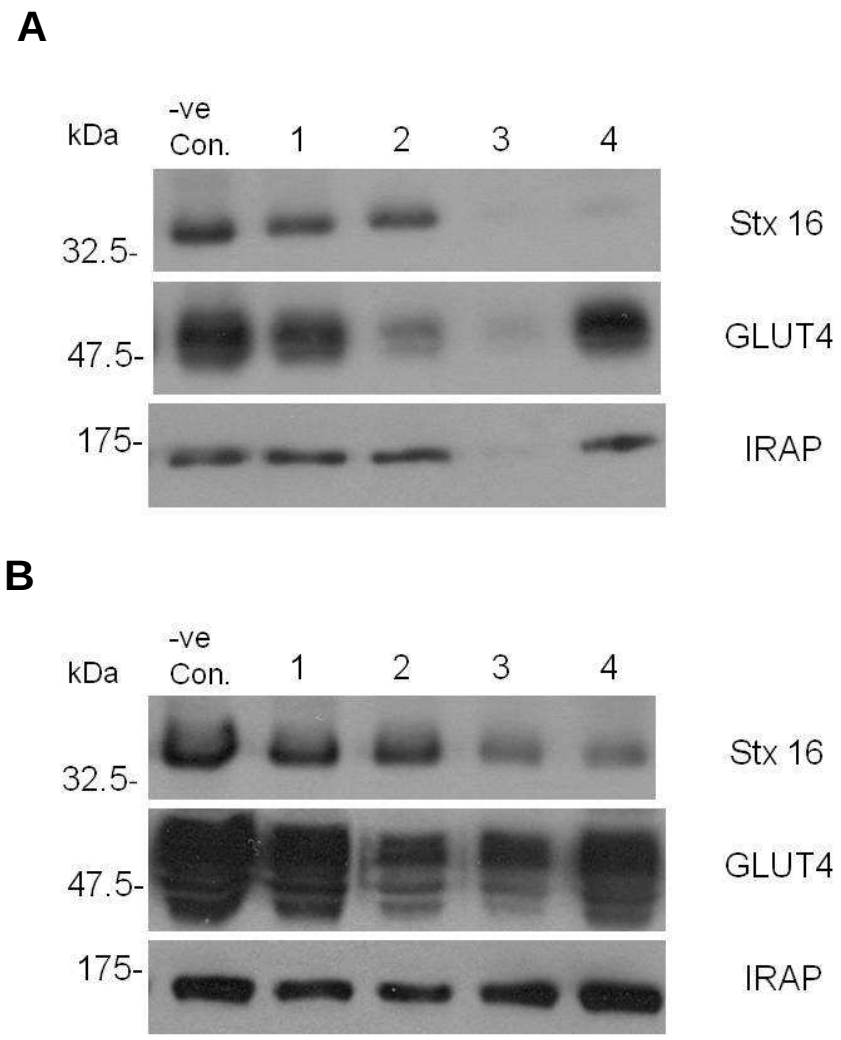

Figure 3.5. Level of GLUT4 in HDM and LDM fractions of stx 16-depleted 3T3-L1 adipocytes.

3T3-L1 fibroblasts were infected with retrovirus expressing negative control (-ve Con.) shRNA or shRNA targeting stx 16 (1-4) as described in section 2.5.1. Lysate from two 10 cm plates of 3T3-L1 adipocytes was fractionated as described in section 2.4.2 into HDM and LDM fractions. 1/20 of the fractions (10 μl) were blotted for stx 16, GLUT4 and IRAP (sections 2.4.4-2.4.6). All antibodies were used at a 1:1000 dilution. The numbers at the side of the blots indicate molecular weight in kDa.

A. HDM fractions.
B. LDM fractions.

The figure shows a representative set of blots (n = 2).

3.3.5 Expression of myc-stx 16A in stx 16 knockdown cells

Once the knockdown of stx 16 expression in 3T3-L1 adipocytes was demonstrated, a way to test the results were due to the depletion of stx 16 was needed. Previous work in the lab had created a myc-tagged human stx 16A in an adenoviral vector. This human stx 16 should be resistant to knockdown by the shRNAs which were designed to target murine stx 16 and do not align with the human stx 16A sequence.

First of all the optimum PFU/cell to use for infection with the myc-stx16A adenovirus in wild type 3T3-L1 adipocytes was determined. Figure 3.6 shows that 1000 PFU/cell resulted in expression of the myc-stx 16A at a similar level as that of endogenous stx 16. Once the optimum PFU/cell was determined, negative control and shRNA4-infected 3T3-L1 adipocytes were infected with or without 1000 PFU/cell myc-stx 16A adenovirus. As shown in figure 3.6, endogenous stx 16 is present in the negative control-infected cells with or without myc-stx 16A adenovirus. Endogenous stx 16 is not present in the shRNA4-infected cells with or without adenovirus as expected. The myc-stx 16A is only present in the cells infected with 1000 PFU/cell adenovirus and is present in both negative control and shRNA4-infected cells.

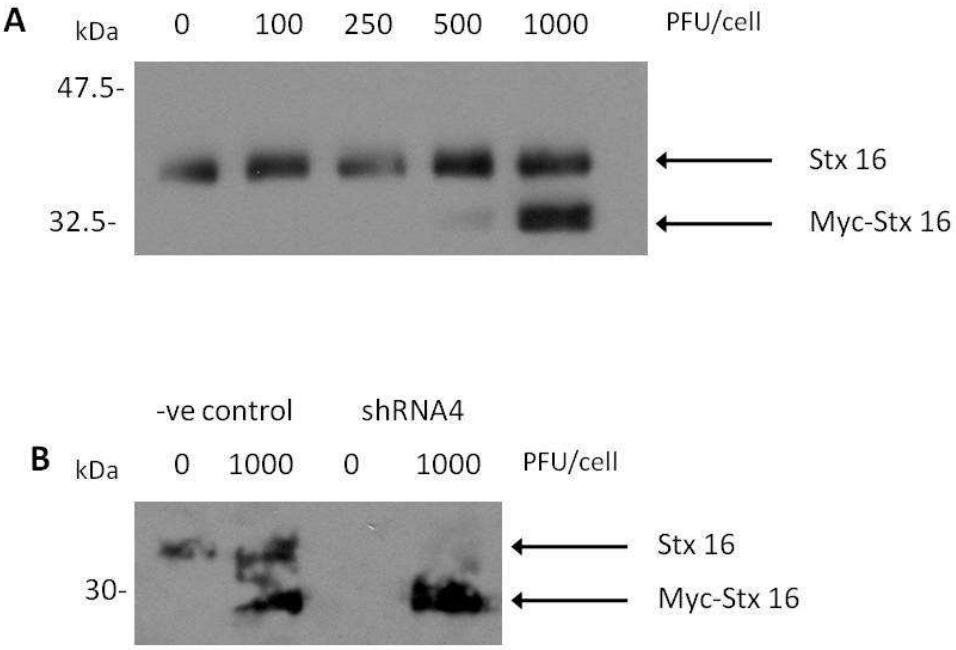

Figure 3.6.Expression of a shRNA-resistant form of myc-stx 16A in stx 16-depleted 3T3-L1 adipocytes.

A. Wild type 3T3-L1 adipocytes were infected at day 6 post-differentiation with adenovirus expressing myc-tagged human stx 16A (Myc-Stx 16) as described in section 2.5.3. A range of 0-1000 PFU/cell was used as indicated in the figure. At day 8 post-differentiation cells were lysed in HES (2.1.9) and the lysates were blotted for stx 16 (sections 2.4.4-2.4.6). 1/10 of the lysate (10 μl) was loaded in each lane. Rabbit stx 16 antiserum was used at a 1:1000 dilution. The bands corresponding to endogenous stx 16 (Stx 16) and Myc-Stx16 are indicated by the arrows. The numbers at the side of the blots indicate molecular weight in kDa.

B. 3T3-L1 fibroblasts were infected with retrovirus expressing negative control (-ve control) shRNA or shRNA targeting stx 16 (shRNA4) as described in section 2.5.1. At day 6 post-differentiation the cells were infected with or without 1000 PFU/cell of adenovirus expressing myc-stx 16A (Myc-Stx 16) as described in section 2.5.3. At day 8 post-differentiation cells were lysed in HES and the lysates were blotted for stx 16 (sections 2.4.4-2.4.6). 1/10 of the lysate (10 μl) was loaded in each lane. Rabbit stx 16 antiserum was used at a 1:1000 dilution. The bands corresponding to endogenous stx 16 (Stx 16) and Myc-Stx16 are indicated by the arrows. The numbers at the side of the blots indicate molecular weight in kDa.

3.4 Discussion

Previous research has shown that stx 16 may have a role in GLUT4 trafficking (Proctor *et al.*, 2006). Proctor *et al.* showed that knockdown of stx 16 using a morpholino antisense oligonucleotide resulted in a marked reduction in insulin-stimulated glucose transport and a 30% loss in total GLUT4 cellular levels. In this chapter a different approach was used to knockdown stx 16 expression to generate 3T3-L1 cells stably depleted in stx 16. These cells were then used to confirm and further investigate the results of this paper.

To knockdown expression of stx 16, a shRNA approach was used. Four different shRNA oligonucleotides (see table in 2.1.5) were designed to target stx 16 using Clontech's online RNAi designer tools. Target sequences were selected according to several criteria. First of all the sequences were 19 bp in length as it has been shown that shRNAs with 19 bp stems give efficient knockdown (Brummelkamp *et al.*, 2002). The maximum hairpin melting temperature (T_m) was set at 45 ^oC to reduce the problem of internal hairpins in the shRNA sequence which can reduce the efficiency of the knockdown achieved. Also the shRNA sequences were selected to have a higher thermal stability at the 5' end of the sense strand compared with the 3' end (in this case, higher thermal stability was a Tm difference of 1 ^oC between the four bases at the 5' end compared with the 3'end). This is thought to promote entry of the targeting strand of the shRNA into the RISC complex and therefore increase efficiency of the knockdown (Schwarz *et al.*, 2003). Clontech's own studies suggested additional criteria for shRNA sequence selection. Sequences were selected to have an optimal GC content of 45%. Also all sequences with stretches of five or more of the same base (polyN) and sequences with a low complexity (alternating sequences or sequences without one of the four bases) were ignored. Finally the sequences were selected according to two position- specific criteria. All selected sequences had an A at position 6 and at least one A or T at residues 18 and 19 (Reynolds *et al.*, 2004). The criteria described above were used to increase the efficiency of the knockdown of stx 16 expression in 3T3-L1 adipocytes. Four different target sequences were selected from the list generated by Clontech's RNAi Target Sequence Selector. The sequences were chosen to target different regions of the stx 16 sequence in the hope that at least one of the four shRNA sequences would knockdown stx 16 expression with high efficiency.

Once the four shRNA sequences were selected, the full oligonucleotides were designed using Clontech's shRNA sequence designer. In this step, the other sequences required for cloning and expression of the shRNA sequence were added to the oligonucleotide sequence. Each oligonucleotide contained the following elements; a *Bam*H I overhang at the 5' end, the 19 nucleotides of the shRNA sense strand, a hairpin loop sequence, the 19 nucloetides of the shRNA antisense strand, a Pol III termination site of 6 consecutive thymidine residues, a *Mlu* I site to allow verification of the cloned inserts and an *Eco*R I overhang at the 3' end of the oligonucleotide. Also if the shRNA sequence did not start with a guanine or adenine, then an extra guanine was added to the 5' end of the shRNA sense strand to allow initiation of Pol III transcription. Once the oligonucleotides had been designed, they were cloned into the RNAi-Ready pSIREN-RetroQ vector (section 2.5.1). The cloned vectors were then transfected into EcoPack2-293 packing cells, which produced retroviral particles. The retroviral particles were then used to infect 3T3-L1 fibroblasts. The retroviral method of shRNA delivery was chosen as it provided a highly efficient way to stably express the shRNAs in 3T3-L1 adipocytes.

Knockdown of stx 16 using shRNA resulted in a reduction of approximately 95% in stx 16 levels using the shRNA4 construct ($P < 0.001$) (Fig. 3.1). This knockdown is similar to the levels achieved by Proctor *et al.* (Proctor *et al.*, 2006).

The knockdown of stx 16 was quantified by densitometry of western blots produced using HRP and ECL. This is one of the most commonly used methods of protein detection and offers rapid and sensitive results with a good signal to noise ratio. However film has a limited linear dynamic range, therefore it was important that several exposures were taken to help ensure that the signal from the blot fell within the linear range.

As stx 16 is part of a t-SNARE complex it was important to investigate the effect of stx 16 knockdown on the levels of other SNARE proteins. Figure 3.2 shows that knockdown of stx 16 by shRNA4 led to a reduction in the level of stx 6 compared with the negative control. Cells infected with shRNA4 showed an approximately 80% reduction in stx 6 ($P < 0.05$). This result contradicts the data of Proctor *et al.* which showed that stx 16 knockdown by a morpholino antisense oligonucleotide did not affect the levels of stx 6 or stxs 4, 8 and 12 (Proctor *et*

al., 2006). This may be due to the differences between the methods of knockdown of stx 16. In the current study, 3T3-L1 fibroblasts were depleted of stx 16 by stable expression of shRNA targeted to stx 16. Antibiotic selection ensured that only cells expressing shRNA remained and the cells were cultured for at least a week post- infection with the shRNA-expressing retrovirus. The shRNA-expressing cells were then differentiated to adipocytes and membranes were prepared and the level of stx 16 and the other proteins tested was determined. This method ensures that all the cells tested were expressing the shRNA and no non-infected cells could alter the result. Also as the cells were cultured for at least a week post-infection and then differentiated, the long-term effects of stx 16 knockdown could be determined. This would allow any changes in expression of other proteins as a consequence of stx 16 knockdown to occur. As a retroviral expression system was used, it meant that the shRNA expression construct was integrated into the cells' DNA and shRNA was continually expressed over the course of the experiment which allowed the long term effects of stx 16 knockdown to be examined.

The method used by Proctor *et al.* involved electroporating 3T3-L1 adipocytes with morpholino antisense oligonucleotide. Lysates were then prepared from the cells 48 hours later and the level of stxs, 4, 8, 12 and 16 was determined. This method does not select for cells containing the morpholino antisense oligonucleotide and so cells which have not been successfully electroporated may affect the results obtained. Also the cells were tested only 48 hours post-electroporation which may not allow time for changes of expression due to stx 16 knockdown to occur. The stability of the morpholino antisense oligonucleotide over a long period of time has not been tested so it is not known how long the morpholino antisense oligonucleotide exerts its effect on stx 16 expression.

Recent data has also shown that knockdown of stx 16 leads to a reduction in stx 6 levels (Ganley *et al.*, 2008). HEK293 cells transfected with short interfering RNA (siRNA) against stx 16 showed an 80% reduction in stx 6. Also cells transfected with siRNA against stx 6 showed a 30% reduction in stx 16. The authors suggest that the majority of stx 6 may be complexed to stx 16 in the cell and that stx 16 is an important stabiliser of stx 6. The siRNA sequence used to knockdown stx 16 by Ganley *et al.* was not the same as any of the shRNA

sequences used in this study (see table in 2.1.5). This is probably because the siRNA sequence was designed to be used against human stx 16 rather than murine stx 16. Vti1a levels were unaffected which suggests that stx 16 is not required to stabilise the levels of Vti1a. Also the level of the related Vti1b was not significantly affected.

As knockdown of stx 16 leads to a reduction in the levels of stx 6 it is possible that some of the effects observed in stx 16-depleted cells are due to the lower levels of stx 6. Stx 6 is part of the same t-SNARE complex as stx 16 with Vti1a (Mallard *et al.*, 2002).Therefore any reduction in the level of stx 6 will have an effect on the trafficking pathways involving that t-SNARE complex. However stx 6 is also a part of several other t-SNARE complexes and seems to be involved in a number of different trafficking pathways involving those complexes (Wendler and Tooze, 2001). This means that the reduction in stx 6 caused by knockdown of stx 16 may have effects other than those involving stx 16. Therefore in order to determine whether the effects observed in stx 16-depleted cells were specific for stx 16, myc-tagged human stx 16A was expressed in negative control and shRNA4-infected cells (Fig. 3.6). If expression of myc- tagged human stx 16 rescues the effects observed in stx 16-depleted cells, the effects should be specific to the function of stx 16 (see discussion of Fig. 3.6 later in this section).

Interestingly, stx 16 knockdown with shRNA4 resulted in an approximately 60% reduction in mVps45 levels ($P < 0.05$). mVps45 is a SM protein which binds to stx 16 and regulates t-SNARE assembly (Dulubova *et al.*, 2002). The data in figure 3.2 suggests that stx 16 depletion leads to a reduction in the recruitment of mVps45 to the membrane.

As mentioned earlier, Proctor *et al.* showed that stx 16 knockdown resulted in a 30% reduction in GLUT4 cellular levels. Figure 3.3 shows that in cells infected with shRNA2 and 4 the level of GLUT4 was reduced by approximately 35% ($P < 0.01$) and 20% ($P < 0.05$) respectively. This suggests that in cells depleted of stx 16, GLUT4 is missorted into a degradative pathway. It would be interesting to investigate whether this loss of GLUT4 was proteasome-dependent using a proteasome inhibitor. Interestingly the levels of GLUT4 did not covary with the level of stx 16 knockdown observed in figure 3.1. This may be because stx 16 expression needs to be knocked down to a high level before an effect on GLUT4

levels is observed. It may be that there are some compensatory mechanisms to preserve the level of GLUT4 in adipocytes. Alternatively, there may have been a problem with the differentiation of shRNA2-infected cells, as the level of GLUT4 was reduced by 35% ($P < 0.05$), even though the level of stx 16 expression was only reduced by approximately 35% ($P < 0.05$). To determine if this was the case with the shRNA2-infected cells the differentiation of the cells could be tested by using Oil Red O staining or by blotting for factors which are upregulated during differentiation such as PPARγ (see discussion of Fig. 3.5).

In contrast the level of IRAP was unaffected in shRNA-infected cells compared with the negative control. This result was unexpected as IRAP traffics in a similar manner to GLUT4 (Garza and Birnbaum, 2000). This suggests that stx 16 depletion affects a pathway which is specific to GLUT4 and not IRAP or that IRAP is more able to compensate for a loss of stx 16 in the cell. Also in figure 3.3 it was noted that the level of TfR was unaffected in shRNA-infected cells compared with the negative control. This result suggests that stx 16 depletion affects a pathway which is specific to GLUT4 and does not affect general endosomal recycling.

After discovering an effect on the total cellular levels of GLUT4, the subcellular distribution of GLUT4 in stx 16-depleted cells was further investigated (Fig. 3.4). In the shRNA4-infected cells, stx 16 is only found in the LDM fraction which represents endosomal membranes and GSVs, but in negative control cells stx 16 is found in both HDM (which represents the ER and Golgi) and LDM fractions. This suggests that even though stx 16 is depleted in shRNA4-infected cells the remaining protein is localised to the endosomal membranes and perhaps the GSVs. In figure 3.4 GLUT4 is found in both HDM and LDM fractions in the negative control and shRNA4 infected-cells. As the reduction in GLUT4 in stx 16-depleted cells is only relatively small there may not be a big change in the distribution of GLUT4 in the different fractions. As the negative control and shRNA4 samples were on separate blots it was not possible to compare the levels of GLUT4 in the LDM and HDM fractions with this data. The TfR and SNAP 23 blots show that the fractions had been properly separated. TfR is located in the LDM fraction as expected and SNAP 23 is found in the P/M fraction where it is normally localised.

Attempts were made to further fractionate the LDM fraction of negative control and shRNA4-infected cells to separate the GSVs using an iodixanol gradient as described in (Hashiramoto and James, 2000) but were unsuccessful (data not shown). An *in vitro* budding assay was also attempted to examine the formation of GSVs as described in (Xu and Kandror, 2002). However initial experiments using wild type cells were unsuccessful (data not shown).

To determine whether stx 16 depletion affects the level of GLUT4 in the HDM and LDM fractions, HDM and LDM samples from negative control and shRNA1-4-infected cells were compared. In figure 3.5, the level of stx 16 in the HDM fraction of shRNA4-infected cells was very low compared with the negative control in agreement with figure 3.4. The level of stx 16 was also reduced in the LDM fraction but not to the same extent. The level of GLUT4 was slightly reduced in the shRNA4 HDM fraction compared with the negative control. In the LDM fractions GLUT4 was reduced to a greater extent in the shRNA4 fraction compared with the negative control. This suggests that of the 20% loss to total GLUT4 levels the majority is lost from the LDM fraction which may suggest that stx 16 depletion leads to a loss of GLUT4 from the GSVs. The level of IRAP in the HDM and LDM fractions of shRNA4-infected cells was similar to that of negative control-infected cells which agrees with the results of figure 3.3 which showed no significant change in the level of total IRAP levels in stx 16-depleted cells. The shRNA3-infected cells showed very different results to that of shRNA4. The shRNA3 HDM and LDM samples had very low levels of stx 16 like shRNA4, however the shRNA3 samples had very low levels of GLUT4 and IRAP in the HDM fraction and also low levels of GLUT4 and IRAP in the LDM fractions. This result was seen in all experiments of this type. These results are much lower than expected considering that in total membrane samples the reduction of GLUT4 levels in the shRNA3-infected cells was approximately 10% and was not significant (Fig. 3.3). A possible explanation for this is that the shRNA3-infected cells had not fully differentiated, which would lead to a low level of GLUT4 and IRAP in the cells. There was not time to fully address this problem. But this problem was one of the reasons why the shRNA3-infected cells were not used in future experiments. One way to avoid this problem in the future would be to test the differentiation of all the shRNA-infected cells to ensure that full differentiation had occurred. As mentioned previously, this could be done by using Oil Red O staining or by blotting for factors which are upregulated during differentiation such as PPARγ.

If stx 16 depletion causes a reduction in GLUT4 levels in the GSVs then this may affect the ability of the cells to transport glucose in response to insulin. Therefore the effect of stx 16 knockdown on insulin-stimulated glucose transport was investigated using a ^{3}H-deoxyglucose assay. Unfortunately consistent and reliable results were not obtained (data not shown).

To confirm that knockdown of stx 16 was responsible for the results shown above, myc-tagged human stx 16A was expressed in negative control and shRNA4-infected cells (Fig. 3.6). First of all the optimum PFU/cell of myc-stx16A adenovirus was determined. Figure 3.6 shows that 1000 PFU/cell was required to express myc- stx 16A in wild type 3T3-L1 adipocytes. The level of expression of myc-stx 16A was similar to endogenous stx 16. The myc-stx 16A runs at a lower molecular weight than endogenous stx 16. This is because human stx 16 has a lower molecular weight of 34 kDa compared with endogenous stx 16 which has a molecular weight of 37 kDa. This difference in molecular weight is due to 22 fewer amino acids in the human stx 16A compared to endogenous murine stx 16 (Fig. 3.7). The majority of these amino acids are missing from a region between the N-terminal peptide that binds to mVps45 and the Habc domain (Dulubova *et al.*, 2002). This is the only major difference between the amino acid sequences of the two proteins. The differences between the human stx 16A and murine stx 16 should not affect the ability of human stx 16A to rescue the main functions of stx 16 to bind its SM protein mVps 45 and to form SNARE complexes. However there is the possibility that human stx 16A may not be able to fully compensate for a lack of endogenous stx 16 in the shRNA4-infected cells, as it will be unable to perform any functions that require the missing region. If this is the case, a shRNA4- resistant version of murine stx 16 will need to be created using site-directed mutagenesis.

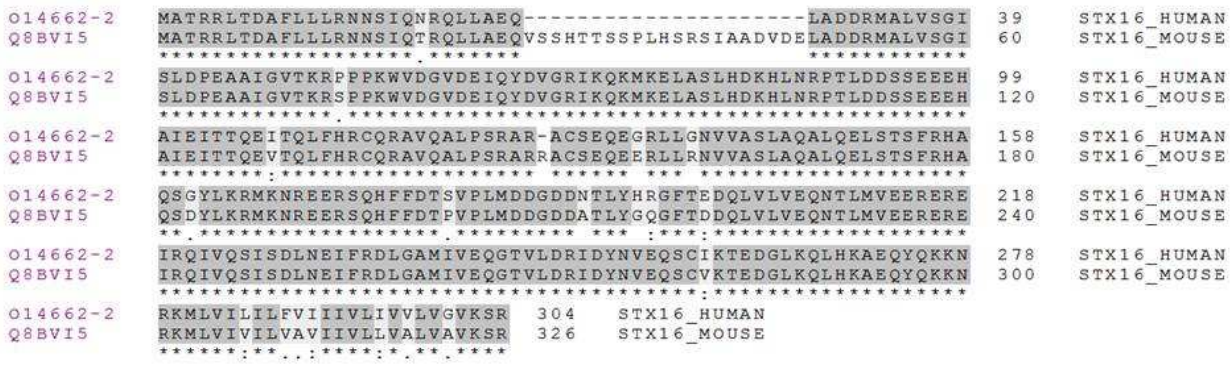

Figure 3.7.Alignment of human and mouse syntaxin 16 amino acid sequences.

Human syntaxin 16 (O14662-2) and mouse syntaxin 16 (Q8BVI5) amino acid sequences were aligned using Clustal W (http://services.uniprot.org/). Identical amino acids are highlighted in grey. ***** denotes the amino acids are identical, **:** denotes a strong similarity between the amino acids and **.** denotes weak similarity between the amino acids.

Once the optimum level of adenovirus was determined, it was used to infect negative control and shRNA4-infected cells. Figure 3.6 shows that shRNA4-infected cells have depleted levels of endogenous stx 16 compared with negative control-infected cells. However the shRNA4-infected cells are able to express the myc-stx 16A, which shows that shRNA4 does not target myc-stx 16A. The samples in figure 3.6 were also blotted for myc to detect myc-stx 16 specifically, however no bands were detected (data not shown). This problem was also encountered in previous work in the lab. It is possible that the myc tag is not correctly folded and therefore the antibody is unable to detect it. Fortunately the myc-stx 16A has a sufficiently different molecular weight for it to be distinguished from endogenous stx 16 in a stx 16 blot. It was hoped that the myc-stx 16A adenovirus would be used in the ^{3}H-deoxyglucose assay, however there was not sufficient time or stock of adenovirus to perform the experiments.

In summary the data in this chapter shows that shRNA can be used to generate 3T3-L1 adipocytes stably depleted of stx 16. The level of knockdown produced by shRNA4 is comparable to that produced by a morpholino antisense oligonucleotide (Proctor *et al.*, 2006). Stx 16 depletion affects the levels of its t-SNARE partner stx 6 and the SM protein mVps45 in membrane samples.

Also stx 16 knockdown by shRNA4 reduces total GLUT4 cellular levels by approximately 20% ($P < 0.05$) which is similar to the level seen in previous work (Proctor *et al.*, 2006). In particular stx 16 knockdown by shRNA4 reduces the level of GLUT4 in the LDM fraction which suggests that stx 16 may affect the level of GLUT4 in GSVs. Finally it was shown that knockdown of stx 16 can be rescued by expression of myc-tagged human stx 16A.

Chapter 4 HA-GLUT4-GFP trafficking assays

4.1 Introduction

The translocation of GLUT4 in response to insulin is an example of regulated membrane trafficking (Bryant *et al.*, 2002). GLUT4 occupies two interrelated, overlapping endosomal cycles (Fig.1.3). A fast-trafficking cycle, involving the plasma membrane and early endosome serves to internalise GLUT4 in the absence of insulin. Once in the endosome, GLUT4 is further sorted into a slow-trafficking pathway, involving the endosome, the TGN and a population of vesicles known as GSVs. It is thought that GLUT4 in the GSVs translocates to the cell surface in response to insulin.

A role for stx 16 in GLUT4 trafficking has been previously described (Proctor *et al.*, 2006). It is important to determine where in the trafficking itinerary of GLUT4, stx 16 functions. It has been proposed that stx 16 functions to control entry of GLUT4 into the slow-trafficking pathway into the GSVs. One way to examine the role of stx 16 in GLUT4 trafficking is to determine the effect stx 16 has on GLUT4 trafficking kinetics. In order to do this the trafficking of HA-GLUT4-GFP was examined.

HA-GLUT4-GFP is a GLUT4 molecule with two tags. It has a HA tag in the first exofacial loop of GLUT4 and a GFP tag at the C-terminus. The HA tag allows any GLUT4 at the cell surface to be labelled and the GFP tag allows total HA-GLUT4-GFP expression in the cell to be determined. This allows translocation or recycling to be normalised for levels of HA-GLUT4-GFP expression using a HA: GFP ratio. The use of HA-GLUT4-GFP as a reporter was first described in primary rat adipose cells (Dawson *et al.*, 2001). This paper showed that HA-GLUT4-GFP localisation and trafficking were identical to that of endogenous GLUT4. Since then HA-GLUT4-GFP has been used in a number of studies (Zeigerer *et al.*, 2002;Karylowski *et al.*, 2004;Zeigerer *et al.*, 2004;Martin *et al.*, 2006;Muretta *et al.*, 2008).

4.2 Aims of this chapter

The aims of this chapter were to develop an assay, which would allow translocation and recycling of GLUT4 to be examined. Initially this involved using a flow cytometry method, but later the assay was developed to be performed in a 96-well plate format for use with a fluorescence plate reader.

4.3 Results

4.3.1 Expression of HA-GLUT4-GFP in 3T3-L1 fibroblasts

In order to investigate GLUT4 trafficking, HA-GLUT4-GFP needed to be expressed in 3T3-L1 fibroblasts. To express HA-GLUT4-GFP, 3T3-L1 fibroblasts were infected with lentivirus expressing HA-GLUT4-GFP as described in section 2.5.2. Cells were infected with a 2-fold serial dilution and the level of HA-GLUT4-GFP expression was determined as the level of GFP fluorescence, using flow cytometry as described in section 2.6.1. Figure 4.1A is the flow cytometry data showing the GFP fluorescence of fibroblasts infected with each serial dilution compared with negative control cells, which were mock-infected. As shown in figure 4.1A the GFP fluorescence of the HA-GLUT4-GFP-infected cells was higher than the negative control at each serial dilution. As the dilution increased the level of GFP fluorescence decreased. The results in figure 4.1A were quantified in terms of mean fluorescence intensity (MFI) (Fig.4.1B) and in terms of the percentage of cells positively expressing HA-GLUT4-GFP (Fig.4.1C). Figure 4.1B shows that the 1 in 2 dilution of lentivirus resulted in the highest level of GFP fluorescence. Also the GFP fluorescence decreased by approximately a factor of 2 with each dilution. Figure 4.1C shows that the 1 in 2 and 1 in 4 dilutions of lentivirus gave the highest levels of infection compared with the negative control.

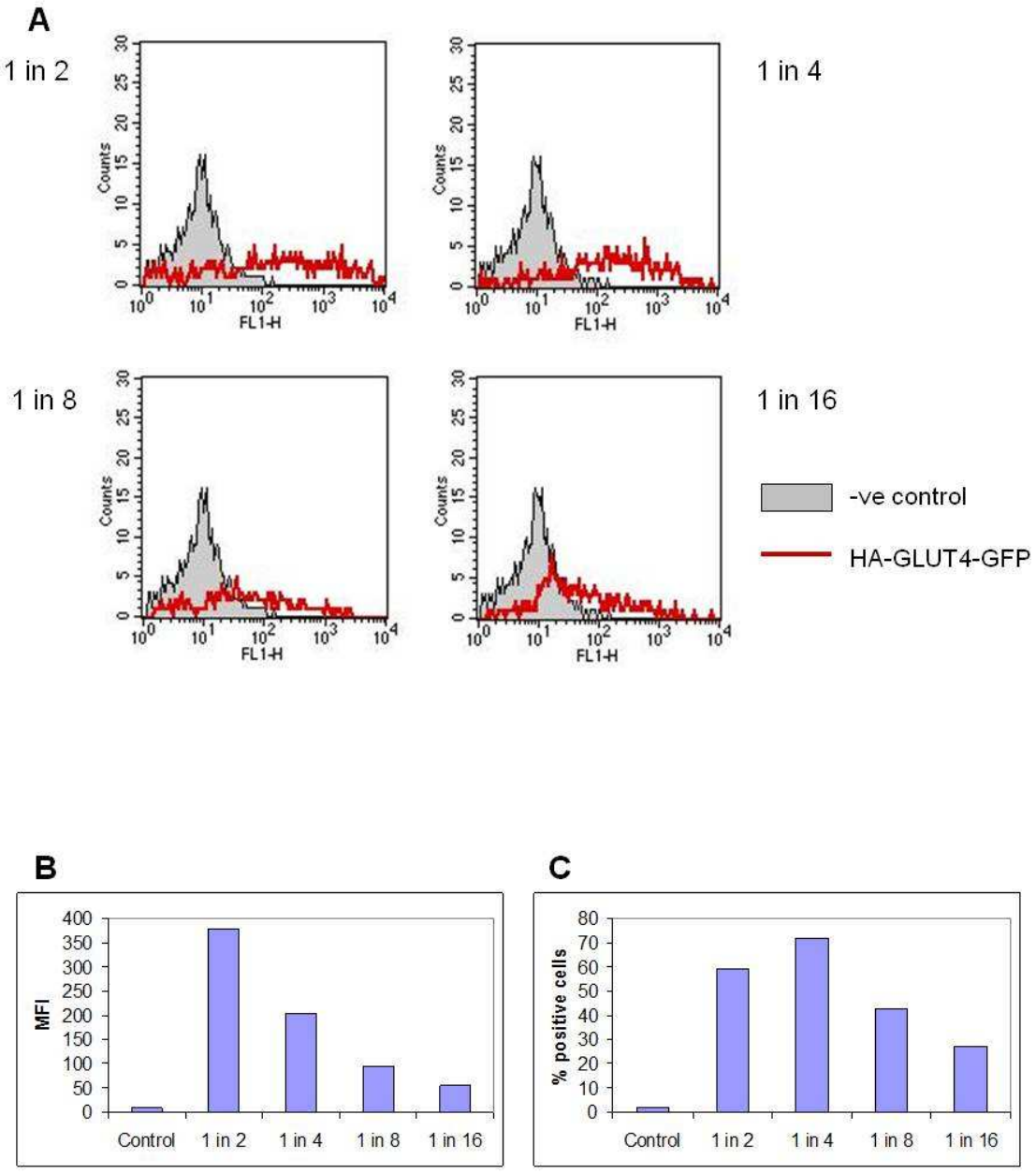

Figure 4.1. Expression of HA-GLUT4-GFP in 3T3-L1 fibroblasts.

A. 3T3-L1 fibroblasts were infected with a 2-fold serial dilution of lentivirus expressing HA-GLUT4-GFP as described in section 2.5.2. Expression levels are proportional to the level of GFP fluorescence, which was determined by flow cytometry as described in section 2.6.1. GFP fluorescence (FL1-H) is shown on the x-axis and the number of cells (counts) is shown on the y-axis. Mock-infected cells were used as a negative control (-ve control). Each panel shows one serial

dilution (1 in 2 to 1 in 16) of HA-GLUT4-GFP lentivirus (shown in red) compared with the negative control (shown in grey).

B. Quantification of the data shown in **A**. The level of GFP fluorescence is expressed in terms of the MFI which is shown on the y-axis (n = 1).

C. Quantification of the data shown in **A**. The percentage of cells positively expressing HA-GLUT4-GFP is shown on the y-axis. If the negative control cells are considered to be not expressing HA-GLUT4-GFP, any cells with a higher GFP fluorescence can be considered to be positively expressing HA-GLUT4-GFP. The percentage of cells positively expressing HA-GLUT4-GFP was determined by calculating the area under the red curve to the right of the negative control (n = 1).

4.3.2 Cell sorting of 3T3-L1 adipocytes.

Recently Muretta *et al.* published a method by which HA-GLUT-GFP trafficking in 3T3-L1 adipocytes could be examined using flow cytometry (Muretta *et al.*, 2008). In this paper they also demonstrated that 3T3-L1 adipocytes could be distinguished using flow cytometry from 3T3-L1 fibroblasts and debris. Therefore before analysing HA-GLUT4-GFP trafficking, wild type 3T3-L1 adipocytes were sorted on the basis on forward scatter (FSC), side scatter (SSC) and autofluorescence in the allophycocyanin (APC) channel into adipocytes, fibroblasts and debris (Fig. 4.2). This was to ensure that in future experiments, the cell populations being analysed by flow cytometry were indeed adipocytes.

As shown in figure 4.2, 3T3-L1 adipocytes formed two populations on the basis of FSC and SSC. The low SSC population (P2) was fibroblasts. 3T3-L1 fibroblasts usually have a long and branched morphology. However, the cells in P2 in figure 4.2 have a rounded morphology. This is probably because the cells became rounded during the cell sorting process and had not settled down fully on the microscope slide. The high SSC population (P1) was further sorted on the basis of autofluorescence in the APC channel. This resulted in two populations. The high autofluorescence population (P4) was debris. The debris has a granular and mis-shapened morphology. The low autofluorescence population (P3) was adipocytes. 3T3-L1 adipocytes contain several lipid droplets of varying size within their cytoplasm.

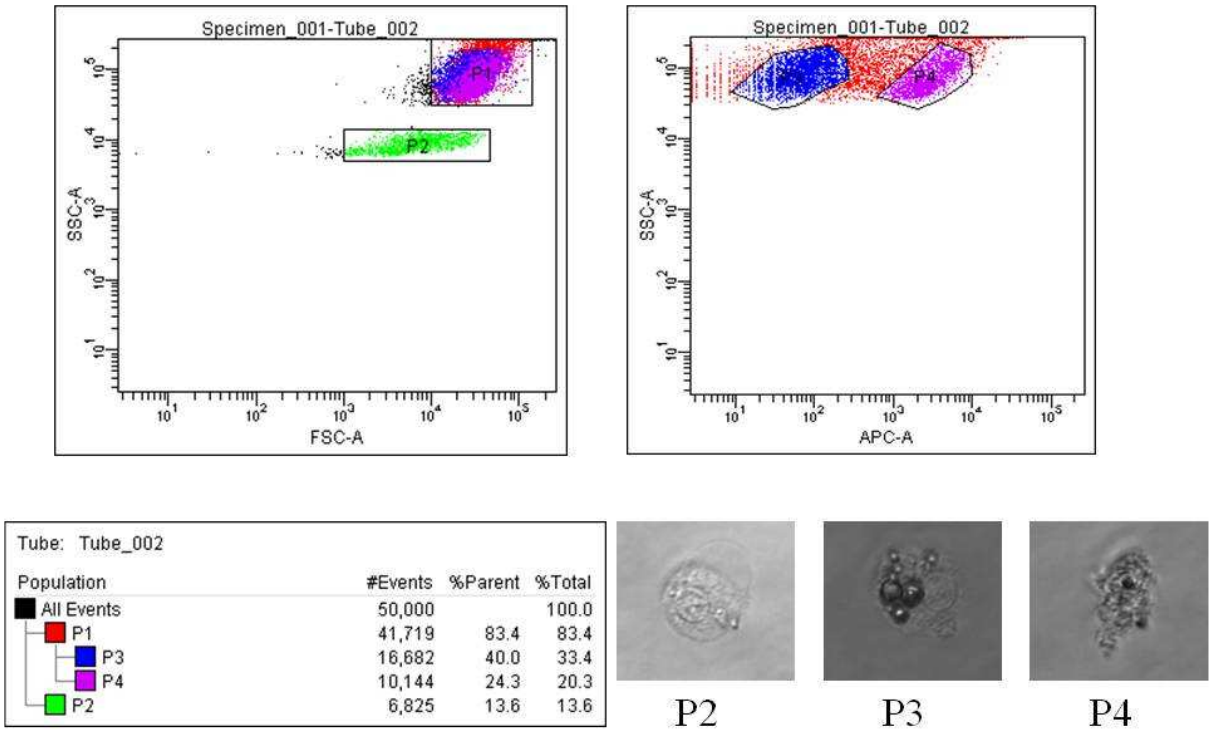

Figure 4.2. Sorting of 3T3-L1 adipocytes.

3T3-L1 adipocytes were sorted as described in section 2.6.2 (n = 1). Cells were sorted on the basis of forward scatter (FSC-A), which represents cell size, and side scatter (SSC-A), which represents cell granularity, into P1 and P2 populations. The P1 population was then sorted into P3 and P4 populations on the basis of autofluorescence in the APC channel (APC-A). The sorted cells were viewed on a Zeiss Axiovert microscope using a x 32 objective lens to determine which was the 3T3-L1 adipocyte population. P2 is 3T3-L1 fibroblasts. P3 is 3T3-L1 adipocytes. P4 is debris. The images shown are representative of the multiple fields of view recorded.

4.3.3 Surface labelling of HA-GLUT4-GFP

To measure the translocation of HA-GLUT4-GFP, 3T3-L1 adipocytes infected with a 1 in 2 dilution of lentivirus were stimulated with or without insulin for 30 minutes. Then the cells were kept on ice and labelled for HA-GLUT4-GFP at the cell surface using a HA primary antibody and a R-Phycoerythrin (RPE)-conjugated secondary antibody. The RPE and GFP fluorescence of the cells was measured using flow cytometry as described in section 2.6.3.

Figure 4.3A shows an example of a flow cytometry analysis for one sample. The cells were gated for high SSC and low autofluorescence in a similar manner to the cell sorting of 3T3-L1 adipocytes in figure 4.2. The top left panel of figure 4.3A shows the FSC and SSC of all the 10,000 cells analysed in the sample. The cells were gated for high SSC as shown by the position of the oval in the top left panel. These gated cells were then analysed in the top right panel. The top right panel of figure 4.3A shows the SSC and autofluorescence in the APC channel of the gated cells. The cells in the top right panel were further gated for low autofluorescence in the APC channel as shown by the position of the oval in the top right panel. The panel at the bottom of figure 4.3A shows the RPE fluorescence of the gated cells (from the top right panel) which represents the level of HA-GLUT4-GFP at the surface. Figure 4.3B shows a comparison of the RPE fluorescence of basal and insulin-stimulated cells. Both basal and insulin-stimulated cells, which were labelled with the isotype control, have low levels of RPE fluorescence. The peaks of both isotype samples are just above 10^0. The level of RPE fluorescence of basal and insulin-stimulated cells labelled with the HA antibody is much higher than the isotype controls. However, there is little difference between the basal HA sample and the insulin-stimulated HA sample. Both HA-labelled samples have a peak at approximately 10^2.

A

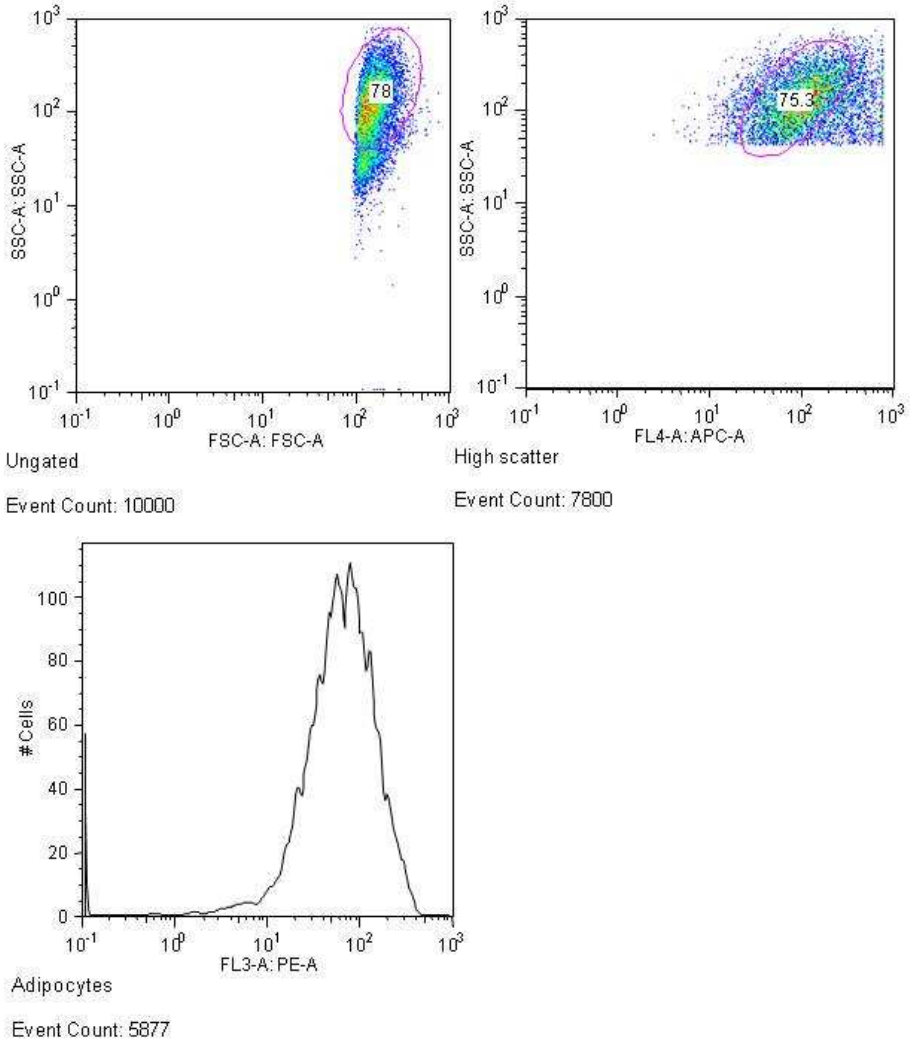
78
75.3
SSC-A: SSC-A
FSC-A: FSC-A
FL4-A: APC-A
Ungated
Event Count: 10000
High scatter
Event Count: 7800
#Cells
FL3-A: PE-A
Adipocytes
Event Count: 5877

B

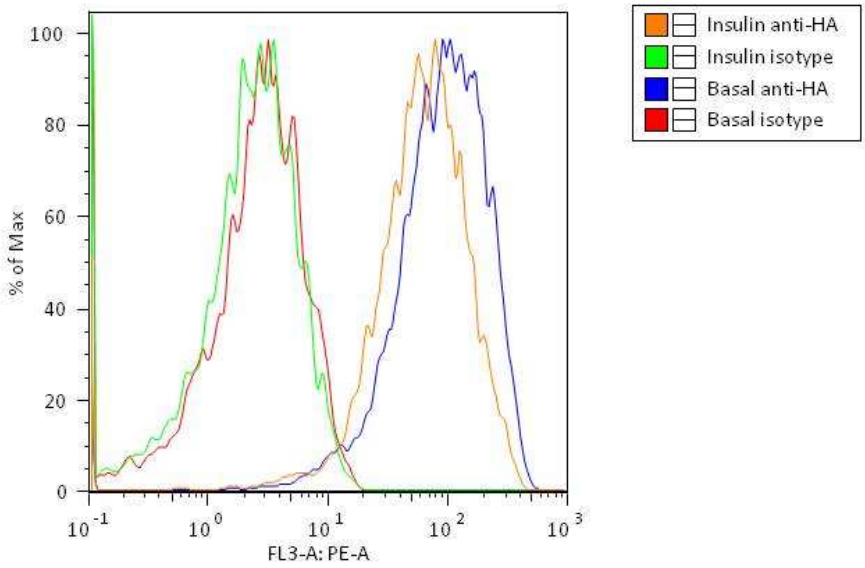
Insulin anti-HA
Insulin isotype
Basal anti-HA
Basal isotype
% of Max
FL3-A: PE-A

Figure 4.3 Surface labelling of HA-GLUT-GFP.

3T3-L1 adipocytes infected with a 1 in 2 dilution of HA-GLUT4-GFP lentivirus (section 2.5.2) were labelled for surface levels of HA-GLUT4-GFP as described in section 2.6.3. Cells were labelled with a HA.11 mouse monoclonal primary antibody or an IgG1 isotype control from murine myeloma clone MOPC21 and a RPE-conjugated goat anti-mouse secondary antibody. The cells were then analysed by flow cytometry.

A. An example of the flow cytometry analysis for one sample. The cells were gated for high side scatter (SSC-A) and then low autofluorescence on the APC channel (FL4-A APC-A). The level of RPE fluorescence which represents the surface level of HA-GLUT4-GFP was then determined. The ovals show where the populations have been gated and the numbers give the percentage of events (cells) in that gated population.

B. A representative comparison of surface levels of HA-GLUT4-GFP (represented by RPE fluorescence) in basal and insulin-stimulated adipocytes expressing HA-GLUT4-GFP (n=2).

4.3.4 Comparison of HA-GLUT4-GFP expression with endogenous GLUT4 expression

In the previous experiment, the level of surface HA-GLUT4-GFP in basal cells was as high as the level in insulin-stimulated cells. This suggested that HA-GLUT4-GFP was on the surface of the cell at high levels in basal conditions. One possibility was that the level of HA-GLUT4-GFP expression was too high and HA-GLUT4-GFP was able to escape the basal retention mechanisms in the cell. Therefore, the level of HA-GLUT4-GFP in membrane samples was determined in cells infected with a 1 in 2 and a 1 in 4 dilution of the lentivirus and this was compared with the level of endogenous GLUT4 in mock-infected negative control cells. Figure 4.4A shows that the level of HA-GLUT4-GFP in the 1 in 2-infected cells was much higher than the level of endogenous GLUT4 in the negative control cells. However, in the 1 in 4-infected cells the level of HA-GLUT4-GFP was similar to endogenous GLUT4 levels. Figure 4.4B shows that HA-GLUT4-GFP is only expressed in the infected cells and not in the negative control cells. Figure 4.4B also confirms that the band at approximately 83 kDa in the GLUT4 blot in figure 4.4A is HA-GLUT4-GFP.

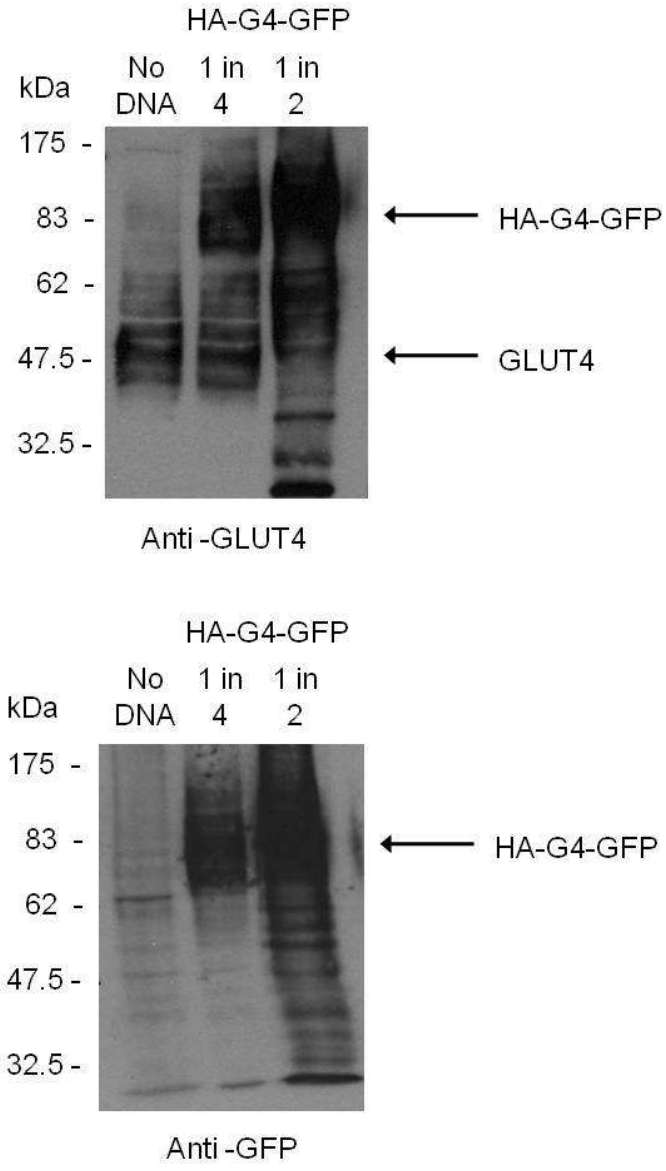

Figure 4.4 Comparison of HA-GLUT4-GFP expression in 3T3-L1 adipocytes with endogenous GLUT4.

Membranes were prepared as described in section 2.4.1 from 3T3-L1 adipocytes infected with a 1 in 2 or a 1 in 4 dilution of HA-GLUT4-GFP lentivirus (section 2.5.2). As a control membranes were also prepared from cells which had been mock-infected (No DNA) (n =1). The membrane samples were separated on a 10% (v/v) SDS-PAGE gel as described in section 2.4.4. 10 μg of protein was loaded in each lane. The proteins were transferred to nitrocellulose as described in section 2.4.5 and then blotted as described in section 2.4.6. The numbers at the side of the blots indicate molecular weight in kDa.

Upper panel. Western blot of GLUT4 using a rabbit anti-GLUT4 C-terminus primary antibody at a 1:1000 dilution.

Lower panel. Western blot of HA-GLUT4-GFP using a rabbit anti-GFP primary antibody at a 1:1000 dilution.

Bands corresponding to GLUT4 and HA-GLUT4-GFP are indicated by the arrows.

4.3.5 Localisation of HA-GLUT4-GFP

It was also important to confirm that HA-GLUT4-GFP was properly localised in basal and insulin-stimulated cells. Cells infected with 1 in 2 and 1 in 4 dilutions of lentivirus were stimulated with or without insulin. To stain for surface HA-GLUT4-GFP, the cells were left unpermeabilised and were stained using a HA primary antibody and a Cy3-conjgated secondary antibody. Cy3 fluorescence and GFP fluorescence were then determined by confocal microscopy. Figure 4.5A shows that in the 1 in 4-infected cells, under basal conditions there is little or no HA-GLUT4-GFP at the cell surface. However insulin stimulation results in much higher levels of HA-GLUT4-GFP at the cell surface. In contrast, in the 1 in 2-infected cells, HA-GLUT4-GFP was present at the cell surface in basal cells and the level at the surface did not increase much with insulin stimulation.

To show that the HA staining represented the location of HA-GLUT4-GFP, the cells were permeablised and then stained for HA. In figure 4.5C GFP and Cy3 fluorescence colocalised in the 1 in 2 and 1 in 4-infected cells in both basal and insulin-stimulated conditions. To confirm that there was no non-specific staining due to the Cy3-conjugated secondary antibody, permeabilised cells were also stained without the HA primary antibody. Figure 4.5B shows that the staining was specific.

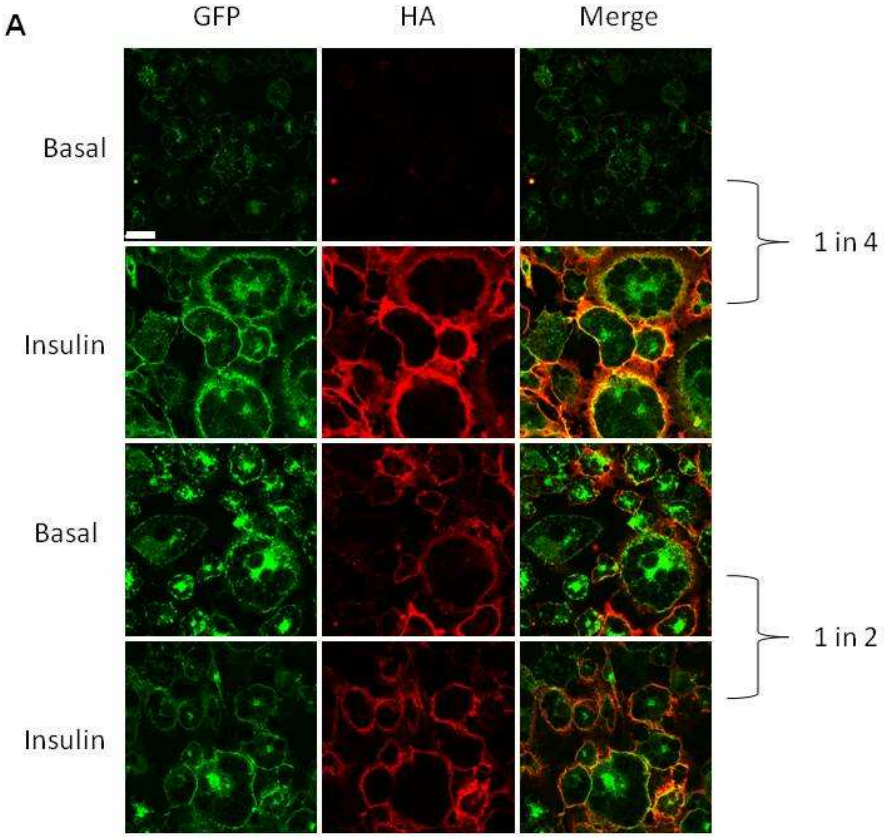
A
GFP
HA
Merge
Basal
Insulin
Basal
Insulin
1 in 4
1 in 2

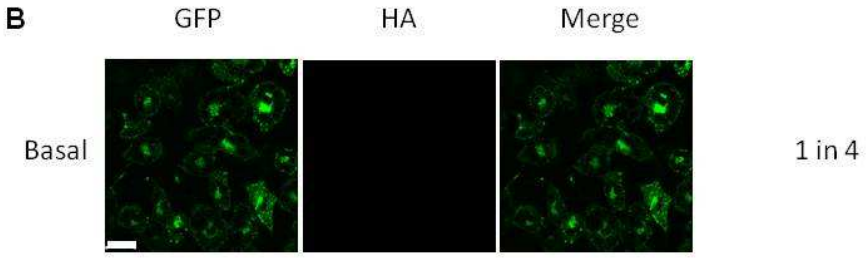
B
GFP
HA
Merge
Basal
1 in 4

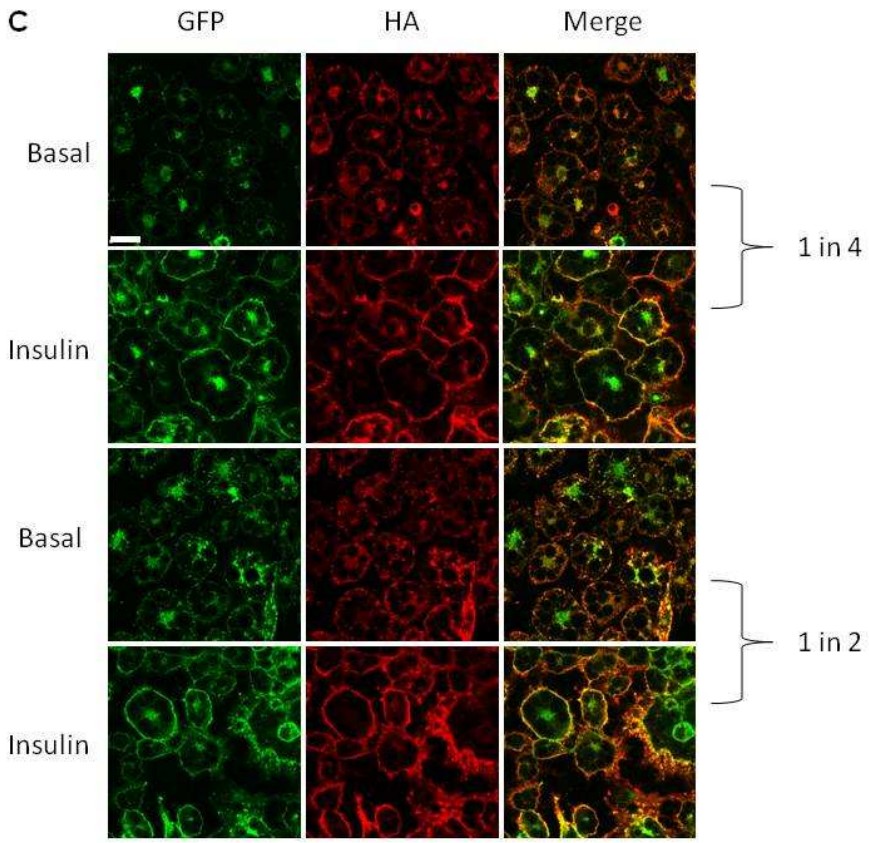

Figure 4.5. Localisation of HA-GLUT4-GFP in 3T3-L1 adipocytes.

3T3-L1 adipocytes were infected with a 1 in 4 or a 1 in 2 dilution of HA-GLUT4-GFP lentivirus as described in section 2.5.2. Basal and insulin-stimulated cells were stained for HA as described in section 2.7.1 (n = 2).

A. Unpermeabilised cells were stained with a HA.11 mouse monoclonal primary antibody and a Cy3-conjugated goat anti-mouse secondary antibody.

B. Permablised cells without HA staining and a Cy3-conjugated goat anti-mouse secondary antibody.

C. Permeabilised cells were stained with a HA.11 mouse monoclonal primary antibody and a Cy3 -conjugated goat anti-mouse secondary antibody.

All images were taken with using a Zeiss LSM Exciter confocal microscope under oil immersion with a x 64 lens. Gain and brightness settings were the same for all images. Scale bar is 20 μm.

4.3.6 Surface labelling of HA-GLUT4-GFP with 1 in 4-infected cells

The experiments of the previous two sections demonstrated that cells infected with a 1 in 4 dilution of lentivirus had more appropriate levels of HA-GLUT4-GFP and the HA-GLUT4-GFP in these cells responded normally to insulin. Therefore, the flow cytometry experiment from section 4.3.3 was repeated using the 1 in 4-infected cells. Figure 4.6 shows a comparison of the RPE fluorescence of basal and insulin-stimulated cells. The results look similar to the results of figure 4.3B. The isotype controls have low levels of RPE fluorescence and peak at about $10^{0.4}$. The RPE fluorescence of the basal and insulin-stimulated cells labelled with HA antibody is much higher than the isotype controls. The basal peak is at 10^{2} and the insulin peak is at $10^{1.7}$.

4.3.7 Confocal staining with RPE-conjugated secondary antibody

The results of the previous section suggested that there was still a problem with the flow cytometry surface labelling assay. One possibility was that the RPE-conjugated secondary antibody used in the flow cytometry assay was not labelling the cells properly. Cells infected with a 1 in 2 and 1 in 4 dilution of lentivirus were stained for surface levels of HA-GLUT4-GFP as described in section 4.3.5, except the RPE-conjugated secondary antibody was used instead of a Cy3-conjugated secondary antibody. Figure 4.7 shows that staining with the RPE secondary antibody was not as strong or as clean as the staining with the Cy3-conjugated secondary antibody (Fig. 4.5). For the insulin-stimulated cells in particular, the ring of staining for HA-GLUT4-GFP at the surface was not as strong or defined.

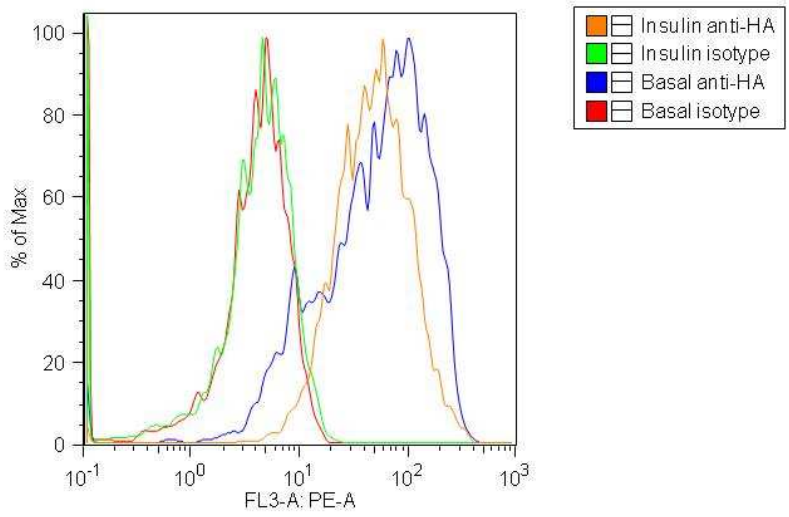

Figure 4.6. Surface labelling of HA-GLUT4-GFP.

3T3-L1 adipocytes infected with a 1 in 4 dilution of HA-GLUT4-GFP lentivirus (section 2.5.2) were labelled for surface levels of HA-GLUT4-GFP as described in section 2.6.3. Cells were labelled with a HA.11 mouse monoclonal primary antibody or an IgG1 isotype control from murine myeloma clone MOPC21 and a RPE-conjugated goat anti-mouse secondary antibody. The cells were then analysed by flow cytometry.

The figure shows a comparison of the surface levels of HA-GLUT4-GFP (represented by RPE fluorescence) in basal and insulin-stimulated adipocytes expressing HA-GLUT4-GFP (n = 1).

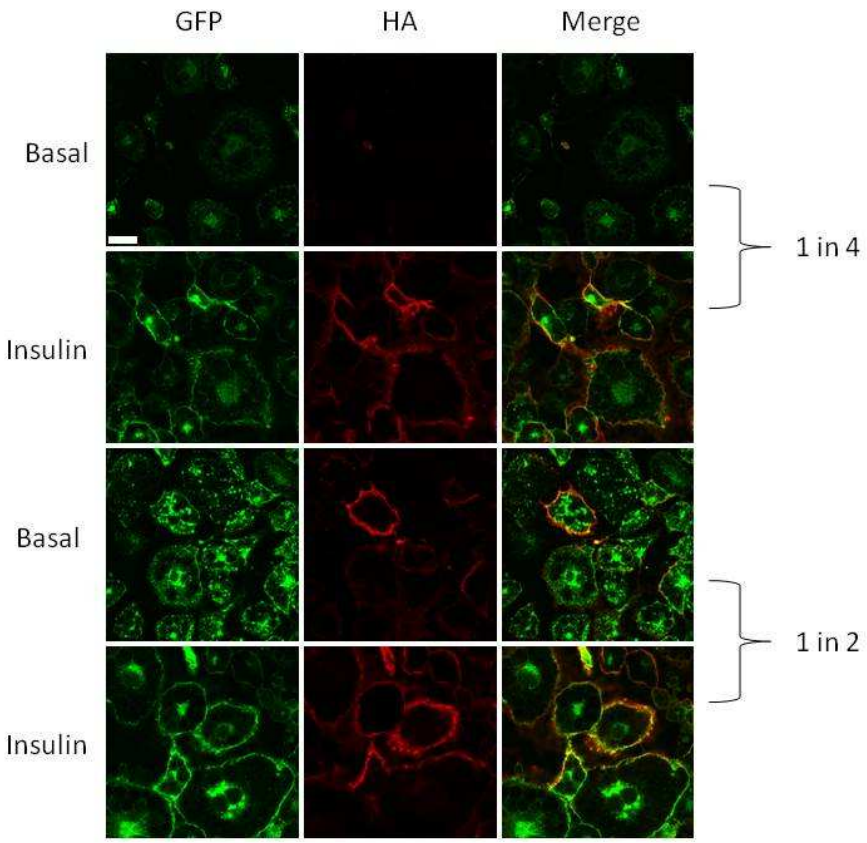

Figure 4.7. HA staining with a RPE secondary antibody.

3T3-L1 adipocytes were infected with a 1 in 4 or a 1 in 2 dilution of HA-GLUT4-GFP lentivirus as described in section 2.5.2. Basal and insulin-stimulated unpermeablised cells were stained for HA as described in section 2.7.1 with a HA.11 mouse monoclonal primary antibody and a RPE-conjugated goat anti-mouse secondary antibody (n = 1).

All images were taken with using a Zeiss LSM Exciter confocal microscope under oil immersion with a x 64 lens. Gain and brightness settings were the same for all images. Scale bar is 20 μm.

4.3.8 Surface labelling of HA-GLUT4-GFP with Cy3-conjugated secondary antibody

The flow cytometry surface labelling assay was repeated as described in section 4.3.6 except a Cy3-conjugated secondary antibody was used to label the cells. Figure 4.8 shows a comparison of the RPE fluorescence (nearest channel to Cy3) of basal and insulin-stimulated cells. The isotype controls had low levels of RPE fluorescence, with peaks at 10^0. The basal cells labelled with HA antibody also had low RPE fluorescence and the peak was almost identical to the isotype controls. The insulin-stimulated cells labelled with HA antibody had a slightly higher level of RPE fluorescence with a peak at $10^{0.1}$.

4.3.9 Surface labelling of HA-GLUT4-GFP 96-well plate assay

The difference between basal and insulin-stimulated levels of surface HA-GLUT4-GFP in the previous experiment was not as big as hoped. It was then decided to try the experiment in a 96-well plate format and use a fluorescence plate reader to measure surface levels of HA-GLUT4-GFP as described in section 2.8.1. In this experiment cells infected with a 1 in 4 dilution of lentivirus were stimulated with or without insulin and then stained for surface levels of HA-GLUT4-GFP using a HA primary antibody and the Cy3-conjugated secondary antibody. Figure 4.9 shows that in response to insulin the level of HA-GLUT4-GFP on the cell surface increased by over four-fold ($P < 0.01$). The mean fluorescence ratio (MFR) (surface: total) of basal cells was 2.17 ± 0.213 (mean ± S.D.) and the MFR of insulin stimulated cells was 9.14 ± 3.48.

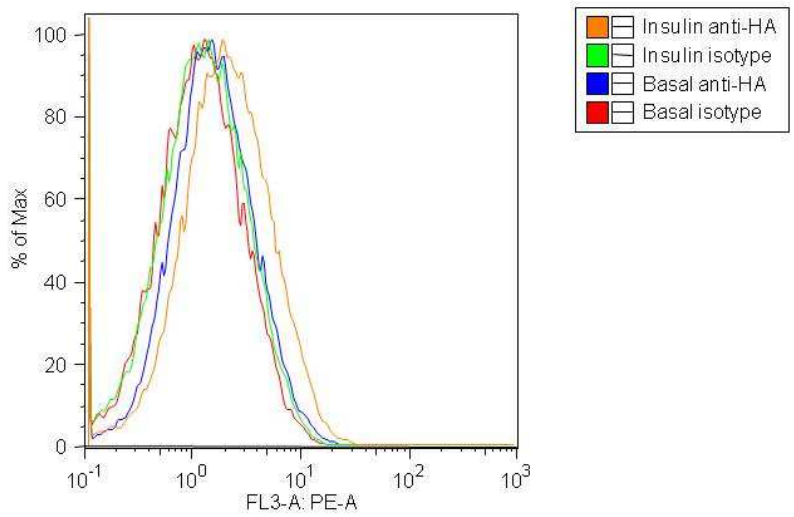

Figure 4.8. Surface labelling of HA-GLUT4-GFP.

3T3-L1 adipocytes infected with a 1 in 4 dilution of HA-GLUT4-GFP lentivirus (section 2.5.2) were labelled for surface levels of HA-GLUT4-GFP as described in section 2.6.3. Cells were labelled with a HA.11 mouse monoclonal primary antibody or an IgG1 isotype control from murine myeloma clone MOPC21 and a Cy3-conjugated goat anti-mouse secondary antibody. The cells were then analysed by flow cytometry.

The figure shows a comparison of the surface levels of HA-GLUT4-GFP represented by RPE fluorescence (nearest channel to Cy3) in basal and insulin-stimulated adipocytes expressing HA-GLUT4-GFP (n = 1). RPE has an Ex/Em of 480/580. Cy3 has an Ex/Em of 550/580. To detect RPE the cells were excited using a 488 nm laser and the emission was detected by channel FL-3 which uses a 585/40 bandpass filter.

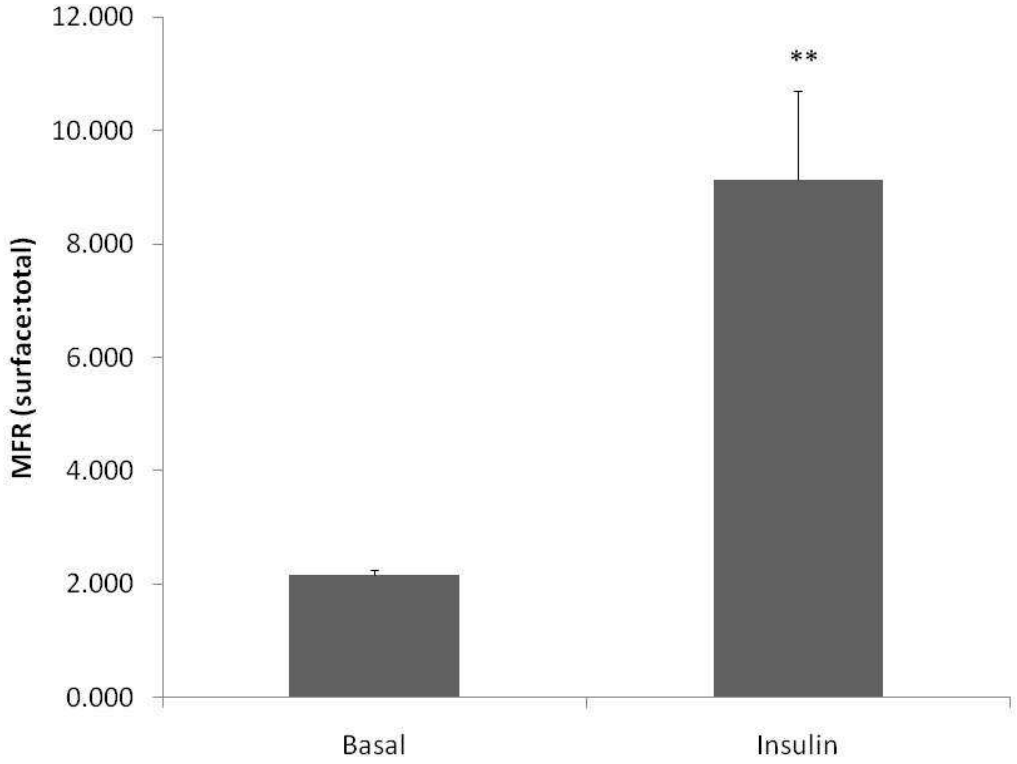

Figure 4.9 Translocation of HA-GLUT4-GFP in response to insulin.

3T3-L1 adipocytes infected with a 1 in 4 dilution of HA-GLUT4-GFP lentivirus (section 2.5.2) were labelled for surface levels of HA-GLUT4-GFP as described in section 2.8.1. Basal or insulin-stimulated cells were labelled with a HA.11 mouse monoclonal primary antibody or an IgG1 isotype control from murine myeloma clone MOPC21 and a Cy3-conjugated goat anti-mouse secondary antibody. The MFR of surface to total HA-GLUT4-GFP was used as a measure of HA-GLUT4-GFP translocation. The MFR was calculated by determining the MFI of HA-GLUT4-GFP at the cell surface (HA/Cy3 fluorescence corrected for isotype/Cy3 fluorescence) and dividing by the MFI of total HA-GLUT4-GFP expression (GFP fluorescence corrected for cells not expressing HA-GLUT4-GFP). The MFR is calculated from 5 independent experiments. Error bars are S.E.M (n = 5) ** denotes Student's T-test $P < 0.01$.

4.3.10 Recycling of HA-GLUT4-GFP

The results of the previous experiment demonstrated that the 96-well plate assay could be used to measure translocation of HA-GLUT4-GFP to the cell surface. Another aspect of GLUT4 trafficking that was important to study was the recycling of GLUT4 through intracellular compartments. For this experiment, basal or insulin-stimulated cells infected with a 1 in 4 dilution of HA-GLUT4-GFP lentivirus were incubated at 37 ^{o}C with Cy3-conjugated HA antibody for various time periods. As the HA epitope is inserted into the first exofacial loop of GLUT4, when Cy3-HA antibody is added to the culture medium, cells expressing HA-GLUT4-GFP accumulate the antibody with time. Any Cy3-HA antibody left on the surface after incubation was washed away and the level of intracellular HA-GLUT4-GFP was determined using a fluorescence plate reader as described in section 2.8.2.

Figure 4.10 shows that under basal conditions the Cy3: GFP ratio increases over time and plateaus at 10 hours. In insulin-stimulated conditions, the Cy3: GFP ratio increases slightly more quickly and starts to plateau at 2 hours. The plateau of the insulin-stimulated cells is lower than the plateau for the basal cells. The basal plateau was at 0.936 and the insulin plateau was at 0.574. The data from figure 4.10 suggests that in insulin-stimulated cells the rate of HA-GLUT4-GFP recycling is slightly higher than the rate in basal cells. Also the data suggests that the level of HA-GLUT4-GFP recycled in insulin-stimulated cells is lower than in basal cells.

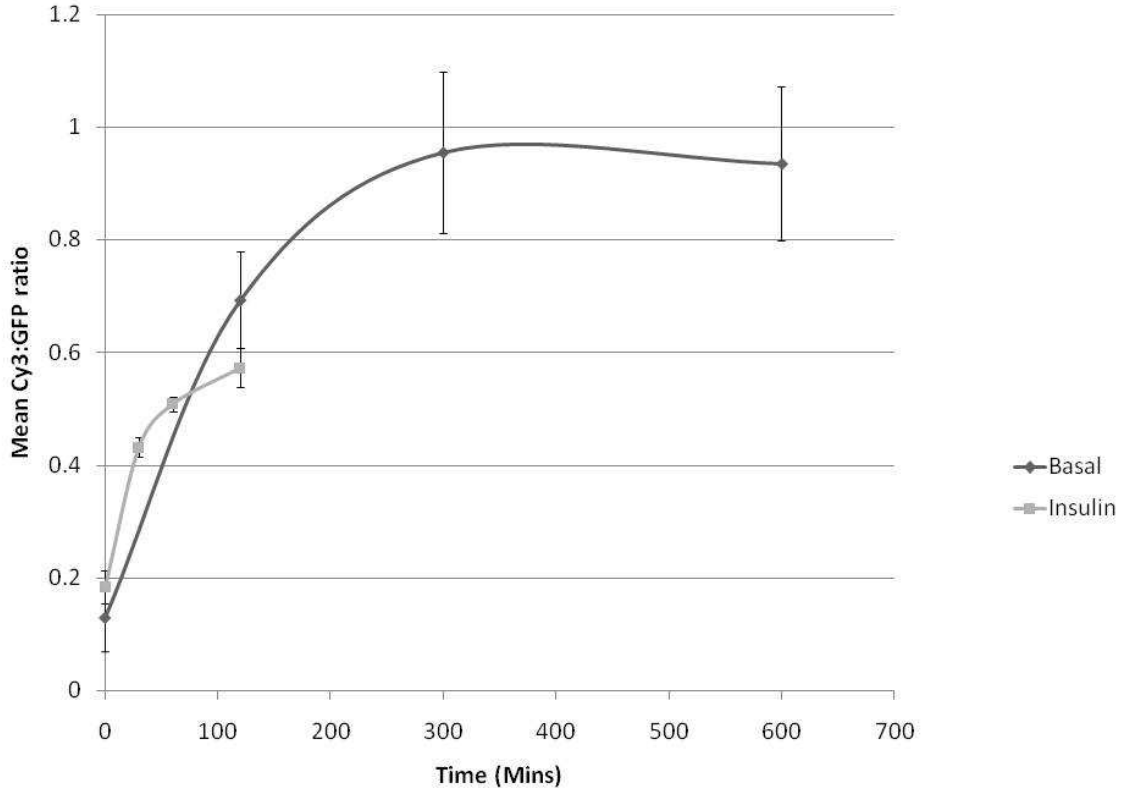

Figure 4.10 Recycling of HA-GLUT4-GFP in response to insulin.

3T3-L1 adipocytes infected with a 1 in 4 dilution of HA-GLUT4-GFP lentivirus (section 2.5.2) were labelled for recycling HA-GLUT4-GFP as described in section 2.8.2. Basal or insulin-stimulated cells were incubated with pre-warmed serum-free DMEM containing 50 μg/ml Cy3-HA.11 and with or without 170 nM insulin for the time periods shown (in minutes). The mean Cy3: GFP ratio at each time point is used as a measure of HA-GLUT4-GFP recycling. The Cy3: GFP ratio is calculated by determining the Cy3 MFI of the HA-GLUT4-GFP infected cells (HA/Cy3 fluorescence corrected for uninfected/Cy3 fluorescence) and dividing by the MFI of total HA-GLUT4-GFP expression (GFP fluorescence corrected for cells not expressing HA-GLUT4-GFP). Error bars are S.E.M (n = 3).

4.4 Discussion

As mentioned in section 4.1, insulin-stimulated GLUT4 translocation is an example of regulated membrane trafficking (Bryant *et al.*, 2002). It has been proposed that stx 16 has a role in GLUT4 trafficking (Proctor *et al.*, 2006). In this chapter a flow cytometry assay and 96-well plate assays were used to examine the trafficking of HA-GLUT4-GFP in 3T3-L1 adipocytes with the hope that these assays could be used to investigate the role of stx 16 in GLUT4 trafficking.

To determine the trafficking of HA-GLUT4-GFP, initially a flow cytometry assay was used which was based on the work of Muretta *et al.* (Muretta *et al.*, 2008). First of all 3T3-L1 fibroblasts were infected with lentivirus expressing HA-GLUT4-GFP. A 1 in 2 and a 1 in 4 dilution of lentivirus gave the greatest infection rate, but the 1 in 2 dilution gave the greatest level of HA-GLUT4-GFP expression (Fig. 4.1). Therefore, the cells infected with a 1 in 2 dilution of lentivirus were used in further experiments.

In the flow cytometry assay used by Muretta *et al.* only 3T3-L1 adipocytes wanted to be analysed for GLUT4 trafficking. However, after differentiation, some fibroblasts remain and the process of removing the adipocytes from their plates results in the formation of debris. To ensure that the cells being analysed by flow cytometry were only adipocytes, wild type 3T3-L1 adipocytes were sorted on the basis of FSC, SSC and autofluorescence in the APC channel (Fig.4.2). First of all, the cells were sorted on the basis of cell size by FSC and on the basis of cell granularity by SSC into the P1 and P2 populations. The P1 population was then sorted into P3 and P4 populations on the basis of autofluorescence in the APC channel. The P2 population with lower FSC and SSC was made up of undifferentiated fibroblasts. The P3 population with higher FSC and SSC but lower autofluorescence in the APC channel was adipocytes. The P4 population with higher FSC and SSC and higher autofluorescence in the APC channel was debris. Figure 4.2 shows that adipocytes could be distinguished from fibroblasts and debris by flow cytometry and that the adipocytes could be separated using a cell sorter.

The results of the first surface labelling experiment using cells infected with a 1 in 2 dilution of lentivirus and a RPE-conjugated secondary antibody were not as

expected. Figure 4.3 shows that there was a high level of RPE fluorescence for basal cells labelled with a HA antibody. This experiment was performed a couple of times and showed similar results. The high RPE fluorescence did not seem to be as a result of non-specific binding as the isotype controls had low RPE fluorescence. The high levels of RPE fluorescence in the basal cells suggested that the cells had a high level of HA-GLUT4-GFP on their cell surface. One possible explanation for this was that the 1 in 2-infected cells were expressing a level of HA-GLUT4-GFP which was too high, and HA-GLUT4-GFP molecules were escaping the retention mechanisms, which keep GLUT4 in intracellular compartments under basal conditions. Therefore, the level of HA-GLUT4-GFP expression was compared in 1 in 2 and 1 in 4-infected cells and was also compared to the level of endogenous GLUT4 found in negative control cells. Figure 4.4 shows that the level of HA-GLUT4-GFP in the 1 in 2-infected cells was much higher than endogenous levels of GLUT4. Whereas, the level of HA-GLUT4-GFP expression in the 1 in 4-infected cells was similar to endogenous GLUT4 levels.

Confocal studies were also performed to confirm that the high level of HA-GLUT4-GFP in the 1 in 2-infected cells was affecting the localisation of HA-GLUT4-GFP under basal conditions. Figure 4.5 shows that the 1 in 2-infected cells did indeed have high levels of surface HA-GLUT4-GFP under basal conditions and also showed that insulin stimulation did not greatly increase the level of HA-GLUT4-GFP at the cell surface compared with basal cells. This confirmed that the results of surface labelling assay in figure 4.3 were probably due to high levels of HA-GLUT4-GFP at the cell surface. In contrast, the level of HA-GLUT4-GFP at the cell surface of basal 1 in 4-infected cells was very low and increased greatly with insulin stimulation.

It was also noted that in figure 4.5, the level of GFP fluorescence in the 1 in 4-infected cells appeared lower in basal conditions compared with insulin-stimulated conditions. This occurred in all images obtained. It is unlikely that insulin stimulation for 30 minutes increased the level of HA-GLUT4-GFP expression. Perhaps the increase in GFP fluorescence is due to the HA-GLUT4-GFP molecules being closer to the cell surface in insulin-stimulated conditions, which may cause the GFP fluorescence to appear brighter.

The results of figure 4.4 and 4.5 suggested that cells infected with a 1 in 4 dilution of lentivirus might be more appropriate to use for the flow cytometry surface labelling assay. The cells had a level of HA-GLUT4-GFP expression that more closely matched endogenous GLUT4 levels. They also had the correct localisation of HA-GLUT4-GFP under basal conditions and were insulin-responsive. In addition, a 1 in 4 dilution of lentivirus produced a high infection rate (Fig. 4.1). Therefore, the 1 in 4-infected cells were used in all future experiments.

Unfortunately, when the 1 in 4-infected cells were used in a surface labelling assay, the results did not improve (Fig. 4.6). They were very similar to the results of figure 4.3. This suggested that the expression level of HA-GLUT4-GFP in the 1 in 2-infected cells was not the only problem with the assay. It was then suggested that there was a problem with the labelling, in particular with the RPE-conjugated secondary antibody. So the RPE-conjugated secondary antibody was used to stain surface HA-GLUT4-GFP and the cells were analysed by confocal microscopy as described in section 4.3.7. When the data of figures 4.5 and 4.7 were compared, the RPE staining was not as strong, clean or as consistent as the Cy3 staining. As the Cy3-conjugated secondary antibody gave better staining in confocal experiments, the flow cytometry surface labelling assay was repeated using the Cy3-conjugated secondary antibody. As there was no Cy3 channel on the flow cytometer the level of surface HA-GLUT4-GFP was measured using the RPE channel which is the closest channel to the Cy3 excitation/emission wavelengths (Ex/Em). Cy3 has an Ex/Em of 550/580 and RPE has an Ex/Em of 480/580. As shown in figure 4.8, using the Cy3-conjugated secondary antibody reduced the high basal fluorescence, which was now almost identical to the isotype control fluorescence. However the fluorescence of the insulin-stimulated cells labelled with HA antibody was much lower than expected and was very close to basal values. This may be due to the fact the RPE channel was not specific to Cy3 fluorescence and therefore it was not as sensitive to changes in Cy3 fluorescence. To detect RPE the cells were excited using a 488 nm laser, which is much lower than the excitation wavelength of Cy3 and the emission was detected by channel FL-3, which uses a 585/40 bandpass filter.

It was then decided to try the surface labelling assay in a 96-well plate format and use a fluorescence plate reader to measure surface levels of HA-GLUT4-GFP.

Figure 4.9 shows that insulin-stimulated HA-GLUT4-GFP translocation was successfully determined. Insulin stimulation resulted in an over four-fold increase in surface HA-GLUT4-GFP compared with basal cells ($P < 0.01$).

Once an assay had been developed to measure HA-GLUT4-GFP translocation to the cell surface, the recycling of HA-GLUT4-GFP was examined using the method described in section 2.8.2. Initial experiments used a mouse HA.11 primary antibody with a Cy3-conjugated secondary antibody but they were not successful (data not shown). It was thought that using separate primary and secondary antibodies may be the reason for the poor results. So a Cy3-conjugated HA antibody was made using a Cy3-labelling kit as described in section 2.4.11.

Using a conjugated antibody improved the results (Fig. 4.10). The Cy3: GFP ratio was used as a measure of recycling, as the time-dependent increase of Cy3-labelled HA-GLUT4-GFP is a measure of the movement of unlabelled intracellular HA-GLUT4-GFP to the cell surface. In basal cells the Cy3: GFP ratio increased over time until it reached a plateau at around 10 hours. This agrees with the results of a similar experiment by Karylowski *et al.* (Karylowski *et al.*, 2004). The rate of recycling of HA-GLUT4-GFP was slightly higher with insulin. The Cy3: GFP ratio increased slightly more quickly and started to plateau at 2 hours.

The curve for insulin-stimulated cells was not as steep as expected. Other work has shown that the Cy3: GFP ratio reaches a plateau at 45 minutes in insulin-stimulated cells (Karylowski *et al.*, 2004). This difference has been suggested by Prof. Timothy McGraw (Weill Cornell Medical College) to be due to variations in cell culture or experimental conditions (personal communication). Karylowski *et al.* used electroporation as a method of expressing HA-GLUT4-GFP in 3T3-L1 adipocytes rather than a lentiviral method. In addition, Karylowski *et al.* used confocal microscopy to analyse the cells (Karylowski *et al.*, 2004). Both of these methods require the replating of differentiated adipocytes, which may have an effect on the trafficking of GLUT4 (Muretta *et al.*, 2008). Finally, Karylowski *et al.* used adipocytes at days 5-7 post-differentiation, rather than at days 8-10 post-differentiation, which may have affected the cells' responsiveness to insulin (Karylowski *et al.*, 2004).

In addition, the level of the plateau reached in insulin-stimulated cells was not as high as the level reached by basal cells. At saturating concentrations of

antibody, the level of the plateau indicates the size of the cycling pool of HA-GLUT4-GFP.The level of recycled GLUT4 should not have been lower in insulin-stimulated cells. In the experiments by Karylowski *et al.* both basal and insulin-stimulated cells reached the same plateau (Karylowski *et al.*, 2004). In fact, other work has suggested that insulin increases the amount of recycling GLUT4 in a dose dependent manner (Govers *et al.*, 2004). Perhaps a higher concentration of insulin was needed to increase the recycling rate further, or possibly the concentration of Cy3-HA antibody was not saturating, which would limit the rate of recycling. However it has been shown that at 50μg/ml the accumulation of Cy3-labelled HA-GLUT4-GFP is not rate limited by antibody binding (Muretta *et al.*, 2008). There was not sufficient time to fully address these problems.

Once the surface labelling assay and the recycling assay had been developed, it was hoped that these assay could be used to investigate the effect of stx 16 knockdown on GLUT4 trafficking. Unfortunately there was not time perform those experiments. The experiments would have required cell lines, which expressed both the shRNA to knockdown stx 16 expression and HA-GLUT4-GFP. This would have involved infecting 3T3-L1s with a retrovirus and a lentivirus. There is nothing in the literature to suggest this had been done before. It was not known whether the infections could be done simultaneously or sequentially. It would have required lots of optimisation to ensure that both constructs were being expressed and to select cells, which were expressing both constructs. Alternatively, the HA-GLUT4-GFP-infected cells could have been transiently transfected with stx 16 shRNA using an electroporation method. However, this method would have involved replating differentiated 3T3-L1 adipocytes, which may have affected HA-GLUT4-GFP recycling by inhibiting static retention of HA-GLUT4-GFP (Muretta *et al.*, 2008).

In summary the data in this chapter shows the development of a surface labelling assay to measure translocation of HA-GLUT4-GFP and an assay to measure the recycling of HA-GLUT4-GFP. This chapter also illustrates the importance of expression levels of HA-GLUT4-GFP, which can adversely affect trafficking.

Chapter 5 Phosphorylation of syntaxin 16

5.1 Introduction

When insulin binds to its receptor, it results in a cascade of signalling events (section 1.3.2) (Kanzaki, 2006). Many of these events involve the activation of kinases and phosphatases. This suggests that phosphorylation status is an important mechanism by which insulin regulates the proteins involved in GLUT4 trafficking. It has been shown that activation of Akt2 is sufficient to stimulate GLUT4 translocation to a similar extent to insulin (Ng et al., 2008). This suggests that phosphorylation of substrates by Akt2 is sufficient to induce GLUT4 translocation. Also it has been shown that insulin-dependent phosphorylation of AS160 is essential for GLUT4 translocation (Stockli et al., 2008). These examples demonstrate the importance of phosphorylation in regulating GLUT4 trafficking.

Vesicle fusion is a highly regulated process. The assembly of cognate SNAREs into a trans-SNARE complex is regulated in a number of ways (Gerst, 2003). Some SNAREs are regulated by SM proteins which regulate the availability and assembly of SNAREs into a trans-SNARE complex. SNAREs can also be regulated by phosphorylation. It has been shown that (de)phosphorylation of t-SNAREs is important for exocytosis and endocytosis in yeast (Marash and Gerst, 2001;Gurunathan *et al.*, 2002) Yeast cells lacking Snc1p and Snc2p (*snc)* are defective in exocytosis. Treatment of *snc* cells with ceramide ameliorated this defect and resulted in the dephosphorylation of Ssop t-SNAREs and the formation of complexes between Ssop and Sec9p t-SNAREs. Mutation of a single PKA phosphoryation site (Ser 79) in Sso1p to alanine was sufficient to rescue *snc* cells in the absence of ceramide. Also recombinant Sso1p phosphorylated *in vitro* by Tpk1p was unable to assemble into complexes with Sec9p (Marash and Gerst, 2001). This data suggests that t-SNARE phosphorylation by PKA inhibits SNARE assembly and subsequent fusion in yeast. The data also suggests a ceramide-regulated pathway can restore exocytosis in *snc* cells by dephosphorylating t-SNAREs.

Yeast cells lacking Tlg1p or Tlg2p t-SNAREs and the v-SNAREs Snc1p and Snc2p are defective in endocytosis. Ceramide treatment restored endocytosis to cells lacking Snc1p, Snc2p and Tlg1p or Tlg2p and also promoted assembly of Tlg1p

and Tlg2p into complexes in *snc* cells. Phosphorylation of Tlg1p and Tlg2p *in vitro* by Tpk1p inhibited complex assembly. Also mutation of single PKA sites in Tlg1p (Ser 31) or Tlg2p (Ser 90) to alanine was sufficient to restore endocytosis in *snc* cells (Gurunathan et al., 2002). This data suggests that like exocytosis, endocytosis is regulated by t-SNARE phosphorylation *in vivo*.

Stx 16 is phosphorylated in adipocytes under basal conditions (Perera et al., 2003). 3T3-L1 adipocytes labelled with ^{32}Pi were treated with or without 1 μM insulin. Autoradiographs showed that stx 16 immunoprecipitated from basal cells was phosphorylated and this phosphorylation decreased by approximately 50% in response to insulin. It is thought that this dephosphorylation controls an important event in GLUT4 trafficking. Recently it has been shown that stx 16 is a functional homologue of Tlg2p (Struthers et al., 2009). Yeast cells lacking Tlg2p (Δ*tlg2*) display multiple endocytic defects. The endocytic defects of Δ*tlg2* cells cause a delay in the degradation of the pheromone receptor Ste3p by vacuolar proteases (Seron et al., 1998). Also the delivery of the lipophilic dye FM4-64 to vacuolar membranes is delayed in these cells. Δ*tlg2* mutants are also sensitive to osmotic stress and exhibit a growth defect on high salt media (Abeliovich et al., 1998). All of these defects were rescued by expression of HA-Tlg2p or HA-Stx 16, but not the expression of an unrelated stx, HA-Stx 4. This suggests that stx 16 can perform the same functions as Tlg2p and is therefore a functional homologue of Tlg2p (Struthers et al., 2009).

Tlg2p is known to be phosphorylated at Ser 90 (Gurunathan et al., 2002). Previous work in the lab by Dr. Kirsty Proctor (University of Glasgow) identified three potential phosphorylation sites in stx 16 using a bioinformatics approach. First of all, NetPhos 2.0 (http://www.cbs.dtu.dk/services/NetPhos/) was used to analyse the stx 16A protein sequence for potential phosphorylation sites. The analysis suggested Ser 94 and Ser 95 as likely candidates with output scores of 0.996 and 0.998 respectively (on a scale of 0.000 to 1.000). These sites were favoured over other high scoring serine residues (Ser 80, Ser 131 and Ser 224) because they were closest in the sequence to the Ser 90 phosphorylation site in Tlg2p. Analysis of the threonine residues revealed Thr 90 as another potential phosphorylation site with an output score of 0.601. Although the output score for Thr 90 was not as high as those for Ser 94 and Ser 95, (and some of the other

threonine residues: Thr 3, Thr105, Thr 178 and Thr 197) it corresponded well to the Ser 90 phosphorylation site in Tlg2p.
The potential phosphorylation sites, Thr 90, Ser 94 and Ser 95 were analysed further using the Scansite program Motif Scan which searches for motifs within proteins that are likely to be phosphorylated by specific protein kinases. The analysis focussed on identifying potential PKA sites within the stx 16A protein sequence, as Tlg2p is phosphorylated at Thr 90 by PKA (Gurunathan *et al.*, 2002). Thr 90 was identified as a potential PKA phosphorylation site. Ser 94 and Ser 95 were identified as potential Casein Kinase II phosphorylation sites. The three potential phosphorylation sites, Thr 90, Ser 94 and Ser 95 have been investigated in this chapter.

The potential sites are at the start of the second predicted helix of the Habc domain in stx 16 (Dulubova et al., 2002). Therefore phosphorylation at one or more of these sites might regulate the ability of stx 16 to adopt a closed confirmation in which the Habc domain binds to the SNARE domain of stx 16 (Struthers et al., 2009). Phosphorylation might also regulate the binding of stx 16 to its SM protein mVps45 (Dulubova *et al.*, 2002;Struthers *et al.*, 2009). Therefore phosphorylation of stx 16 may regulate the assembly of stx 16 into SNARE complexes and subsequent fusion.

5.2 Aims of this chapter

The aim of this chapter was to determine the phosphorylation site of stx 16. Two complementary approaches were used to determine the phosphorylation site. First of all, stx 16 mutants of the three potential phosphorylation sites were screened in yeast cells lacking Tlg2p to determine whether expression of the stx 16 mutants could complement the phenotypes of Δ*tlg2* cells. Also several techniques were used to determine the phosphorylation site of endogenous stx 16 in 3T3-L1 adipocytes.

5.3 Results

5.3.1 Yeast studies

5.3.1.1 Site-directed mutagenesis of stx 16

Recent work which showed stx 16 was a functional homologue of Tlg2p used a HA-tagged human stx 16A plasmid to express stx 16 in Δ*tlg2* yeast cells (Struthers et al., 2009). Single alanine mutants of the three potential stx 16 phosphorylation sites (Thr 90, Ser 94 and Ser 95) and a triple alanine mutant had been made previously in the lab by Dr. Scott Shanks (University of Glasgow). Single phosphomimetic aspartic acid mutants of stx 16 were made by site-directed mutagenesis as described in section 2.2.11 using the primers described in section 2.1.5. After mutagenesis, the plasmids were sequenced on both strands as described in section 2.2.7.

5.3.1.2 Expression of Tlg2p and stx 16 mutants in Δ*tlg2* yeast

Δ*tlg2* yeast cells were transformed with stx 16 mutants and the expression of the HA-tagged stx 16 mutants and Tlg2p was determined. Figure 5.1 shows an example of a set of transformations. Δ*tlg2* yeast cells were transformed with pHA-Tlg2, pHA-Stx 16, pHA-Stx 4 or pHA-Stx 16 T90A, S94A, S95A. As a control wild type and Δ*tlg2* cells were transformed with the empty vector (pVT102U). Figure 5.1 shows that wild type cells did not express any HA-tagged proteins and expressed a low level of Tlg2p. Δ*tlg2* cells did not express any Tlg2p as expected. Cells transformed with pHA-Stx 16, pHA-Stx 4 or pHA-Stx 16 T90A, S94A, S95A all expressed the HA-tagged proteins but to different levels. The expression of HA-Tlg2p in cells transformed with pHA-Tlg2 could not be detected on the HA blot but a high level of Tlg2p was present in the Tlg2p blot suggesting that HA-Tlg2p was in fact overexpressed in these cells.

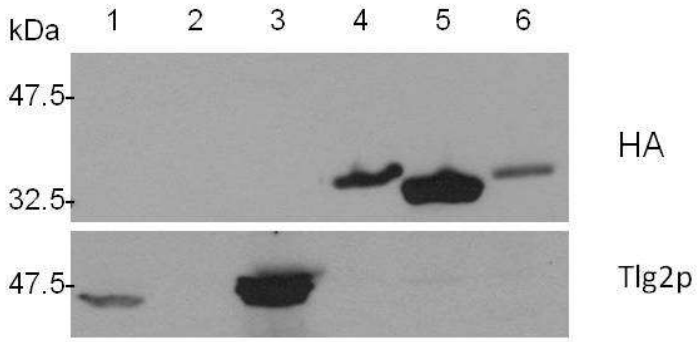

Figure 5.1. Expression of HA-Stx 16 and phosphosite mutant in yeast.

RPY10 Δ*tlg2* (NOzY4) yeast strains were transformed as described in section 2.9.3 with pHA-Tlg2, pHA-Stx 16 (pSGS025) pHA-Stx 4 (pSGS036), or pHA-Stx 16 T90A, S94A, S95A. As a control wild type RPY10 and RPY10 Δ*tlg2* cells were transformed with the empty vector (pVT102U) (n = 6). 10 μl of the samples prepared as described in section 2.9.4 were separated on a 10% (v/v) SDS-PAGE gel, transferred to nitrocellulose and blotted (sections 2.4.4- 2.4.6). The samples were blotted for the HA-tagged proteins using a rat anti-HA primary antibody at a 1:1000 dilution. The samples were blotted for Tlg2p using a rabbit anti-Tlg2p antiserum at a 1:100 dilution after blocking overnight with 5% (w/v) low-fat milk powder. The numbers at the side of the blots indicate molecular weight in kDa.

Lane 1: RPY10 + pVT102U

Lane 2: RPY10 Δ*tlg2* + pVT102U

Lane 3: RPY10 Δ*tlg2* + pHA-Tlg2

Lane 4: RPY10 Δ*tlg2* + pHA-Stx 16

Lane 5: RPY10 Δ*tlg2* + pHA-Stx 4

Lane 6: RPY10 Δ*tlg2* + pHA-Stx 16 T90A, S94A, S95A

5.3.1.3 Ste3p-myc endocytosis assay

Yeast lacking Tlg2p have delayed endocytosis and degradation of the Ste3p receptor (Seron et al., 1998). This is due to delayed trafficking of Ste3p to the vacuole. Expression of HA-Stx 16 rescues this defect (Struthers et al., 2009). Ste3p-myc endocytosis and degradation was determined in wild type yeast cells, Δ*tlg2* cells and Δ*tlg2* cells expressing HA-Stx 16 or HA-Stx 16 T90A, S94A and S95A. As a control wild type and Δ*tlg2* yeast cells were transformed with pVT102U empty vector. Figure 5.2 shows that in wild type cells Ste3p-myc was efficiently endocytosed and degraded within 80 minutes. In Δ*tlg2* cells the degradation of Ste3p-myc was delayed. This is in agreement with previous work with Δ*tlg2* cells (Seron *et al.*, 1998;Struthers *et al.*, 2009). The level of Ste3p-myc at the 20 minute time point and all subsequent time points was increased compared with wild type cells and Ste3p-myc was still present after 80 minutes. This suggests that trafficking of Ste3p to the vacuole is impaired, resulting in the delayed degradation of Ste3p by vacuolar proteases. Expression of HA-Stx 16 partially rescued this effect. The rate of Ste3p-myc degradation was increased and the amount of Ste3p-myc present after 80 minutes was decreased. This suggests that Ste3p trafficking has been restored by expression of HA-Stx 16. This also suggests that stx 16 can function in place of Tlg2p in Ste3p trafficking. However expression of HA-Stx16 T90A, S94A, S95A gave a phenotype similar to Δ*tlg2* cells. The level of Ste3p-myc was stabilised and only started to degrade at 80 minutes. This suggests that Ste3p trafficking was not restored by expression of HA-Stx16 T90A, S94A, S95A.

5.3.1.4 KCl osmotic stress assay

Yeast lacking Tlg2p are sensitive to osmotic stress and have reduced growth on high salt plates (Abeliovich et al., 1998). Expression of HA-Stx 16 rescues this defect (Struthers et al., 2009). Wild type, Δ*tlg2* cells and Δ*tlg2* cells expressing HA-Tlg2p, HA-Stx 4, HA-Stx 16, HA-Stx 16 T90A, HA-Stx 16 S94A or HA-Stx 16 S95A were plated on S-D –Ura –Met plates with or without 1.5 M KCl. As a control wild type and Δ*tlg2* yeast cells were transformed with pVT102U empty vector. Figure 5.3 shows that all yeast strains grew well on S-D –Ura –Met plates. All strains grew less well on plates containing 1.5M KCl. The Δ*tlg2* cells were particularly affected. The level of growth was reduced across all dilutions,

particularly in the 3rd and 4th dilution compared with the wild type cells. This agrees with previous experiments on Δ*tlg2* cells (Abeliovich *et al.*, 1998;Struthers *et al.*, 2009). The expression of HA-Tlg2p in Δ*tlg2* cells increased growth at all dilutions which shows that the osmotic stress phenotype was due to a lack of Tlg2p expression. Expression of HA-Stx 4 did not increase the growth of Δ*tlg2* cells which shows that stx 4 cannot rescue the osmotic stress phenotype. Expression of HA-Stx 16 increased growth of Δ*tlg2* cells across all dilutions, which shows that stx 16 can rescue the osmotic stress phenotype in Δ*tlg2* cells. Also expression HA-Stx 16 T90A or HA-Stx 16 S94A increased growth of Δ*tlg2* cells across all dilutions. However expression of HA-Stx 16 S95A did not increase growth of Δ*tlg2* cells.

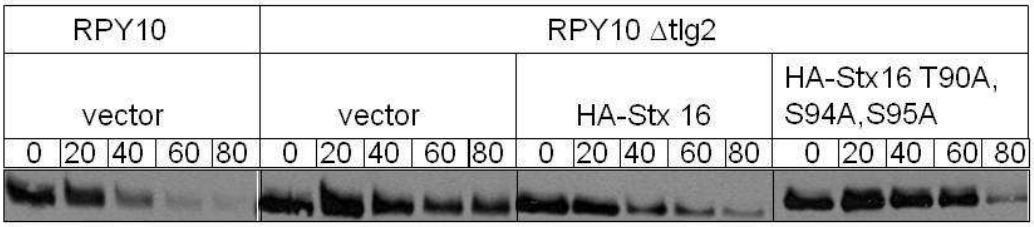

Figure 5.2 Ste3p-myc endocytosis assay.

RPY10 Δ*tlg2* (NOzY4) yeast strains were transformed as described in section 2.9.3 with pHA-Stx 16 (pSGS025) or pHA-Stx 16 T90A, S94A, S95A. As a control wild type RPY10 and RPY10 Δ*tlg2* cells were transformed with the empty vector (pVT102U). All the strains were transformed with pSL2099 expressing the Ste3p-myc fusion protein. Ste3p-myc endocytosis was determined as described in section 2.9.4 (n = 1). To ensure equal loading, each sample was resuspended at the same OD_{600}/ml concentration. 10 μl of the samples were separated on a 10% (v/v) SDS-PAGE gel, transferred to nitrocellulose and blotted as described in sections 2.4.4, 2.4.5 and 2.4.6. The samples were blotted for Ste3p-myc using a mouse anti-myc primary antibody at a 1:250 dilution.

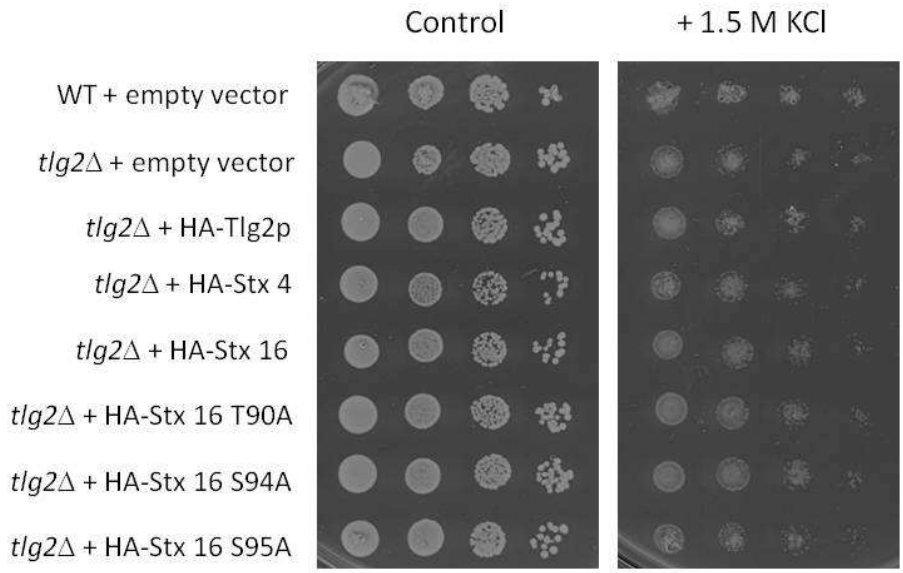

Figure 5.3 KCl osmotic stress assay.

Δ*tlg2* (NOzY3) yeast strains were transformed as described in section 2.9.3 with pHA-Tlg2, pHA-Stx 4 (pSGS036), pHA-Stx 16 (pSGS025), pHA-Stx 16 T90A, pHA-Stx 16 S94A and pHA-Stx 16 S95A. As a control wild type (SF838-9D) or Δ*tlg2* (NOzY3) cells were transformed with the empty vector (pVT102U). Aliquots (5 μl) of 1 OD_{600}/ml cultures and ten-fold serial dilutions were spotted on S-D –Ura –Met plates with or without 1.5 M KCl in triplicate as described in section 2.9.6 (n=1).

5.3.2 3T3-L1 adipocyte studies

5.3.2.1 Phosphopeptide purification kit

Several attempts to determine the phosphorylation site of stx 16 in 3T3-L1 adipocytes had proved unsuccessful (see section 5.4). The Fingerprint Proteomics unit at the University of Dundee offered a service to determine the phosphorylation site of protein immunoprecipitated from cell lysates. However this required large amounts of protein (enough protein to be visible by colloidal Coomassie staining). Early attempts to immunoprecipitate the required amount of stx 16 to send for analysis were unsuccessful (data not shown). So a phosphopeptide enrichment technique was used in the hope that this would provide enough sample to be analysed by mass spectrometry. Stx 16 was immunoprecipitated from basal and insulin-stimulated 3T3-L1 adipocytes as described section 2.4.7. The immunoprecipitated proteins were left bound to the Protein A-agarose and were denatured and digested as described in section 2.4.10. Two phosphopeptide enrichment methods were used to purify the phosphopeptides. A TiO_2 method described in section 2.4.10.1 and a SCIMAC method described in section 2.4.10.2. As a control an immunoprecipitation reaction from basal cells was run in tandem with the samples to be used for phosphopeptide purification. This immunoprecipitation was separated on an SDS-PAGE gel and blotted for stx 16 to ensure that stx 16 had been correctly immunoprecipitated. Figure 5.4 shows immunoprecipitations performed before purifying for phosphopeptides using the TiO_2 method and the SCIMAC method. The figure shows that stx 16 was successfully immunoprecipitated in both cases. A low level of stx 16 was present in the IgG supernatant. But no stx 16 was detected in the stx 16 supernatant. No stx 16 was immunoprecipitated with the control IgG antiserum but a large amount of stx 16 was immunoprecipitated with the rabbit stx 16 antiserum.

When the samples were analysed by mass spectrometry, unfortunately no phosphopeptides were detected. Therefore a sample of the pre-purification digest was sent for analysis. Again no phosphopeptides were detected.

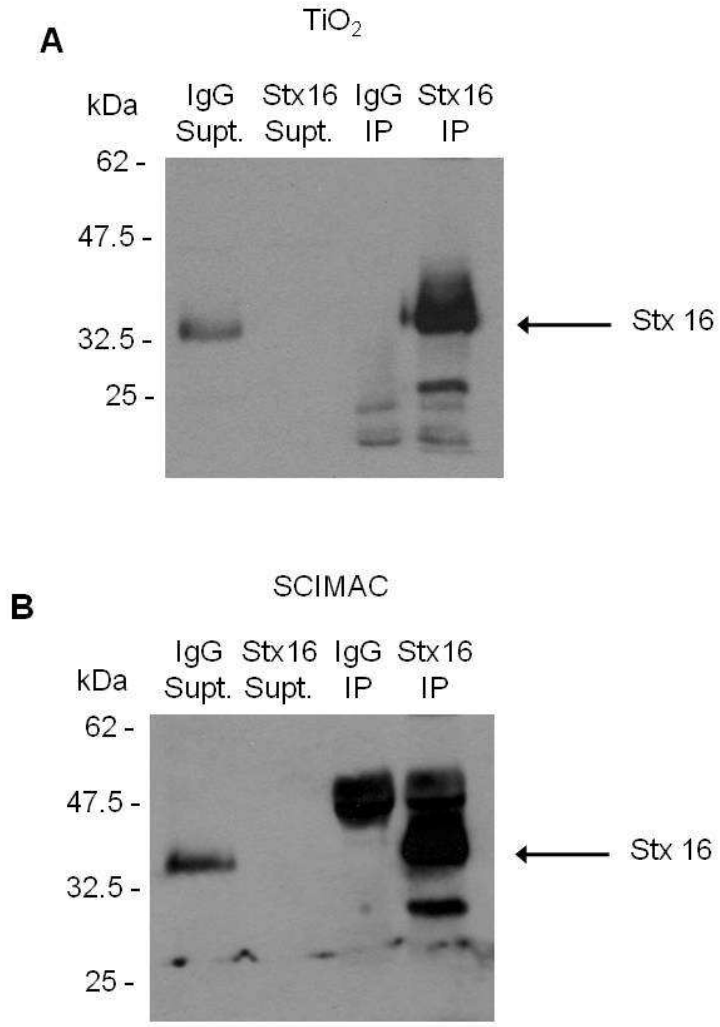

Figure 5.4 Immunoprecipitation of stx 16 for proteomic analysis.

Endogenous stx 16 was immunoprecipitated from 3T3-L1 adipocytes as described in section 2.4.7. Three 10 cm plates were used for each immunoprecipitation. Rabbit stx 16 antiserum (Stx 16) was used to immunoprecipitate stx 16. As a control rabbit anti-sheep IgG antiserum (IgG) was used. 20 μl (1/50) of the unbound supernatant after immunoprecipitation was loaded in the first two lanes (IgG supt., Stx 16 supt.). In the second two lanes the immunoprecipitates were loaded (IgG IP and Stx 16 IP). The samples were separated on a 10% (v/v) SDS-PAGE gel, transferred to nitrocellulose and blotted for stx 16 as described in sections 2.4.4, 2.4.5 and 2.4.6. To blot for stx 16, rabbit stx 16 antiserum was used as the primary antibody at a 1:1000 dilution and a Protein-A-HRP secondary was used at a 1:2500 dilution. The numbers at the side of the blots indicate molecular weight in kDa. Other stx 16 immunoprecipitation reactions were run in parallel and used in proteomic analysis and were not put on a gel.

A. Stx 16 Immunoprecipitation prior to trypsin digest and phosphopeptide purification by TiO_2.

B. Stx 16 Immunoprecipitation prior to trypsin digest and phosphopeptide purification by SCIMAC.

Bands corresponding to stx 16 are indicated by the arrows.

5.4 Discussion

Stx 16 is known to be phosphorylated in adipocytes under basal conditions (Perera et al., 2003). It is proposed that dephosphorylation of stx 16 in response to insulin could regulate an important event in GLUT4 trafficking. In this chapter the insulin-regulated phosphorylation site of stx 16 was examined. The phosphorylation site of stx 16 was studied in both yeast and 3T3-L1 adipocytes. It was hoped that once the phosphorylation site had been determined, the effect of stx 16 phosphorylation on GLUT4 trafficking and protein interactions involving stx 16 could be investigated.

In this study, the phosphorylation of stx 16 in adipocytes was not tested, as it had been previously shown that stx 16 is phosphorylated under basal conditions (Perera *et al.*, 2003). Perera *et al.* showed that stx 16 immunoprecipitated from basal cells labelled with ^{32}Pi was phosphorylated and that this phosphorylation decreased by approximately 50% in response to insulin. This experiment was performed three times. Other unpublished work performed by Dr. Kirsty Proctor (University of Glasgow) investigated the kinetics of stx 16 dephosphorylation. Insulin-stimulated dephosphorylation was shown to be evident within 5 minutes of the addition of insulin and maximum dephosphorylation occurred after 15 minutes. In addition to the experiments above, the phosphorylation of stx 16 could also have been detected by blotting stx 16 immunoprecipitates from basal and insulin –stimulated adipocytes with phosphotyrosine, phosphoserine and phosphothreonine antibodies. Alternatively the stx 16 immunoprecipitates could have been stained with the Pro-Q® Diamond Phosphoprotein blot stain by Molecular Probes®.

Recently stx 16 had been shown to be a functional homologue of Tlg2p (Struthers et al., 2009). It was thought this would be a useful way of screening mutants of the potential phosphorylation sites in stx 16. Dr. Scott Shanks (University of Glasgow) had already made single alanine mutants of the three potential stx 16 phosphorylation sites (Thr 90, Ser 94 and Ser 95) and a triple alanine mutant. Single phosphomimetic aspartic acid mutants of stx 16 were made by site-directed mutagenesis as described in section 5.3.1.1.

Before the phosphorylation site mutants could be used in any experiments, their expression in yeast had to be confirmed. Figure 5.1 shows an example of a set of transformations. All of the HA-tagged proteins were expressed in yeast at a similar level or higher level than endogenous Tlg2p in the wild type yeast strain. It was not possible to detect the expression of HA-Tlg2p by anti-HA blot but HA-Tlg2p was detected by anti-Tlg2p blot. This may be because the pHA-Tlg2 plasmid was not made in house and the HA tag had a different sequence to the HA tags of the other proteins. The HA antibody may not have been able to bind to the HA-tagged Tlg2p. HA-Stx 4 was to be used as a control to show that expression of an unrelated stx did not complement Δ*tlg2* yeast and therefore the effects seen were specific to stx 16.

Once the expression of the phosphorylation site mutants was confirmed in yeast, they were used in a Ste3p-myc endocytosis assay which had been previously used to show that stx 16 expression can complement Δ*tlg2* yeast (Struthers et al., 2009). Figure 5.2 shows that while HA-Stx 16 expression rescued the delayed Ste3p-myc degradation seen in Δ*tlg2* cells, the expression of HA-Stx 16 T90A, S94A, S95A did not. A control of Δ*tlg2* cells expressing HA-Stx 4 was not used in this experiment as their growth was poor. This may have been due to the very high level of HA-Stx 4 expression in the cells which was seen in figure 5.1. However it has already been shown that stx 4 expression does not complement Δ*tlg2* yeast in this assay (Struthers et al., 2009). The assay was repeated with the stx 16 single alanine mutants, however the differences in Ste3p-myc degradation were too subtle to determine which single alanine mutants rescued Δ*tlg2* cells and which did not.

A carboxypeptidase Y (CPY)-invertase assay was then used to screen the stx 16 mutants as this assay gave more quantitative data (Darsow et al., 2000). Unfortunately initial experiments involving wild type yeast cells, Δ*tlg2* cells and Δ*tlg2* cells expressing HA-Tlg2p, HA-Stx 4 or HA-Stx 16 were unsuccessful. The results did not show any difference between wild type and Δ*tlg2* cells (data not shown).

As the Ste3p-myc assay and the CPY-invertase assay had been unsuccessful in determining the phosphorylation site of stx 16, another assay was tried. Expression of stx 16 can rescue the osmotic stress phenotype of Δ*tlg2* yeast cells

(Struthers et al., 2009). Figure 5.3 shows that expression of stx 16 rescued the growth defect of Δ*tlg2* cells on high salt medium. Stx 16 T90A and stx 16 S94A expression also rescued the growth defect of Δ*tlg2* cells. However stx 16 S95A expression did not. This result will need to be confirmed by repeat experiments and the phosphorylation site will also need to be confirmed in 3T3-L1 adipocytes.

The difference between the growth of wild type and Δ*tlg2* cells on high salt medium was not as big as that seen by Struthers *et al* (Struthers *et al.*, 2009). The same yeast strains as those used by Struthers *et al.* were used in this experiment. However the plates did not contain 50 μM $CuCl_2$ as the plasmids used to transform the yeast cells contained a constitutive ADH promoter and not a Cu^{2+}-controlled CUP1 promoter. This may account for the difference in growth of the strains on high salt medium.

The Ste3p receptor endocytosis assay and the osmotic stress assay allow the phosphorylation site of stx 16 to be investigated. Information from these assays could then be used to inform experiments on stx 16 in 3T3-L1 adipocytes which would investigate GLUT4 trafficking. Any suggestion of a phosphorylation site using the Ste3p receptor assay and the osmotic stress assay would need to be further investigated to ensure that the effects seen in the phosphosite mutants were due to changes in phosphorylation and not for example, changes in protein folding or protein interactions.

Ser 95 is at the start of the second predicted helix of the Habc domain in stx 16 (Dulubova et al., 2002). So phosphorylation at Ser 95 might regulate the ability of stx 16 to adopt a closed confirmation (Struthers et al., 2009). Alternatively phosphorylation might regulate the binding of stx 16 to its SM protein mVps45 (Dulubova *et al.*, 2002;Struthers *et al.*, 2009) or other SNARE proteins such as stx 6 (Perera et al., 2003). The effect of phosphorylation of stx 16 on its interactions with mVps45 or stx 6 could be examined by expressing the alanine mutant and phosphomimetic aspartic acid mutant of Ser 95 in stx 16-depleted cells and then performing co-immunoprecipitation assays. Alternatively the stx16 Ser 95 mutants, mVps45 and stx 6 could be expressed in *E.Coli* and *in vitro* binding assays performed.

While the phosphorylation site of stx 16 was investigated using yeast, experiments were also performed using 3T3-L1 adipocytes to determine the insulin-regulated phosphorylation site of stx 16. Before starting any experiments to determine the site, several different alanine mutants and aspartic acid phosphomimetic mutants of a myc-tagged stx 16 were made. It was hoped that these mutants could be used in future assays to examine the phosphorylation site of stx 16. Previously ^{32}Pi labelling had been used to determine the phosphorylation site of stx 16 using stx 16 T90A and stx 16 S94A, S95A made by Dr. Kirsty Proctor (University of Glasgow). Unfortunately those experiments had been unsuccessful.

Therefore a different approach was taken. It was hoped that expressing the phosphorylation site alanine mutants of stx 16 in 3T3-L1 adipocytes, then purifying lysates for phosphoproteins and blotting for the myc-tagged stx 16 mutants would identify the phosphorylation site. Unfortunately initial attempts to use the phophosprotein kit to purify endogenous phosphorylated stx 16 as described in section 2.4.9 from basal and insulin-stimulated wild type 3T3-L1 adipocytes were unsuccessful. The concentration of the eluate which contained phosphorylated proteins was too low for endogenous stx 16 to be detected by western blot (data not shown).This was the case in all attempts with the kit. The low concentration of the eluate also meant it was not possible to detect other proteins known to be phosphorylated in insulin-stimulated 3T3-L1 adipocytes, for example PKB/Akt. This would have shown whether the phosphoprotein kit was working correctly.

Since the phosphoprotein purification kit had been unsuccessful, a new approach was taken. Instead of using stx 16 mutants, the phosphorylation site of endogenous stx 16 in 3T3-L1 adipocytes was investigated. The Fingerprint Proteomics unit at the University of Dundee offered a service to determine the phosphorylation site of protein immunoprecipitated from cell lysates. So stx 16 was immunoprecipitated from basal and insulin stimulated 3T3-L1 adipocytes so that the insulin-regulated phosphorylation site of stx 16 could be determined. The Fingerprint Proteomics unit required large amounts of protein to determine the phosphorylation site. However initial attempts at immunoprecipitating stx 16 did not provide sufficient protein to send for analysis (data not shown). After investigating solutions to the problem and discussing it with the Fingerprint

Proteomics unit, it was suggested that a phosphopeptide enrichment kit may compensate for the low levels of stx 16 protein immunoprecipitated. Therefore after immunoprecipitation, the protein bound to the Protein A-agarose was denatured, digested and enriched for phosphopeptides as described in section 5.3.2.1. Both TiO_2 and SCIMAC phosphopeptide enrichment kits were used as the methods enrich different profiles of peptides (Bodenmiller *et al.*, 2007). The TiO2 method tends to isolate singly phosphorylated, acidic phosphopeptides. Whereas, the SCIMAC method tends to isolate more doubly phosphorylated phosphopeptides. As no single method can isolate the whole phosphoproteome, using the two different kits would give a better chance of enriching a phosphopeptide which contained the insulin-regulated phosphorylation site of stx 16.

Unfortunately when the samples were sent for analysis, no phosphopeptides were detected. Figure 5.4 shows that stx 16 was successfully immunoprecipitated before digestion and phosphopeptide enrichment. So the problem did not seem to be the immunoprecipitation protocol. It was thought that either there was a problem with the phosphopeptide enrichment kits or that the concentration of peptides after digestion was too low for enrichment. Therefore a sample of the digested immunoprecipitate prior to phosphopeptide enrichment was sent for analysis. In this case peptides were detected but they were not phosphorylated. This was unexpected as the immunoprecipitation protocol and buffers were designed for immunoprecipitation of phosphoproteins. The immunoprecipitation buffer contained several phosphatase inhibitors (sodium orthovanadate, sodium fluoride, sodium pyrophosphate and β-glycerol phosphate), which should have protected any phosphorylated proteins during the immunoprecipitation. Perhaps there was not enough stx 16 phosphorylated under basal conditions for analysis.

As the phosphopeptide kits were unsuccessful, it was decided to go back to the previous method of immunoprecipitating endogenous stx 16, staining by colloidal Coomassie to detect the band of immunoprecipitated stx 16 and sending the band for phosphosite analysis. As this method had been unsuccessful previously, it was necessary to optimise the immunoprecipitation protocol further. To increase the amount of stx 16 immunoprecipitated, the concentration of the cell lysate used was increased. However increasing the concentration of the lysate

resulted in non-specific binding by the control IgG antiserum (data not shown). The optimal concentration of lysate for stx 16 immunoprecipitation was three 10 cm plates per immunoprecipitation. Unfortunately there was not enough stx 16 immunoprecipitated to be visible by colloidal Coomassie staining which is the required level of protein for analysis.

As the immunoprecipitation reactions using a rabbit antiserum were unsuccessful in precipitating sufficient quantities of stx 16 to send for analysis, an alternative antibody was used to immunoprecipitate stx 16. A mouse monoclonal anti-stx 16 antibody was used to immunoprecipitate stx 16 from three 10 cm plates of 3T3-L1 adipocytes in the hope that this antibody might be more efficient at immunoprecipitating stx 16. Unfortunately, immunoprecipitation of stx 16 using the mouse monoclonal anti-stx 16 antibody was not as successful as immunoprecipitation using the rabbit stx 16 antiserum (data not shown). There was still some stx 16 remaining in the stx 16 supernatant which had not been bound by the antibody. Also a band specific for the immunoprecipitated stx 16 was not visible by colloidal Coomassie staining. Increasing the amount of mouse monoclonal antibody used in the immunoprecipitation increased the non-specific binding of the control IgG (data not shown).

Therefore it seems unlikely that the phosphorylation site of stx 16 will be determined by analysis of immunoprecipitated endogenous stx 16. Alternatively a tagged version of stx 16 could be overexpressed in 3T3-L1 adipocytes, immunoprecipitated and analysed for its phosphorylation site. This would require a virus, perhaps adenovirus to overexpress the tagged stx 16. If overexpression of a tagged stx 16 in 3T3-L1 adipocytes proves difficult, perhaps the phosphorylation site of stx 16 could be determined *in vitro*. Stx 16 protein could be expressed in *E.Coli* and then incubated with cell lysate from basal and insulin-stimulated 3T3-L1 adipocytes before its phosphorylation site is analysed.

Once the phosphorylation site of stx 16 has been determined, the effect of stx 16 phosphorylation can be determined by expressing the alanine mutants and phosphomimetic aspartic acid mutants of the phosphorylation site in stx 16-depleted cells. The effect of stx 16 phosphorylation on GLUT4 trafficking could be investigated using a ^{3}H-deoxyglucose assay or the HA-GLUT4-GFP assays described in chapter 4. Also the effect of phosphorylation of stx 16 on its

interactions with other proteins, for example, stx 6 or mVps45 could be examined by co-immunoprecipitation or *in vitro* binding assays.

In addition to stx 16, there are other syntaxins which have been found to be phosphorylated. Stx 1 is phosphorylated by several kinases including, casein kinase I (CKI) (Dubois *et al.*, 2002), CKII (Bennett *et al.*, 1993;Hirling and Scheller, 1996;Foster *et al.*, 1998;Risinger and Bennett, 1999;Dubois *et al.*, 2002), calcium/calmodulin-dependent protein kinase II (CaMKII) (Hirling and Scheller, 1996;Ohyama *et al.*, 2002) and death-associated protein (DAP) kinase (Tian *et al.*, 2003). Also stx 4 is phosphorylated by CKII (Foster *et al.*, 1998;Risinger and Bennett, 1999) and PKA (Foster *et al.*, 1998).

Stx 1 is phosphorylated by CKI on Thr 21 (Dubois *et al.*, 2002). This phosphorylation site was determined *in vitro* using kinase assays, trypsin digestion, mass spectrometry and solid phase sequencing of ^{32}Pi- labelled peptides. Stx 1 is phosphorylated by CKII on Ser 14. This site was initially identified by *in vitro* kinase assays using recombinant stx 1 fragments and consensus site analysis (Bennett *et al.*, 1993;Risinger and Bennett, 1999). More recently the CKII phosphorylation site has been confirmed *in vitro* by the same method used for the CKI site (Dubois *et al.*, 2002). Foletti *et al.* have also shown that stx 1 is phosphorylated at Ser 14 *in vivo* using a phospho-specific antibody (Foletti *et al.*, 2000). Phosphorylation of stx 1 by CKII enhances its interaction with synaptotagmin I (Risinger and Bennett, 1999). Phosphorylated stx 1 also associates with SNAP 25 and localises to discrete domains of axonal plasma membranes which may define fusion sites (Foletti *et al.*, 2000). In addition, phosphorylation of stx 1 at Ser 14 decreases the N-terminal interaction of stx 1 with Munc 18-1 at the plasma membrane and reduces vesicle mobility and exocytosis (Rickman and Duncan, 2010).

Stx 1 is also phosphorylated by CaMKII at Thr 161 in the linker domain (Ohyama *et al.*, 2002). This site was determined by *in vitro* kinase assay, consensus site analysis and site-directed mutagenesis. Phosphorylation at Thr 161 by CaMKII does not affect binding of CaMKII to stx 1 (Ohyama *et al.*, 2002). In addition, stx 1 has been found to be phosphorylated by DAP kinase. Stx 1 is phosphorylated by DAP kinase at Ser 188 in the linker domain of stx 1 both *in vitro* and *in vivo* in a Ca^{2+}-dependent manner (Tian *et al.*, 2003). To determine the phosphorylation

site, recombinant stx 1 fragments were incubated with DAP kinase, and then site-directed mutagenesis was used to make alanine mutants of potential serine and threonine residues. The S188A mutant was not phosphorylated *in vitro*. To test that phosphorylation by DAP kinase occurred *in vivo* back-phosphorylation assays were performed in HEK 293T cells co-transfected with stx 1 and DAP kinase cDNAs. A decrease in the *in vitro* back-phosphorylation of stx 1 in Ca^{2+}-stimulated cell lysates was observed, which reflects *in vivo* phosphorylation of stx 1 by DAP kinase in response to Ca^{2+}. Stx 1 phosphorylation by DAP kinase decreases stx 1 binding to Munc 18-1 (Tian *et al.*, 2003).

Stx 4 phosphorylation by CKII was determined by *in vitro* kinase assays (Foster *et al.*, 1998;Risinger and Bennett, 1999). No phosphorylation site was determined, however phosphoamino acid analysis performed by acidic hydrolysis followed by thin layer chromatography revealed that stx 4 was phosphorylated on a Thr residue (Risinger and Bennett, 1999). Stx 4 is also phosphorylated by PKA *in vitro* (Foster *et al.*, 1998). No phosphorylation site was determined, but it was shown that phosphorylation of stx 4 by PKA disrupted its binding to SNAP 23. The authors suggest that PKA may modulate stx 4-dependent SNARE complex formation to regulate exocytosis in non-neuronal cells.

The studies described above, suggest that an *in vitro* method might be more successful in determining the phosphorylation site of stx 16. The studies also suggest that phosphorylation of stx 16 may affect its interactions with other SNAREs, for example stx 6 and its SM protein mVps45. In addition phosphorylation may affect vesicle trafficking in the stx 16 pathway, which may lead to changes in GLUT4 trafficking.

In summary the data in this chapter shows an investigation into the phosphorylation site of stx 16. Further work is needed to determine the insulin-regulated phosphorylation site of stx 16 in 3T3-L1 adipocytes.

Chapter 6 Discussion

In fat and muscle cells, under basal conditions the level of GLUT4 at the cell surface is very low. Insulin stimulation greatly increases the level of GLUT4 at the cell surface by stimulating the translocation of GLUT4 from unique intracellular storage sites to the plasma membrane (Suzuki and Kono, 1980;Cushman and Wardzala, 1980).The translocation of GLUT4 is an example of regulated membrane trafficking (Bryant *et al.*, 2002). GLUT4 occupies two interrelated, overlapping endosomal cycles. A fast-trafficking cycle involving the early endosome serves to internalise GLUT4 in the absence of insulin. Once in the endosome GLUT4 is further sorted into a slow-trafficking pathway involving the endosome, TGN and GSVs. It is thought that GLUT4 in the GSVs translocates to the cell surface in response in insulin (Fig. 1.3).

How is this process regulated and what are the proteins involved? How is basal retention of GLUT4 achieved? One place to look for answers to these questions is the proteins involved in the membrane trafficking of GLUT4. Membrane trafficking involves the fusion of vesicles with specific target membranes. This process is mediated by SNARE proteins (Hong, 2005). The SNAREs involved in the fusion of GLUT4 vesicles with the plasma membrane have been previously described (Thurmond and Pessin, 2001).GSVs contain the v-SNARE VAMP2 (Martin *et al.*, 1996) which has been shown to be important for insulin-stimulated translocation of GSVs to the plasma membrane (Martin *et al.*, 1998). VAMP2 binds to the t-SNAREs stx 4 and SNAP 23 present on the plasma membrane. Once bound, the resulting fusion leads to insertion of GLUT4 into the plasma membrane. The assembly of the trans-SNARE complex between VAMP2, stx 4 and SNAP 23 is regulated by the SM protein Munc18c (Brandie *et al.*, 2008).

However the SNAREs involved in the intracellular trafficking of GLUT4 remain poorly understood. The t-SNARE stx 6 has been implicated in GLUT4 trafficking. Stx 6 is highly enriched in GLUT4 vesicles and colocalises with GLUT4 in a subdomain of the TGN. Stx 6 also translocates to the cell surface in response to insulin (Shewan *et al.*, 2003). Overexpression of the cytosolic domain of stx 6 increases basal glucose transport and cell surface levels of GLUT4. Also stx 6 cytosolic domain slows the reversal of insulin-stimulated glucose transport and reduces the rate of GLUT4 internalisation after insulin withdrawal. The stx 6

cytosolic domain also perturbs subendosomal sorting of GLUT4 into GSVs (Perera *et al.*, 2003). These data suggest that stx 6 may be involved in trafficking of GLUT4 into its storage site(s).

Another SNARE which had been identified to have a role in GLUT4 trafficking is stx 16. Stx 16 has been shown to bind stx 6 (Perera *et al.*, 2003) and is known to function in the same trafficking step from the early endosome to the TGN (Mallard *et al.*, 2002).There is a lot of data to support a role for stx 16 in GLUT4 trafficking. Like stx 6, stx 16 colocalises with GLUT4 in a subdomain of the TGN and is highly enriched in GLUT4 vesicles. Also insulin stimulation results in the translocation of stx 16 to the cell surface (Shewan *et al.*, 2003). More recent data has shown that overexpression of the cytosolic domain of stx 16 significantly slows the reversal of insulin-stimulated glucose transport. Also depletion of stx 16 using a morpholino antisense oligonucleotide reduces insulin-stimulated glucose transport over a range of insulin concentrations. It was also observed in these cells that the total cellular levels of GLUT4 were reduced by 30% which suggested that GLUT4 was being missorted into a degradative pathway (Proctor *et al.*, 2006). The above data suggests that stx 16 may control GLUT4 sequestration in its storage site(s).

The aim of this thesis was to further investigate the role of stx 16 in GLUT4 trafficking.

In chapter 3 a different approach was used to knockdown stx 16 expression in 3T3-L1 adipocytes. 3T3-L1 fibroblasts were infected with retrovirus expressing one of four different shRNAs which targeted stx 16 to generate cells which were stably depleted of stx 16. This is very different to the method of knockdown employed by Proctor *et al.* in which 3T3-L1 adipocytes were transiently depleted of stx 16 by electroporation with a morpholino antisense oligonucleotide (Proctor *et al.*, 2006). Of the four shRNAs designed, shRNA4 resulted in the greatest level of stx 16 knockdown of 95% (Fig. 3.1). This level of knockdown is comparable to the level of knockdown achieved by Proctor *et al.* (Proctor *et al.*, 2006).

It was observed in the shRNA4-infected cells that the level of the t-SNARE stx 6 was reduced by 80% (Fig.3.2). This is in contrast to the data of Proctor *et* al. which showed that knockdown of stx 16 by a morpholino antisense

oligonucleotide did not affect the levels of stx 6 or stxs 4, 8 and 12 (Proctor *et al.*, 2006). This contradiction may be due to the differences in the knockdown methods used. Other more recent data has also shown that stx 16 knockdown results in a reduction in stx 6 levels (Ganley *et al.*, 2008). HEK293 cells transfected with siRNA against stx 16 showed an 80% reduction in stx 6, which is the same reduction seen in figure 3.2. The results of Ganley *et al.* and the data in figure 3.2 suggest that stx 16 is an important stabiliser of stx 6. In addition to affecting stx 6 levels, stx 16 knockdown also seemed to reduce the level of mVps45 recruited to the membrane. Figure 3.3 showed that membrane samples from shRNA4-infected cells had approximately 60% less mVps45 compared with the negative control-infected cells.

Cells infected with shRNA4 also exhibited a 20% reduction in total cellular levels of GLUT4 (Fig 3.3). This is similar to the 30% reduction in GLUT4 levels seen in stx 16-depleted cells by Proctor *et al.* (Proctor *et al.*, 2006). This suggests that GLUT4 is missorted into a degradative pathway in stx 16-depleted cells. A proteasome inhibitor would reveal whether the loss of GLUT4 is proteasome-dependent. Further study into the loss of GLUT4 showed that the majority of the loss occurred from the LDM fraction (Fig 3.5). The LDM fraction contains the GSVs, so stx 16 depletion may lead to a loss of GLUT4 from the GSVs. Further fractionation of the LDM fraction using an iodixanol gradient to separate the GSVs as described by Hashiramoto *et al.* (Hashiramoto and James, 2000) would reveal whether the loss of GLUT4 in stx 16-depleted cells is occurring from the GSVs. Also the formation of GSVs could be examined in stx 16-depleted cells using the *in vitro* budding assay described by Xu *et al.* (Xu and Kandror, 2002). Unfortunately initial attempts at these experiments were unsuccessful.

Further work is required to confirm whether the loss of GLUT4 in stx 16-depleted cells affects insulin-stimulated glucose transport. Proctor *et al.* showed that depletion of stx 16 by a morpholino antisense oligonucleotide resulted in a reduction in insulin-stimulated glucose transport (Proctor *et al.*, 2006). Therefore a similar effect would be expected in shRNA4-infected cells. The reversal of insulin-stimulated glucose transport could also be tested. Expression of myc-stx 16A in the stx 16-depleted cells would confirm whether all the results described above were due to stx 16 depletion.

In order to investigate the effect of stx 16 on GLUT4 trafficking, assays were developed to measure the translocation and recycling of HA-GLUT4-GFP. Infection of 3T3-L1 fibroblasts with a 1 in 4 dilution of lentivirus expressing HA-GLUT4-GFP resulted in adipocytes which expressed HA-GLUT4-GFP to a similar level as endogenous GLUT4 (Fig. 4.4). These cells had the correct localisation of HA-GLUT4-GFP under basal conditions and exhibited insulin-stimulated translocation of HA-GLUT4-GFP to the cell surface (Fig. 4.5). A flow cytometry method was unsuccessful in determining HA-GLUT4-GFP translocation in these cells (Fig.4.8). This may have been due to problems with the Cy3-conjugated secondary antibody and the specificity of the channels in the flow cytometer. An alternative method using a 96-well plate successfully determined HA-GLUT4-GFP translocation in response to insulin (Fig. 4.9). Insulin stimulation resulted in an over four-fold increase in surface HA-GLUT4-GFP compared with basal cells. The recycling of HA-GLUT4-GFP was also examined. In basal cells the Cy3: GFP ratio increased over time until it reached a plateau at around 10 hours (Fig. 4.10). The recycling of HA-GLUT4-GFP under basal conditions was similar to that seen in an experiment by Karylowski *et al.* (Karylowski *et al.*, 2004). However the recycling of HA-GLUT4-GFP in insulin-stimulated conditions was not as expected. The rate of HA-GLUT4-GFP recycling was higher with insulin but it was not as high as that seen by Karylowski *et al.* In figure 4.10 the Cy3: GFP ratio increased until it reached a plateau at 2 hours. However the plateau was reached at around 45 minutes in insulin-stimulated cells in experiments by Karylowski *et al.* (Karylowski *et al.*, 2004). Also the level of the plateau reached in insulin-stimulated cells was not as high as the level reached by basal cells (Fig. 4.10). These problems may have been due to variations in cell culture or experimental conditions or perhaps the concentration of the Cy3-HA antibody was not saturating.

Further work is needed to solve the problems with the HA-GLUT4-GFP recycling assay. Once the problems have been rectified, the assays can be used to investigate the role of stx 16 on GLUT4 trafficking kinetics.

Stx 16 is phosphorylated in adipocytes under basal conditions (Perera *et al.*, 2003). Insulin stimulation decreases the phosphorylation of stx 16. It is thought that this dephosphorylation regulates an important event in GLUT4 trafficking. Recently it has been shown that stx 16 is a functional homologue of Tlg2p

(Struthers *et al.*, 2009). Tlg2p is phosphorylated at Ser 90 by PKA (Gurunathan *et al.*, 2002). Previous work in the lab by Dr. Kirsty Proctor (University of Glasgow) identified three potential phosphorylation sites in stx 16 using a bioinformatics approach to identify potential PKA phosphorylation sites. They are Thr 90, Ser 94 and Ser 95. In chapter 5 the insulin-regulated phosphorylation site of stx 16 was examined. Two complementary approaches were used to investigate the phosphorylation site of stx 16. Stx 16 mutants of the three potential phosphorylation sites were screened in yeast cells lacking Tlg2p to determine whether expression of the stx 16 mutants could complement the phenotypes of $\Delta tlg2$ cells. Also several techniques were used to determine the phosphorylation site of endogenous stx 16 in 3T3-L1 adipocytes.

Screening of a stx 16 triple alanine mutant in $\Delta tlg2$ yeast using a Ste3p-myc endocytosis assay confirmed that phosphorylation at one or more of the potential phosphorylation sites is important for stx 16 function (Fig. 5.2). Further work screening the single alanine mutants in a KCl osmotic stress assay, suggested that Ser 95 may be the site of stx 16 phosphorylation (Fig. 5.3). This result needs to be confirmed by repeat experiments and the phosphorylation site will also need to be confirmed in 3T3-L1 adipocytes. Several attempts were made to determine the phosphorylation site of endogenous stx 16 in 3T3-L1 adipocytes. Phosphoprotein and phosphopeptide purification kits and immunoprecipitation methods were employed but unfortunately none of them were successful.

Ser 95 is at the start of the second predicted helix of the Habc domain in stx 16 (Dulubova et al., 2002). So phosphorylation at Ser 95 might regulate the ability of stx 16 to adopt a closed confirmation (Struthers et al., 2009). Alternatively phosphorylation might regulate the binding of stx 16 to its SM protein mVps45 (Dulubova *et al.*, 2002;Struthers *et al.*, 2009) or other SNARE proteins such as stx 6 (Perera et al., 2003).

Further work is required to determine the phosphorylation site of endogenous stx 16. As previous attempts to obtain samples for proteomic analysis were unsuccessful, alternative methods to purify stx 16 from basal and insulin-stimulated adipocytes are required. A tagged version of stx 16 could be overexpressed in 3T3-L1 adipocytes, immunoprecipitated and analysed for its

phosphorylation site. Alternatively the phosphorylation site of stx 16 could be determined *in vitro*. Stx 16 protein could be expressed in *E.Coli* and then incubated with cell lysate from basal and insulin-stimulated 3T3-L1 adipocytes before its phosphorylation site is analysed. Once the phosphorylation site of stx 16 has been determined the effect of alanine mutants and phosphomimetic aspartic acid mutants on GLUT4 trafficking could be determined using a ^{3}H-deoxyglucose assay or the HA-GLUT4-GFP assays. Also the effect of phosphorylation of stx 16 on its interactions with other proteins, for example, stx 6 or mVps45 could be examined by co-immunoprecipitation or *in vitro* binding assays.

In summary this thesis presents a further investigation into the role of stx 16 in GLUT4 trafficking. Blockade of stx 16 function by shRNA knockdown results in a loss of GLUT4 from the cell, which may represent a depletion of GLUT4 in the GSVs due to missorting of GLUT4 to a degradative pathway.

The data in the thesis and in the current literature suggest the following model for stx 16 function in GLUT4 trafficking. Stx 16 is localised in a subdomain of the TGN and mediates trafficking of vesicles from the early endosome to the TGN. This would suggest that stx 16 mediates entry of GLUT4 into the slow-trafficking pathway (Fig. 1.3) by fusion of GLUT4 vesicles with the stx 16/stx 6 t-SNAREs in the TGN subdomain. Enriched GLUT4 in the TGN is then packaged into GSVs which translocate and fuse with the plasma membrane in response to insulin. Stx 16 and stx 6 are also packaged into the GSVs during this process which would explain the translocation of stx 16 and stx 6 to the plasma membrane in response to insulin (Shewan *et al.*, 2003). This enrichment of stx 16 and stx 6 in the GSVs may be part of the maturation process for the GSVs.

Knockdown of stx 16 in this model would result in GLUT4 being unable to enter the slow trafficking pathway as the GLUT4 vesicles cannot fuse with the TGN subdomain and therefore cannot be packaged into GSVs. This would lead to slow reversal of insulin-stimulated glucose transport and high basal glucose transport as GLUT4 is stuck in the fast trafficking cycle between the plasma membrane and the endsome. This agrees with data that shows that overexpression of the cytosolic domain of stx 6 increases basal glucose transport (Perera *et al.*, 2003) and is also consistent with previous data which shows that overexpression of the

cytosolic domain of stx 16 significantly slows the reversal of insulin-stimulated glucose transport (Proctor *et al.*, 2006).

Also depletion of stx 16 in 3T3-L1 adipocytes would lead to a lack of GLUT4 in GSVs which would result in reduced glucose transport in response to insulin. Proctor *et al.* have shown that depletion of stx 16 using a morpholino antisense oligonucleotide reduces insulin-stimulated glucose transport over a range of insulin concentrations (Proctor *et al.*, 2006). In addition, the missorting of GLUT4 might result in its degradation, which would explain the loss of total GLUT4 observed in this thesis and by Proctor *et al.* (Proctor *et al.*, 2006).

Further work is required to investigate the impact of stx 16 knockdown on GLUT4 trafficking in more detail. Future studies on the role of stx 16 in GLUT4 trafficking should attempt to elucidate its precise role in basal retention of GLUT4. Where in the trafficking itinerary of GLUT4 does stx 16 exert its effect? Does stx 16 control entry of GLUT4 into the slow-trafficking pathway into the GSVs, or does stx 16 regulate exit of GLUT4 from the GSV compartment? Kinetic studies on GLUT4 trafficking using the HA-GLUT4-GFP assay described in chapter 4 and knockdown of stx 16 by shRNA will hopefully give answers to these questions.

Knockdown of stx 16 also reduces stx 6 levels and mVps45 recruitment to the membrane which may have an impact on vesicle fusion in this pathway. The loss of stx 6 in stx 16-depleted cells suggests that stx 16 is an important stabiliser of stx 6. In normal cells the majority of stx 6 may be in complex with stx 16 and stx 6 may be degraded if it is not bound to stx 16 in a t-SNARE complex. This suggests that stx 16 is important for t-SNARE complex formation in this pathway. Stx 16 knockdown also leads to a reduction in mVps45 at the membrane, which suggests that mVps45 is recruited to t-SNARE complexes in the membrane by binding to stx 16. Therefore knockdown of stx 16 would result in a reduction in t-SNARE complex and trans-SNARE complex formation. It would be interesting to determine whether expression of the shRNA resistant, myc-tagged human stx 16A would result in stabilisation of stx 6 and increased recruitment of mVps45 to the membrane in stx 16-depleted cells. Other data in the lab has found that mVps45 depletion in 3T3-L1 adipocytes results in a significant reduction in insulin-stimulated glucose transport and GLUT4 translocation (Roccisana, Bryant

and Gould, unpublished). This suggests a model in which stx 16, stx 6 and mVps45 act in concert in the intracellular sorting of GLUT4.

The data in this thesis also suggests that phosphorylation of stx 16 is important for its function and suggests Ser 95 as a potential site of phosphorylation. The phosphorylation site of stx 16 needs to be confirmed in 3T3-L1 adipocytes and its importance in GLUT4 trafficking further investigated.

The data in the thesis and in the current literature suggest the following model for how phosphorylation may affect stx 16 function.
Stx 16 is phosphorylated in basal conditions (Perera *et al.*, 2003). Insulin decreases this phosphorylation. Dephosphorylation of SNAREs has been shown to lead to t-SNARE complex assembly (Marash and Gerst, 2001;Gurunathan *et al.*, 2002). Therefore insulin stimulation may promote stx 16 t-SNARE complex formation. The potential phosphorylation site for stx 16 lies at the start of the second helix of the Habc domain (Dulubova *et al.*, 2002), therefore phosphorylation of stx 16 might regulate the conformation of stx 16, for example its ability to adopt the closed confirmation (Struthers *et al.*, 2009).

This might lead to the following model of how stx 16 phosphorylation might regulate GLUT4 trafficking. Basal stx 16 is phosphorylated and is in a closed conformation unable to bind to other t-SNAREs in its t-SNARE complex for example stx 6. Insulin stimulation leads to stx 16 dephosphorylation (or reduced phosphorylation) which leads to stx 16 adopting an open conformation (this may occur the other way around in which the open confirmation of stx 16 leads its dephosphorylation.) This leads to stx 16 assembly into the a t-SNARE complex with stx 6 and Vti1a which allows GLUT4 vesicles to fuse with the subdomain of the TGN and allows GLUT4 to enter GSVs which can then fuse with the plasma membrane.

How stx 16 is regulated by the SM protein mVps45 and by phosphorylation needs further investigation. Also the effect of insulin on this regulation needs to be examined. There are several questions still remaining: Is phosphorylation of stx 16 required for the adoption of the closed conformation? Does dephosphorylation of stx 16 and/or binding of mVps45 control opening of stx 16 to allow SNARE complex formation? Or is stx 16 dephosphorylated as a consequence of it adopting the open formation? Does phosphorylation of stx 16

affect its binding to mVps45? mVps45 binds to both the open and closed conformation of stx 16. (Struthers *et al.*, 2009) Is this regulated by phosphorylation of stx 16?

Finally, is mVps45 phosphorylated by insulin and how does this affect its binding to stx16? One possible mechanism could be the following: Insuiln stimulation leads to mVps45 phosphorylation; mVps45 dissociates from the closed conformation of stx 16; Stx 16 opens and mVps45 binds to the N-terminus of stx 16; Stx 16 is dephosphorylated which leads to stx 16 SNARE complex formation.

These questions could be examined by using a combination of phosphorylation site mutations with mutations which result in the open conformation of stx 16. Also the phosphorylation site mutants of stx 16 could be used with mVps45 mutants which affect its ability to bind stx 16 and its ability to be phosphorylated by insulin. The effects of these mutants on *in vitro* and *in vivo* binding of stx 16 to mVps45 and the ability of stx 16 to form SNARE complexes can then be determined.

In addition to furthering our understanding of the role of stx 16 in GLUT4 trafficking, and the regulation of this role, the studies described above will hopefully give insight into other mechanisms controlling basal retention of GLUT4 and how they are regulated by insulin. These studies may also bridge the gap in understanding between insulin signalling and GLUT4 trafficking. Understanding how GLUT4 trafficking events are controlled on a molecular level will hopefully aid in the development of novel treatments for type II diabetes.

References

Abel,E.D., Peroni,O., Kim,J.K., Kim,Y.B., Boss,O., Hadro,E., Minnemann,T., Shulman,G.I., and Kahn,B.B. (2001). Adipose-selective targeting of the GLUT4 gene impairs insulin action in muscle and liver. Nature *409*, 729-733.

Abeliovich,H., Grote,E., Novick,P., and Ferro-Novick,S. (1998). Tlg2p, a yeast syntaxin homolog that resides on the Golgi and endocytic structures. J. Biol. Chem. *273*, 11719-11727.

Ahn,M.Y., Katsanakis,K.D., Bheda,F., and Pillay,T.S. (2004). Primary and essential role of the adaptor protein APS for recruitment of both c-Cbl and its associated protein CAP in insulin signaling. J. Biol. Chem. *279*, 21526-21532.

Alessi,D.R., James,S.R., Downes,C.P., Holmes,A.B., Gaffney,P.R., Reese,C.B., and Cohen,P. (1997). Characterization of a 3-phosphoinositide-dependent protein kinase which phosphorylates and activates protein kinase Balpha. Curr. Biol. *7*, 261-269.

Amessou,M., Fradagrada,A., Falguieres,T., Lord,J.M., Smith,D.C., Roberts,L.M., Lamaze,C., and Johannes,L. (2007). Syntaxin 16 and syntaxin 5 are required for efficient retrograde transport of several exogenous and endogenous cargo proteins. J. Cell Sci. *120*, 1457-1468.

Antonin,W., Fasshauer,D., Becker,S., Jahn,R., and Schneider,T.R. (2002). Crystal structure of the endosomal SNARE complex reveals common structural principles of all SNAREs. Nat. Struct. Biol. *9*, 107-111.

Aran,V., Brandie,F.M., Boyd,A.R., Kantidakis,T., Rideout,E.J., Kelly,S.M., Gould,G.W., and Bryant,N. (2009). Characterisation of two distinct binding modes between Syntaxin 4 and Munc18c. Biochem. J.

Bai,L., Wang,Y., Fan,J., Chen,Y., Ji,W., Qu,A., Xu,P., James,D.E., and Xu,T. (2007). Dissecting Multiple Steps of GLUT4 Trafficking and Identifying the Sites of Insulin Action. Cell Metab *5*, 47-57.

Baumann,C.A., Ribon,V., Kanzaki,M., Thurmond,D.C., Mora,S., Shigematsu,S., Bickel,P.E., Pessin,J.E., and Saltiel,A.R. (2000). CAP defines a second signalling pathway required for insulin-stimulated glucose transport. Nature *407*, 202-207.

Bennett,M.K., Miller,K.G., and Scheller,R.H. (1993). Casein kinase II phosphorylates the synaptic vesicle protein p65. J. Neurosci. *13*, 1701-1707.

Berwick,D.C., Dell,G.C., Welsh,G.I., Heesom,K.J., Hers,I., Fletcher,L.M., Cooke,F.T., and Tavare,J.M. (2004). Protein kinase B phosphorylation of PIKfyve regulates the trafficking of GLUT4 vesicles. J. Cell Sci. *117*, 5985-5993.

Bethani,I., Lang,T., Geumann,U., Sieber,J.J., Jahn,R., and Rizzoli,S.O. (2007). The specificity of SNARE pairing in biological membranes is mediated by both proof-reading and spatial segregation. EMBO J. *26*, 3981-3992.

Blot,V. and McGraw,T.E. (2008). Molecular mechanisms controlling GLUT4 intracellular retention. Mol. Biol. Cell *19*, 3477-3487.

Bodenmiller,B., Mueller,L.N., Mueller,M., Domon,B., and Aebersold,R. (2007). Reproducible isolation of distinct, overlapping segments of the phosphoproteome. Nat. Methods *4*, 231-237.

Bogan,J.S., Hendon,N., McKee,A.E., Tsao,T.S., and Lodish,H.F. (2003). Functional cloning of TUG as a regulator of GLUT4 glucose transporter trafficking. Nature *425*, 727-733.

Bonifacino,J.S. and Traub,L.M. (2003). Signals for sorting of transmembrane proteins to endosomes and lysosomes. Annu. Rev. Biochem. *72*, 395-447.

Brandie,F.M., Aran,V., Verma,A., McNew,J.A., Bryant,N.J., and Gould,G.W. (2008). Negative regulation of syntaxin4/SNAP-23/VAMP2-mediated membrane fusion by Munc18c in vitro. PLoS. ONE. *3*, e4074.

Broadie,K., Prokop,A., Bellen,H.J., O'Kane,C.J., Schulze,K.L., and Sweeney,S.T. (1995). Syntaxin and synaptobrevin function downstream of vesicle docking in Drosophila. Neuron *15*, 663-673.

Brozinick,J.T., Jr., McCoid,S.C., Reynolds,T.H., Nardone,N.A., Hargrove,D.M., Stevenson,R.W., Cushman,S.W., and Gibbs,E.M. (2001). GLUT4 overexpression in db/db mice dose-dependently ameliorates diabetes but is not a lifelong cure. Diabetes *50*, 593-600.

Brummelkamp,T.R., Bernards,R., and Agami,R. (2002). A system for stable expression of short interfering RNAs in mammalian cells. Science *296*, 550-553.

Brunger,A.T. (2005). Structure and function of SNARE and SNARE-interacting proteins. Q. Rev. Biophys. *38*, 1-47.

Bryant,N.J., Govers,R., and James,D.E. (2002). Regulated transport of the glucose transporter GLUT4. Nat. Rev. Mol. Cell Biol. *3*, 267-277.

Bryant,N.J. and James,D.E. (2001). Vps45p stabilizes the syntaxin homologue Tlg2p and positively regulates SNARE complex formation. EMBO J. *20*, 3380-3388.

Capilla,E., Suzuki,N., Pessin,J.E., and Hou,J.C. (2007). The glucose transporter 4 FQQI motif is necessary for Akt substrate of 160-kilodalton-dependent plasma membrane translocation but not Golgi-localized (gamma)-ear-containing Arf-binding protein-dependent entry into the insulin-responsive storage compartment. Mol. Endocrinol. *21*, 3087-3099.

Carpp,L.N., Ciufo,L.F., Shanks,S.G., Boyd,A., and Bryant,N.J. (2006). The Sec1p/Munc18 protein Vps45p binds its cognate SNARE proteins via two distinct modes. J. Cell Biol. *173*, 927-936.

Carpp,L.N., Shanks,S.G., Struthers,M.S., and Bryant,N.J. (2007). Cellular levels of the syntaxin Tlg2p are regulated by a single mode of binding to Vps45p. Biochem. Biophys. Res. Commun. *363*, 857-860.

Chang,L., Chiang,S.H., and Saltiel,A.R. (2007). TC10alpha is required for insulin-stimulated glucose uptake in adipocytes. Endocrinology *148*, 27-33.

Chen,H.J., Remmler,J., Delaney,J.C., Messner,D.J., and Lobel,P. (1993). Mutational analysis of the cation-independent mannose 6-phosphate/insulin-like growth factor II receptor. A consensus casein kinase II site followed by 2 leucines

near the carboxyl terminus is important for intracellular targeting of lysosomal enzymes. J. Biol. Chem. *268*, 22338-22346.

Chen,Y.A. and Scheller,R.H. (2001). SNARE-mediated membrane fusion. Nat. Rev. Mol. Cell Biol. *2*, 98-106.

Chiang,S.H., Baumann,C.A., Kanzaki,M., Thurmond,D.C., Watson,R.T., Neudauer,C.L., Macara,I.G., Pessin,J.E., and Saltiel,A.R. (2001). Insulin-stimulated GLUT4 translocation requires the CAP-dependent activation of TC10. Nature *410*, 944-948.

Chou,M.M., Hou,W., Johnson,J., Graham,L.K., Lee,M.H., Chen,C.S., Newton,A.C., Schaffhausen,B.S., and Toker,A. (1998). Regulation of protein kinase C zeta by PI 3-kinase and PDK-1. Curr. Biol. *8*, 1069-1077.

Cope,D.L., Lee,S., Melvin,D.R., and Gould,G.W. (2000). Identification of further important residues within the Glut4 carboxy-terminal tail which regulate subcellular trafficking. FEBS Lett. *481*, 261-265.

Corvera,S., Chawla,A., Chakrabarti,R., Joly,M., Buxton,J., and Czech,M.P. (1994). A double leucine within the GLUT4 glucose transporter COOH-terminal domain functions as an endocytosis signal. J. Cell Biol. *126*, 979-989.

Cosson,P. and Letourneur,F. (1994). Coatomer interaction with di-lysine endoplasmic reticulum retention motifs. Science *263*, 1629-1631.

Coster,A.C., Govers,R., and James,D.E. (2004). Insulin stimulates the entry of GLUT4 into the endosomal recycling pathway by a quantal mechanism. Traffic. *5*, 763-771.

Cushman,S.W. and Wardzala,L.J. (1980). Potential mechanism of insulin action on glucose transport in the isolated rat adipose cell. Apparent translocation of intracellular transport systems to the plasma membrane. J. Biol. Chem. *255*, 4758-4762.

D'Andrea-Merrins,M., Chang,L., Lam,A.D., Ernst,S.A., and Stuenkel,E.L. (2007). Munc18c Interaction with Syntaxin 4 Monomers and SNARE Complex Intermediates in GLUT4 Vesicle Trafficking. J. Biol. Chem. *282*, 16553-16566.

Darsow,T., Odorizzi,G., and Emr,S.D. (2000). Invertase fusion proteins for analysis of protein trafficking in yeast. Methods Enzymol. *327*, 95-106.

Davis,N.G., Horecka,J.L., and Sprague,G.F., Jr. (1993). Cis- and trans-acting functions required for endocytosis of the yeast pheromone receptors. J. Cell Biol. *122*, 53-65.

Dawson,K., viles-Hernandez,A., Cushman,S.W., and Malide,D. (2001). Insulin-regulated trafficking of dual-labeled glucose transporter 4 in primary rat adipose cells. Biochem. Biophys. Res. Commun. *287*, 445-454.

Domanska,M.K., Kiessling,V., Stein,A., Fasshauer,D., and Tamm,L.K. (2009). Single vesicle millisecond fusion kinetics reveals number of SNARE complexes optimal for fast SNARE-mediated membrane fusion. J. Biol. Chem. *284*, 32158-32166.

Dubois,T., Kerai,P., Learmonth,M., Cronshaw,A., and Aitken,A. (2002). Identification of syntaxin-1A sites of phosphorylation by casein kinase I and casein kinase II. Eur. J. Biochem. *269*, 909-914.

Dugani,C.B. and Klip,A. (2005). Glucose transporter 4: cycling, compartments and controversies. EMBO Rep. *6*, 1137-1142.

Dulubova,I., Yamaguchi,T., Gao,Y., Min,S.W., Huryeva,I., Sudhof,T.C., and Rizo,J. (2002). How Tlg2p/syntaxin 16 'snares' Vps45. EMBO J. *21*, 3620-3631.

Eguez,L., Lee,A., Chavez,J.A., Miinea,C.P., Kane,S., Lienhard,G.E., and McGraw,T.E. (2005). Full intracellular retention of GLUT4 requires AS160 Rab GTPase activating protein. Cell Metab *2*, 263-272.

Fasshauer,D. (2003). Structural insights into the SNARE mechanism. Biochim. Biophys. Acta *1641*, 87-97.

Fasshauer,D., Antonin,W., Margittai,M., Pabst,S., and Jahn,R. (1999). Mixed and non-cognate SNARE complexes. Characterization of assembly and biophysical properties. J. Biol. Chem. *274*, 15440-15446.

Fasshauer,D., Sutton,R.B., Brunger,A.T., and Jahn,R. (1998). Conserved structural features of the synaptic fusion complex: SNARE proteins reclassified as Q- and R-SNAREs. Proc. Natl. Acad. Sci. U. S. A *95*, 15781-15786.

Foletti,D.L., Lin,R., Finley,M.A., and Scheller,R.H. (2000). Phosphorylated syntaxin 1 is localized to discrete domains along a subset of axons. J. Neurosci. *20*, 4535-4544.

Foster,L.J., Yeung,B., Mohtashami,M., Ross,K., Trimble,W.S., and Klip,A. (1998). Binary interactions of the SNARE proteins syntaxin-4, SNAP23, and VAMP-2 and their regulation by phosphorylation. Biochemistry *37*, 11089-11096.

Fratti,R.A., Collins,K.M., Hickey,C.M., and Wickner,W. (2007). Stringent 3Q.1R composition of the SNARE 0-layer can be bypassed for fusion by compensatory SNARE mutation or by lipid bilayer modification. J. Biol. Chem. *282*, 14861-14867.

Funaki,M., Randhawa,P., and Janmey,P.A. (2004). Separation of insulin signaling into distinct GLUT4 translocation and activation steps. Mol. Cell Biol. *24*, 7567-7577.

Furgason,M.L., Macdonald,C., Shanks,S.G., Ryder,S.P., Bryant,N.J., and Munson,M. (2009). The N-terminal peptide of the syntaxin Tlg2p modulates binding of its closed conformation to Vps45p. Proc. Natl. Acad. Sci. U. S. A *106*, 14303-14308.

Ganley,I.G., Espinosa,E., and Pfeffer,S.R. (2008). A syntaxin 10-SNARE complex distinguishes two distinct transport routes from endosomes to the trans-Golgi in human cells. J. Cell Biol. *180*, 159-172.

Garippa,R.J., Judge,T.W., James,D.E., and McGraw,T.E. (1994). The amino terminus of GLUT4 functions as an internalization motif but not an intracellular retention signal when substituted for the transferrin receptor cytoplasmic domain. J. Cell Biol. *124*, 705-715.

Garvey,W.T., Maianu,L., Huecksteadt,T.P., Birnbaum,M.J., Molina,J.M., and Ciaraldi,T.P. (1991). Pretranslational suppression of a glucose transporter protein causes insulin resistance in adipocytes from patients with non-insulin-dependent diabetes mellitus and obesity. J. Clin. Invest *87*, 1072-1081.

Garza,L.A. and Birnbaum,M.J. (2000). Insulin-responsive aminopeptidase trafficking in 3T3-L1 adipocytes. J. Biol. Chem. *275*, 2560-2567.

Genoud,S., Pralong,W., Riederer,B.M., Eder,L., Catsicas,S., and Muller,D. (1999). Activity-dependent phosphorylation of SNAP-25 in hippocampal organotypic cultures. J. Neurochem. *72*, 1699-1706.

Gerst,J.E. (2003). SNARE regulators: matchmakers and matchbreakers. Biochim. Biophys. Acta *1641*, 99-110.

Gotte,M. and von Mollard,G.F. (1998). A new beat for the SNARE drum. Trends Cell Biol. *8*, 215-218.

Govers,R., Coster,A.C., and James,D.E. (2004). Insulin increases cell surface GLUT4 levels by dose dependently discharging GLUT4 into a cell surface recycling pathway. Mol. Cell Biol. *24*, 6456-6466.

Gurunathan,S., Marash,M., Weinberger,A., and Gerst,J.E. (2002). t-SNARE phosphorylation regulates endocytosis in yeast. Mol. Biol. Cell *13*, 1594-1607.

Han,X., Wang,C.T., Bai,J., Chapman,E.R., and Jackson,M.B. (2004). Transmembrane segments of syntaxin line the fusion pore of Ca2+-triggered exocytosis. Science *304*, 289-292.

Hashiramoto,M. and James,D.E. (2000). Characterization of insulin-responsive GLUT4 storage vesicles isolated from 3T3-L1 adipocytes. Mol. Cell Biol. *20*, 416-427.

Hepp,R., Puri,N., Hohenstein,A.C., Crawford,G.L., Whiteheart,S.W., and Roche,P.A. (2005). Phosphorylation of SNAP-23 regulates exocytosis from mast cells. J. Biol. Chem. *280*, 6610-6620.

Heyward,C.A., Pettitt,T.R., Leney,S.E., Welsh,G.I., Tavare,J.M., and Wakelam,M.J. (2008). An intracellular motif of GLUT4 regulates fusion of GLUT4-containing vesicles. BMC. Cell Biol. *9*, 25.

Hirling,H. and Scheller,R.H. (1996). Phosphorylation of synaptic vesicle proteins: modulation of the alpha SNAP interaction with the core complex. Proc. Natl. Acad. Sci. U. S. A *93*, 11945-11949.

Holman,G.D. and Sandoval,I.V. (2001). Moving the insulin-regulated glucose transporter GLUT4 into and out of storage. Trends Cell Biol. *11*, 173-179.

Hong,W. (2005). SNAREs and traffic. Biochim. Biophys. Acta *1744*, 493-517.

Hou,J.C., Suzuki,N., Pessin,J.E., and Watson,R.T. (2006). A specific dileucine motif is required for the GGA-dependent entry of newly synthesized insulin-responsive aminopeptidase into the insulin-responsive compartment. J. Biol. Chem. *281*, 33457-33466.

Hresko,R.C. and Mueckler,M. (2005). mTOR.RICTOR is the Ser473 kinase for Akt/protein kinase B in 3T3-L1 adipocytes. J. Biol. Chem. *280*, 40406-40416.

Hu,S.H., Latham,C.F., Gee,C.L., James,D.E., and Martin,J.L. (2007). Structure of the Munc18c/Syntaxin4 N-peptide complex defines universal features of the N-peptide binding mode of Sec1/Munc18 proteins. Proc. Natl. Acad. Sci. U. S. A *104*, 8773-8778.

Hua,Y. and Scheller,R.H. (2001). Three SNARE complexes cooperate to mediate membrane fusion. Proc. Natl. Acad. Sci. U. S. A *98*, 8065-8070.

Huang,S., Lifshitz,L.M., Jones,C., Bellve,K.D., Standley,C., Fonseca,S., Corvera,S., Fogarty,K.E., and Czech,M.P. (2007). Insulin stimulates membrane fusion and GLUT4 accumulation in clathrin coats on adipocyte plasma membranes. Mol. Cell Biol. *27*, 3456-3469.

Hunt,J.M., Bommert,K., Charlton,M.P., Kistner,A., Habermann,E., Augustine,G.J., and Betz,H. (1994). A post-docking role for synaptobrevin in synaptic vesicle fusion. Neuron *12*, 1269-1279.

Ishikura,S., Bilan,P.J., and Klip,A. (2007). Rabs 8A and 14 are targets of the insulin-regulated Rab-GAP AS160 regulating GLUT4 traffic in muscle cells. Biochem. Biophys. Res. Commun. *353*, 1074-1079.

Jahn,R. (2004). Principles of exocytosis and membrane fusion. Ann. N. Y. Acad. Sci. *1014*, 170-178.

Jahn,R. and Grubmuller,H. (2002). Membrane fusion. Curr. Opin. Cell Biol. *14*, 488-495.

Jahn,R. and Scheller,R.H. (2006). SNAREs--engines for membrane fusion. Nat. Rev. Mol. Cell Biol. *7*, 631-643.

Jiang,L., Fan,J., Bai,L., Wang,Y., Chen,Y., Yang,L., Chen,L., and Xu,T. (2008). Direct quantification of fusion rate reveals a distal role for AS160 in insulin-stimulated fusion of GLUT4 storage vesicles. J. Biol. Chem. *283*, 8508-8516.

Joost,H.G. and Thorens,B. (2001). The extended GLUT-family of sugar/polyol transport facilitators: nomenclature, sequence characteristics, and potential function of its novel members (review). Mol. Membr. Biol. *18*, 247-256.

Kane,S., Sano,H., Liu,S.C., Asara,J.M., Lane,W.S., Garner,C.C., and Lienhard,G.E. (2002). A method to identify serine kinase substrates. Akt phosphorylates a novel adipocyte protein with a Rab GTPase-activating protein (GAP) domain. J. Biol. Chem. *277*, 22115-22118.

Kanzaki,M. (2006). Insulin receptor signals regulating GLUT4 translocation and actin dynamics. Endocr. J. *53*, 267-293.

Kanzaki,M. and Pessin,J.E. (2001). Insulin-stimulated GLUT4 translocation in adipocytes is dependent upon cortical actin remodeling. J. Biol. Chem. *276*, 42436-42444.

Kanzaki,M., Watson,R.T., Hou,J.C., Stamnes,M., Saltiel,A.R., and Pessin,J.E. (2002). Small GTP-binding protein TC10 differentially regulates two distinct

populations of filamentous actin in 3T3L1 adipocytes. Mol. Biol. Cell *13*, 2334-2346.

Karylowski,O., Zeigerer,A., Cohen,A., and McGraw,T.E. (2004). GLUT4 is retained by an intracellular cycle of vesicle formation and fusion with endosomes. Mol. Biol. Cell *15*, 870-882.

Keller,S.R., Scott,H.M., Mastick,C.C., Aebersold,R., and Lienhard,G.E. (1995). Cloning and characterization of a novel insulin-regulated membrane aminopeptidase from Glut4 vesicles. J. Biol. Chem. *270*, 23612-23618.

Khan,A.H., Capilla,E., Hou,J.C., Watson,R.T., Smith,J.R., and Pessin,J.E. (2004). Entry of newly synthesized GLUT4 into the insulin-responsive storage compartment is dependent upon both the amino terminus and the large cytoplasmic loop. J. Biol. Chem. *279*, 37505-37511.

Koumanov,F., Jin,B., Yang,J., and Holman,G.D. (2005). Insulin signaling meets vesicle traffic of GLUT4 at a plasma-membrane-activated fusion step. Cell Metab *2*, 179-189.

Kupriyanova,T.A., Kandror,V., and Kandror,K.V. (2002). Isolation and characterization of the two major intracellular Glut4 storage compartments. J. Biol. Chem. *277*, 9133-9138.

Lalioti,V., Vergarajauregui,S., and Sandoval,I.V. (2001). Targeting motifs in GLUT4 (review). Mol. Membr. Biol. *18*, 257-264.

Larance,M., Ramm,G., and James,D.E. (2008). The GLUT4 code. Mol. Endocrinol. *22*, 226-233.

Larance,M. *et al.* (2005). Characterization of the role of the Rab GTPase-activating protein AS160 in insulin-regulated GLUT4 trafficking. J. Biol. Chem. *280*, 37803-37813.

Le Good,J.A., Ziegler,W.H., Parekh,D.B., Alessi,D.R., Cohen,P., and Parker,P.J. (1998). Protein kinase C isotypes controlled by phosphoinositide 3-kinase through the protein kinase PDK1. Science *281*, 2042-2045.

Lee,W. and Jung,C.Y. (1997). A synthetic peptide corresponding to the GLUT4 C-terminal cytoplasmic domain causes insulin-like glucose transport stimulation and GLUT4 recruitment in rat adipocytes. J. Biol. Chem. *272*, 21427-21431.

Leney,S.E. and Tavare,J.M. (2009). The molecular basis of insulin-stimulated glucose uptake: signalling, trafficking and potential drug targets. J. Endocrinol. *203*, 1-18.

Lewis,M.J. and Pelham,H.R. (1992). Ligand-induced redistribution of a human KDEL receptor from the Golgi complex to the endoplasmic reticulum. Cell *68*, 353-364.

Li,F., Pincet,F., Perez,E., Eng,W.S., Melia,T.J., Rothman,J.E., and Tareste,D. (2007). Energetics and dynamics of SNAREpin folding across lipid bilayers. Nat. Struct. Mol. Biol. *14*, 890-896.

Li,L.V., Bakirtzi,K., Watson,R.T., Pessin,J.E., and Kandror,K.V. (2009). The C-terminus of GLUT4 targets the transporter to the perinuclear compartment but not to the insulin-responsive vesicles. Biochem. J. *419*, 105-12, 1.

Li,L.V. and Kandror,K.V. (2005). Golgi-localized, gamma-ear-containing, Arf-binding protein adaptors mediate insulin-responsive trafficking of glucose transporter 4 in 3T3-L1 adipocytes. Mol. Endocrinol. *19*, 2145-2153.

Littleton,J.T., Chapman,E.R., Kreber,R., Garment,M.B., Carlson,S.D., and Ganetzky,B. (1998). Temperature-sensitive paralytic mutations demonstrate that synaptic exocytosis requires SNARE complex assembly and disassembly. Neuron *21*, 401-413.

Liu,J., Kimura,A., Baumann,C.A., and Saltiel,A.R. (2002). APS facilitates c-Cbl tyrosine phosphorylation and GLUT4 translocation in response to insulin in 3T3-L1 adipocytes. Mol. Cell Biol. *22*, 3599-3609.

Livingstone,C., James,D.E., Rice,J.E., Hanpeter,D., and Gould,G.W. (1996). Compartment ablation analysis of the insulin-responsive glucose transporter (GLUT4) in 3T3-L1 adipocytes. Biochem. J. *315 (Pt 2)*, 487-495.

Lizunov,V.A., Matsumoto,H., Zimmerberg,J., Cushman,S.W., and Frolov,V.A. (2005). Insulin stimulates the halting, tethering, and fusion of mobile GLUT4 vesicles in rat adipose cells. J. Cell Biol. *169*, 481-489.

Lu,X., Zhang,Y., and Shin,Y.K. (2008). Supramolecular SNARE assembly precedes hemifusion in SNARE-mediated membrane fusion. Nat. Struct. Mol. Biol. *15*, 700-706.

Mallard,F., Tang,B.L., Galli,T., Tenza,D., Saint-Pol,A., Yue,X., Antony,C., Hong,W., Goud,B., and Johannes,L. (2002). Early/recycling endosomes-to-TGN transport involves two SNARE complexes and a Rab6 isoform. J. Cell Biol. *156*, 653-664.

Malsam,J., Kreye,S., and Sollner,T.H. (2008). Membrane fusion: SNAREs and regulation. Cell Mol. Life Sci. *65*, 2814-2832.

Marash,M. and Gerst,J.E. (2001). t-SNARE dephosphorylation promotes SNARE assembly and exocytosis in yeast. EMBO J. *20*, 411-421.

Martin,L.B., Shewan,A., Millar,C.A., Gould,G.W., and James,D.E. (1998). Vesicle-associated membrane protein 2 plays a specific role in the insulin-dependent trafficking of the facilitative glucose transporter GLUT4 in 3T3-L1 adipocytes. J. Biol. Chem. *273*, 1444-1452.

Martin,O.J., Lee,A., and McGraw,T.E. (2006). GLUT4 distribution between the plasma membrane and the intracellular compartments is maintained by an insulin-modulated bipartite dynamic mechanism. J. Biol. Chem. *281*, 484-490.

Martin,S., Millar,C.A., Lyttle,C.T., Meerloo,T., Marsh,B.J., Gould,G.W., and James,D.E. (2000). Effects of insulin on intracellular GLUT4 vesicles in adipocytes: evidence for a secretory mode of regulation. J. Cell Sci. *113 Pt 19*, 3427-3438.

Martin,S., Tellam,J., Livingstone,C., Slot,J.W., Gould,G.W., and James,D.E. (1996). The glucose transporter (GLUT-4) and vesicle-associated membrane

protein-2 (VAMP-2) are segregated from recycling endosomes in insulin-sensitive cells. J. Cell Biol. *134*, 625-635.

Martinez-Arca,S., Lalioti,V.S., and Sandoval,I.V. (2000). Intracellular targeting and retention of the glucose transporter GLUT4 by the perinuclear storage compartment involves distinct carboxyl-tail motifs. J. Cell Sci. *113 (Pt 10)*, 1705-1715.

Maxfield,F.R. and McGraw,T.E. (2004). Endocytic recycling. Nat. Rev. Mol. Cell Biol. *5*, 121-132.

McNew,J.A., Parlati,F., Fukuda,R., Johnston,R.J., Paz,K., Paumet,F., Sollner,T.H., and Rothman,J.E. (2000a). Compartmental specificity of cellular membrane fusion encoded in SNARE proteins. Nature *407*, 153-159.

McNew,J.A., Weber,T., Engelman,D.M., Sollner,T.H., and Rothman,J.E. (1999). The length of the flexible SNAREpin juxtamembrane region is a critical determinant of SNARE-dependent fusion. Mol. Cell *4*, 415-421.

McNew,J.A., Weber,T., Parlati,F., Johnston,R.J., Melia,T.J., Sollner,T.H., and Rothman,J.E. (2000b). Close is not enough: SNARE-dependent membrane fusion requires an active mechanism that transduces force to membrane anchors. J. Cell Biol. *150*, 105-117.

Miinea,C.P., Sano,H., Kane,S., Sano,E., Fukuda,M., Peranen,J., Lane,W.S., and Lienhard,G.E. (2005). AS160, the Akt substrate regulating GLUT4 translocation, has a functional Rab GTPase-activating protein domain. Biochem. J. *391*, 87-93.

Muretta,J.M., Romenskaia,I., and Mastick,C.C. (2008). Insulin releases Glut4 from static storage compartments into cycling endosomes and increases the rate constant for Glut4 exocytosis. J. Biol. Chem. *283*, 311-323.

Murphy,G.A., Solski,P.A., Jillian,S.A., Perez de la,O.P., D'Eustachio,P., Der,C.J., and Rush,M.G. (1999). Cellular functions of TC10, a Rho family GTPase: regulation of morphology, signal transduction and cell growth. Oncogene *18*, 3831-3845.

Nagy,G., Matti,U., Nehring,R.B., Binz,T., Rettig,J., Neher,E., and Sorensen,J.B. (2002). Protein kinase C-dependent phosphorylation of synaptosome-associated protein of 25 kDa at Ser187 potentiates vesicle recruitment. J. Neurosci. *22*, 9278-9286.

Nagy,G., Reim,K., Matti,U., Brose,N., Binz,T., Rettig,J., Neher,E., and Sorensen,J.B. (2004). Regulation of releasable vesicle pool sizes by protein kinase A-dependent phosphorylation of SNAP-25. Neuron *41*, 417-429.

Ng,Y., Ramm,G., Lopez,J.A., and James,D.E. (2008). Rapid activation of Akt2 is sufficient to stimulate GLUT4 translocation in 3T3-L1 adipocytes. Cell Metab *7*, 348-356.

Nielander,H.B., Onofri,F., Valtorta,F., Schiavo,G., Montecucco,C., Greengard,P., and Benfenati,F. (1995). Phosphorylation of VAMP/synaptobrevin in synaptic vesicles by endogenous protein kinases. J. Neurochem. *65*, 1712-1720.

Ohyama,A. *et al.* (2002). Regulation of exocytosis through Ca2+/ATP-dependent binding of autophosphorylated Ca2+/calmodulin-activated protein kinase II to syntaxin 1A. J. Neurosci. *22*, 3342-3351.

Okada,T., Kawano,Y., Sakakibara,T., Hazeki,O., and Ui,M. (1994). Essential role of phosphatidylinositol 3-kinase in insulin-induced glucose transport and antilipolysis in rat adipocytes. Studies with a selective inhibitor wortmannin. J. Biol. Chem. *269*, 3568-3573.

Palacios,S., Lalioti,V., Martinez-Arca,S., Chattopadhyay,S., and Sandoval,I.V. (2001). Recycling of the insulin-sensitive glucose transporter GLUT4. Access of surface internalized GLUT4 molecules to the perinuclear storage compartment is mediated by the Phe5-Gln6-Gln7-Ile8 motif. J. Biol. Chem. *276*, 3371-3383.

Parlati,F., Varlamov,O., Paz,K., McNew,J.A., Hurtado,D., Sollner,T.H., and Rothman,J.E. (2002). Distinct SNARE complexes mediating membrane fusion in Golgi transport based on combinatorial specificity. Proc. Natl. Acad. Sci. U. S. A *99*, 5424-5429.

Paumet,F., Rahimian,V., and Rothman,J.E. (2004). The specificity of SNARE-dependent fusion is encoded in the SNARE motif. Proc. Natl. Acad. Sci. U. S. A *101*, 3376-3380.

Peng,R. and Gallwitz,D. (2004). Multiple SNARE interactions of an SM protein: Sed5p/Sly1p binding is dispensable for transport. EMBO J. *23*, 3939-3949.

Perera,H.K., Clarke,M., Morris,N.J., Hong,W., Chamberlain,L.H., and Gould,G.W. (2003). Syntaxin 6 regulates Glut4 trafficking in 3T3-L1 adipocytes. Mol. Biol. Cell *14*, 2946-2958.

Pessin,J.E., Thurmond,D.C., Elmendorf,J.S., Coker,K.J., and Okada,S. (1999). Molecular basis of insulin-stimulated GLUT4 vesicle trafficking. Location! Location! Location! J. Biol. Chem. *274*, 2593-2596.

Pilch,P.F. (2008). The mass action hypothesis: formation of Glut4 storage vesicles, a tissue-specific, regulated exocytic compartment. Acta Physiol (Oxf) *192*, 89-101.

Piper,R.C., Whitters,E.A., and Stevens,T.H. (1994). Yeast Vps45p is a Sec1p-like protein required for the consumption of vacuole-targeted, post-Golgi transport vesicles. Eur. J. Cell Biol. *65*, 305-318.

Polgar,J., Lane,W.S., Chung,S.H., Houng,A.K., and Reed,G.L. (2003). Phosphorylation of SNAP-23 in activated human platelets. J. Biol. Chem. *278*, 44369-44376.

Proctor,K.M., Miller,S.C., Bryant,N.J., and Gould,G.W. (2006). Syntaxin 16 controls the intracellular sequestration of GLUT4 in 3T3-L1 adipocytes. Biochem. Biophys. Res. Commun. *347*, 433-438.

Ramm,G., Slot,J.W., James,D.E., and Stoorvogel,W. (2000). Insulin recruits GLUT4 from specialized VAMP2-carrying vesicles as well as from the dynamic endosomal/trans-Golgi network in rat adipocytes. Mol. Biol. Cell *11*, 4079-4091.

Reynolds,A., Leake,D., Boese,Q., Scaringe,S., Marshall,W.S., and Khvorova,A. (2004). Rational siRNA design for RNA interference. Nat. Biotechnol. *22*, 326-330.

Ribon,V., Printen,J.A., Hoffman,N.G., Kay,B.K., and Saltiel,A.R. (1998). A novel, multifuntional c-Cbl binding protein in insulin receptor signaling in 3T3-L1 adipocytes. Mol. Cell Biol. *18*, 872-879.

Ribon,V. and Saltiel,A.R. (1997). Insulin stimulates tyrosine phosphorylation of the proto-oncogene product of c-Cbl in 3T3-L1 adipocytes. Biochem. J. *324 (Pt 3)*, 839-845.

Rickman,C. and Duncan,R.R. (2010). Munc18/Syntaxin interaction kinetics control secretory vesicle dynamics. J. Biol. Chem. *285*, 3965-3972.

Risinger,C. and Bennett,M.K. (1999). Differential phosphorylation of syntaxin and synaptosome-associated protein of 25 kDa (SNAP-25) isoforms. J. Neurochem. *72*, 614-624.

Robinson,M.S. (2004). Adaptable adaptors for coated vesicles. Trends Cell Biol. *14*, 167-174.

Rothman,J.E. and Wieland,F.T. (1996). Protein sorting by transport vesicles. Science *272*, 227-234.

Rothman,J.H. and Stevens,T.H. (1986). Protein sorting in yeast: mutants defective in vacuole biogenesis mislocalize vacuolar proteins into the late secretory pathway. Cell *47*, 1041-1051.

Sakamoto,K. and Holman,G.D. (2008). Emerging role for AS160/TBC1D4 and TBC1D1 in the regulation of GLUT4 traffic. Am. J. Physiol Endocrinol. Metab *295*, E29-E37.

Saltiel,A.R. and Kahn,C.R. (2001). Insulin signalling and the regulation of glucose and lipid metabolism. Nature *414*, 799-806.

Sano,H., Eguez,L., Teruel,M.N., Fukuda,M., Chuang,T.D., Chavez,J.A., Lienhard,G.E., and McGraw,T.E. (2007). Rab10, a Target of the AS160 Rab GAP, Is Required for Insulin-Stimulated Translocation of GLUT4 to the Adipocyte Plasma Membrane. Cell Metab *5*, 293-303.

Sano,H., Kane,S., Sano,E., Miinea,C.P., Asara,J.M., Lane,W.S., Garner,C.W., and Lienhard,G.E. (2003a). Insulin-stimulated phosphorylation of a Rab GTPase-activating protein regulates GLUT4 translocation. J. Biol. Chem. *278*, 14599-14602.

Sano,H., Kane,S., Sano,E., Miinea,C.P., Asara,J.M., Lane,W.S., Garner,C.W., and Lienhard,G.E. (2003b). Insulin-stimulated phosphorylation of a Rab GTPase-activating protein regulates GLUT4 translocation. J. Biol. Chem. *278*, 14599-14602.

Sano,H., Roach,W.G., Peck,G.R., Fukuda,M., and Lienhard,G.E. (2008). Rab10 in insulin-stimulated GLUT4 translocation. Biochem. J. *411*, 89-95.

Sarbassov,D.D., Guertin,D.A., Ali,S.M., and Sabatini,D.M. (2005). Phosphorylation and regulation of Akt/PKB by the rictor-mTOR complex. Science *307*, 1098-1101.

Satoh,S., Nishimura,H., Clark,A.E., Kozka,I.J., Vannucci,S.J., Simpson,I.A., Quon,M.J., Cushman,S.W., and Holman,G.D. (1993). Use of bismannose photolabel to elucidate insulin-regulated GLUT4 subcellular trafficking kinetics in rat adipose cells. Evidence that exocytosis is a critical site of hormone action. J. Biol. Chem. *268*, 17820-17829.

Scales,S.J., Chen,Y.A., Yoo,B.Y., Patel,S.M., Doung,Y.C., and Scheller,R.H. (2000). SNAREs contribute to the specificity of membrane fusion. Neuron *26*, 457-464.

Schiavo,G., Benfenati,F., Poulain,B., Rossetto,O., Polverino de,L.P., Dasgupta,B.R., and Montecucco,C. (1992). Tetanus and botulinum-B neurotoxins block neurotransmitter release by proteolytic cleavage of synaptobrevin. Nature *359*, 832-835.

Schoch,S., Deak,F., Konigstorfer,A., Mozhayeva,M., Sara,Y., Sudhof,T.C., and Kavalali,E.T. (2001). SNARE function analyzed in synaptobrevin/VAMP knockout mice. Science *294*, 1117-1122.

Schwarz,D.S., Hutvagner,G., Du,T., Xu,Z., Aronin,N., and Zamore,P.D. (2003). Asymmetry in the assembly of the RNAi enzyme complex. Cell *115*, 199-208.

Schweizer,A., Kornfeld,S., and Rohrer,J. (1997). Proper sorting of the cation-dependent mannose 6-phosphate receptor in endosomes depends on a pair of aromatic amino acids in its cytoplasmic tail. Proc. Natl. Acad. Sci. U. S. A *94*, 14471-14476.

Semenza,J.C., Hardwick,K.G., Dean,N., and Pelham,H.R. (1990). ERD2, a yeast gene required for the receptor-mediated retrieval of luminal ER proteins from the secretory pathway. Cell *61*, 1349-1357.

Seron,K. *et al.* (1998). A yeast t-SNARE involved in endocytosis. Mol. Biol. Cell *9*, 2873-2889.

Shewan,A.M., Marsh,B.J., Melvin,D.R., Martin,S., Gould,G.W., and James,D.E. (2000). The cytosolic C-terminus of the glucose transporter GLUT4 contains an acidic cluster endosomal targeting motif distal to the dileucine signal. Biochem. J. *350 Pt 1*, 99-107.

Shewan,A.M., van Dam,E.M., Martin,S., Luen,T.B., Hong,W., Bryant,N.J., and James,D.E. (2003). GLUT4 recycles via a trans-Golgi network (TGN) subdomain enriched in Syntaxins 6 and 16 but not TGN38: involvement of an acidic targeting motif. Mol. Biol. Cell *14*, 973-986.

Shi,J., Huang,G., and Kandror,K.V. (2008). Self-assembly of Glut4 Storage Vesicles during Differentiation of 3T3-L1 Adipocytes. J. Biol. Chem. *283*, 30311-30321.

Shi,J. and Kandror,K.V. (2005). Sortilin is essential and sufficient for the formation of Glut4 storage vesicles in 3T3-L1 adipocytes. Dev. Cell *9*, 99-108.

Shi,J. and Kandror,K.V. (2007). The Luminal Vps10p Domain of Sortilin Plays the Predominant Role in Targeting to Insulin-responsive Glut4-containing Vesicles. J. Biol. Chem. *282*, 9008-9016.

Shimazaki,Y., Nishiki,T., Omori,A., Sekiguchi,M., Kamata,Y., Kozaki,S., and Takahashi,M. (1996). Phosphorylation of 25-kDa synaptosome-associated protein. Possible involvement in protein kinase C-mediated regulation of neurotransmitter release. J. Biol. Chem. *271*, 14548-14553.

Simonsen,A., Bremnes,B., Ronning,E., Aasland,R., and Stenmark,H. (1998). Syntaxin-16, a putative Golgi t-SNARE. Eur. J. Cell Biol. *75*, 223-231.

Slot,J.W., Geuze,H.J., Gigengack,S., Lienhard,G.E., and James,D.E. (1991). Immuno-localization of the insulin regulatable glucose transporter in brown adipose tissue of the rat. J. Cell Biol. *113*, 123-135.

Sollner,T., Whiteheart,S.W., Brunner,M., Erdjument-Bromage,H., Geromanos,S., Tempst,P., and Rothman,J.E. (1993). SNAP receptors implicated in vesicle targeting and fusion. Nature *362*, 318-324.

Song,X.M., Hresko,R.C., and Mueckler,M. (2008). Identification of amino acid residues within the C terminus of the Glut4 glucose transporter that are essential for insulin-stimulated redistribution to the plasma membrane. J. Biol. Chem. *283*, 12571-12585.

Sorensen,J.B., Wiederhold,K., Muller,E.M., Milosevic,I., Nagy,G., de Groot,B.L., Grubmuller,H., and Fasshauer,D. (2006). Sequential N- to C-terminal SNARE complex assembly drives priming and fusion of secretory vesicles. EMBO J. *25*, 955-966.

Stenbit,A.E., Tsao,T.S., Li,J., Burcelin,R., Geenen,D.L., Factor,S.M., Houseknecht,K., Katz,E.B., and Charron,M.J. (1997). GLUT4 heterozygous knockout mice develop muscle insulin resistance and diabetes. Nat. Med. *3*, 1096-1101.

Stephens,D.J., Crump,C.M., Clarke,A.R., and Banting,G. (1997). Serine 331 and tyrosine 333 are both involved in the interaction between the cytosolic domain of TGN38 and the mu2 subunit of the AP2 clathrin adaptor complex. J. Biol. Chem. *272*, 14104-14109.

Stockli,J., Davey,J.R., Hohnen-Behrens,C., Xu,A., James,D.E., and Ramm,G. (2008). REGULATION OF GLUT4 TRANSLOCATION BY THE RABGAP AS160/TBC1D4. ROLE OF PHOSPHORYLATION AND MEMBRANE ASSOCIATION. Mol. Endocrinol.

Stokoe,D., Stephens,L.R., Copeland,T., Gaffney,P.R., Reese,C.B., Painter,G.F., Holmes,A.B., McCormick,F., and Hawkins,P.T. (1997). Dual role of phosphatidylinositol-3,4,5-trisphosphate in the activation of protein kinase B. Science *277*, 567-570.

Struthers,M.S., Shanks,S.G., Macdonald,C., Carpp,L.N., Drozdowska,A.M., Kioumourtzoglou,D., Furgason,M.L., Munson,M., and Bryant,N.J. (2009). Functional homology of mammalian syntaxin 16 and yeast Tlg2p reveals a conserved regulatory mechanism. J. Cell Sci. *122*, 2292-2299.

Sudhof,T.C. and Rothman,J.E. (2009). Membrane fusion: grappling with SNARE and SM proteins. Science *323*, 474-477.

Suzuki,K. and Kono,T. (1980). Evidence that insulin causes translocation of glucose transport activity to the plasma membrane from an intracellular storage site. Proc. Natl. Acad. Sci. U. S. A *77*, 2542-2545.

Tahara,M., Coorssen,J.R., Timmers,K., Blank,P.S., Whalley,T., Scheller,R., and Zimmerberg,J. (1998). Calcium can disrupt the SNARE protein complex on sea urchin egg secretory vesicles without irreversibly blocking fusion. J. Biol. Chem. *273*, 33667-33673.

Tang,B.L., Low,D.Y., Lee,S.S., Tan,A.E., and Hong,W. (1998). Molecular cloning and localization of human syntaxin 16, a member of the syntaxin family of SNARE proteins. Biochem. Biophys. Res. Commun. *242*, 673-679.

Taylor,E.B. *et al.* (2008). Discovery of TBC1D1 as an insulin-, AICAR-, and contraction-stimulated signaling nexus in mouse skeletal muscle. J. Biol. Chem. *283*, 9787-9796.

Teng,F.Y., Wang,Y., and Tang,B.L. (2001). The syntaxins. Genome Biol. *2*, REVIEWS3012.

Thingholm,T.E., Jorgensen,T.J., Jensen,O.N., and Larsen,M.R. (2006). Highly selective enrichment of phosphorylated peptides using titanium dioxide. Nat. Protoc. *1*, 1929-1935.

Thurmond,D.C. and Pessin,J.E. (2000). Discrimination of GLUT4 vesicle trafficking from fusion using a temperature-sensitive Munc18c mutant. EMBO J. *19*, 3565-3575.

Thurmond,D.C. and Pessin,J.E. (2001). Molecular machinery involved in the insulin-regulated fusion of GLUT4-containing vesicles with the plasma membrane (review). Mol. Membr. Biol. *18*, 237-245.

Tian,J.H., Das,S., and Sheng,Z.H. (2003). Ca2+-dependent phosphorylation of syntaxin-1A by the death-associated protein (DAP) kinase regulates its interaction with Munc18. J. Biol. Chem. *278*, 26265-26274.

Toonen,R.F. and Verhage,M. (2003). Vesicle trafficking: pleasure and pain from SM genes. Trends Cell Biol. *13*, 177-186.

Tsui,M.M. and Banfield,D.K. (2000). Yeast Golgi SNARE interactions are promiscuous. J. Cell Sci. *113 (Pt 1)*, 145-152.

Ungermann,C., Sato,K., and Wickner,W. (1998). Defining the functions of trans-SNARE pairs. Nature *396*, 543-548.

van Vliet,C., Thomas,E.C., Merino-Trigo,A., Teasdale,R.D., and Gleeson,P.A. (2003). Intracellular sorting and transport of proteins. Prog. Biophys. Mol. Biol. *83*, 1-45.

Verhey,K.J., Yeh,J.I., and Birnbaum,M.J. (1995). Distinct signals in the GLUT4 glucose transporter for internalization and for targeting to an insulin-responsive compartment. J. Cell Biol. *130*, 1071-1079.

Vernet,T., Dignard,D., and Thomas,D.Y. (1987). A family of yeast expression vectors containing the phage f1 intergenic region. Gene *52*, 225-233.

von Mollard,G.F., Nothwehr,S.F., and Stevens,T.H. (1997). The yeast v-SNARE Vti1p mediates two vesicle transport pathways through interactions with the t-SNAREs Sed5p and Pep12p. J. Cell Biol. *137*, 1511-1524.

Watson,R.T., Khan,A.H., Furukawa,M., Hou,J.C., Li,L., Kanzaki,M., Okada,S., Kandror,K.V., and Pessin,J.E. (2004). Entry of newly synthesized GLUT4 into the insulin-responsive storage compartment is GGA dependent. EMBO J. *23*, 2059-2070.

Watson,R.T., Shigematsu,S., Chiang,S.H., Mora,S., Kanzaki,M., Macara,I.G., Saltiel,A.R., and Pessin,J.E. (2001). Lipid raft microdomain compartmentalization of TC10 is required for insulin signaling and GLUT4 translocation. J. Cell Biol. *154*, 829-840.

Weber,T., Zemelman,B.V., McNew,J.A., Westermann,B., Gmachl,M., Parlati,F., Sollner,T.H., and Rothman,J.E. (1998). SNAREpins: minimal machinery for membrane fusion. Cell *92*, 759-772.

Wendler,F. and Tooze,S. (2001). Syntaxin 6: the promiscuous behaviour of a SNARE protein. Traffic. *2*, 606-611.

White,M.F. (1998). The IRS-signalling system: a network of docking proteins that mediate insulin action. Mol. Cell Biochem. *182*, 3-11.

Xu,T., Binz,T., Niemann,H., and Neher,E. (1998). Multiple kinetic components of exocytosis distinguished by neurotoxin sensitivity. Nat. Neurosci. *1*, 192-200.

Xu,T., Rammner,B., Margittai,M., Artalejo,A.R., Neher,E., and Jahn,R. (1999). Inhibition of SNARE complex assembly differentially affects kinetic components of exocytosis. Cell *99*, 713-722.

Xu,Z. and Kandror,K.V. (2002). Translocation of small preformed vesicles is responsible for the insulin activation of glucose transport in adipose cells. Evidence from the in vitro reconstitution assay. J. Biol. Chem. *277*, 47972-47975.

Yang,B., Gonzalez,L., Jr., Prekeris,R., Steegmaier,M., Advani,R.J., and Scheller,R.H. (1999). SNARE interactions are not selective. Implications for membrane fusion specificity. J. Biol. Chem. *274*, 5649-5653.

Yeh,T.Y., Sbodio,J.I., Tsun,Z.Y., Luo,B., and Chi,N.W. (2007). Insulin-stimulated exocytosis of GLUT4 is enhanced by IRAP and its partner tankyrase. Biochem. J. *402*, 279-290.

Yu,C., Cresswell,J., Loffler,M.G., and Bogan,J.S. (2007). The GLUT4 regulating protein TUG is essential for highly insulin responsive glucose uptake in 3T3-L1 adipocytes. J. Biol. Chem.

Zaid,H., Antonescu,C.N., Randhawa,V.K., and Klip,A. (2008). Insulin action on glucose transporters through molecular switches, tracks and tethers. Biochem. J. *413*, 201-215.

Zeigerer,A., Lampson,M.A., Karylowski,O., Sabatini,D.D., Adesnik,M., Ren,M., and McGraw,T.E. (2002). GLUT4 retention in adipocytes requires two intracellular insulin-regulated transport steps. Mol. Biol. Cell *13*, 2421-2435.

Zeigerer,A., McBrayer,M.K., and McGraw,T.E. (2004). Insulin stimulation of GLUT4 exocytosis, but not its inhibition of endocytosis, is dependent on RabGAP AS160. Mol. Biol. Cell *15*, 4406-4415.

Zeng,Q., Tran,T.T., Tan,H.X., and Hong,W. (2003). The cytoplasmic domain of Vamp4 and Vamp5 is responsible for their correct subcellular targeting: the N-terminal extenSion of VAMP4 contains a dominant autonomous targeting signal for the trans-Golgi network. J. Biol. Chem. *278*, 23046-23054.

Zerial,M. and McBride,H. (2001). Rab proteins as membrane organizers. Nat. Rev. Mol. Cell Biol. *2*, 107-117.

Zimmet,P., Alberti,K.G., and Shaw,J. (2001). Global and societal implications of the diabetes epidemic. Nature *414*, 782-787.

Zisman,A. *et al.* (2000). Targeted disruption of the glucose transporter 4 selectively in muscle causes insulin resistance and glucose intolerance. Nat. Med. *6*, 924-928.